Electrification and Automation of Mobility Infrastructure: Unintended Consequences and Their Solutions via Connectivity, Modeling, and Control

by

Soomin Woo

A dissertation submitted in partial satisfaction of the

requirements for the degree of

Doctor of Philosophy

in

Engineering- Civil and Environmental Engineering

in the

Graduate Division

of the

University of California, Berkeley

Committee in charge:

Professor Scott J. Moura, Chair
Professor Alexander Skabardonis
Professor Francesco Borrelli
Professor Rhonda Righter

Fall 2021

Electrification and Automation of Mobility Infrastructure:
Unintended Consequences and Their Solutions via Connectivity, Modeling, and Control

Abstract

Electrification and Automation of Mobility Infrastructure:
Unintended Consequences and Their Solutions via Connectivity, Modeling, and Control

by

Soomin Woo

Doctor of Philosophy in Engineering- Civil and Environmental Engineering

University of California, Berkeley

Professor Scott J. Moura, Chair

It is estimated that there were 1.3 billion vehicles in the world at the end of 2016, which is almost two times more than the number of vehicles 20 years before. With the ever-growing population of vehicles, transportation has caused many problems. It was the sector with the most significant contribution to greenhouse gas emissions in the United States in 2019. About 90% of the fuel burned in transportation is based on petroleum, a non-renewable energy source. The transportation system is also unsafe. For instance, with 1.10 fatalities per 100 million vehicle miles traveled in the United States in 2019.

To resolve these problems, significant innovations have been made in vehicle technology via electrification, automation, and communication. For instance, electric vehicles (EVs) can vastly reduce greenhouse gas emissions and utilize sustainable energy, such as solar-generated electricity. Also, Connected and Automated Vehicles (CAVs) promise to improve road safety, enhance traffic network performance, and increase fuel efficiency by safely driving with smaller headways and smaller air drag.

As more vehicles adopt these advanced technologies, the urban system will find new opportunities and unintended consequences for the related infrastructure, such as the charging facilities, the electrical energy grid, and the traffic network. In this dissertation, we identify some of these issues and enable vehicle electrification and automation technologies to enhance the systematic performance of urban infrastructure through connectivity.

First, we investigate the problem of optimally planning an EV charging infrastructure, subject to the electrical grid pricing and the random charging demand. The facility planner faces a trade-off problem, where the operator has to pay a high price to achieve a high quality of service in charging EVs or pay a low cost but provide a low quality of service. We propose a Pareto-optimal planning solution that uses demand management strategies and achieves a higher quality of service at a lower cost.

Second, we study the relationship between the electrical energy grid and the charging schedule of an EV fleet on a large, regional scale. We identify the opportunities in shifting the EV charging schedule both in time and space to benefit the grid operation in terms of the cost, the renewable energy mix, and the greenhouse gas emissions. We evaluate the maximum potential gain to the grid based on real data from the individual vehicles and the energy grid operation. We recommend an optimal model to schedule the EV charging sessions.

Third, we analyze the balance between the operation of Connected Automated Vehicles (CAVs) and the traffic network performance. We find that in mixed traffic of CAVs and human-driven vehicles, naive operation strategies of CAVs can induce more lane changes and create unnecessary congestion. We propose and validate an operation strategy for CAVs that ensures the maximal performance of the traffic network while allowing the CAVs to enjoy the benefits of automation and connection.

To my parents, my sisters, and my grandparents,

for always believing in me.

Contents

List of Figures

List of Tables

Acknowledgments

Over the past, I had many excellent mentors that encouraged my passion for science. First, I express my sincere gratitude to my advisor Professor Scott Moura for his knowledge, trust, and care. He is a prime example of who I strive to be - a true educator and a brilliant academic who genuinely cares for the students and produces exceptional and innovative research. I am very fortunate to have had him as an advisor, and I am very excited to continue working with him in the future.

I thank Professor Alexander Skabardonis for guiding me through the numerous challenges during the Ph.D. program. He provided me with many opportunities for research, teaching, and scholarships, and of course, with his humor. My sincere thanks also go to Doctor Timothy Lipman, Doctor Xiao-Yun Lu, and Doctor Hao Liu, who gave me opportunities to collaborate on their outstanding research. Without their precious support, I would not have conducted this research and grown academically.

I would also like to thank Professors Carlos Daganzo and Michael Cassidy for their insight on my research. They taught me that I should always strive to pave a new path in research rather than 'only adding a delta' to the existing research. I also appreciate the rest of my thesis committee, Professors Rhonda Righter and Francesco Borrelli, for their insightful comments and encouragement on my research. I send my gratitude to Professor Hwasoo Yeo, who believed in me and encouraged me to dream big and pursue my career in the US.

My Ph.D. life would have been very difficult without my amazing friends and colleagues. I am lucky to have Elpiniki Apostolaki-Iosifidou, Ayse Tugba Ozturk, Zhe Fu, Sangjae Bae, Hongcai Zhang, David Kan, Juan Caicedo Castro, Mauricio Martínez, Bassel Sadek, Saehong Park, Teng Zeng, Dylan Kato, Ibrahim Itani, Mathilde Badoual, Guillaume Goujard, Preet Gill, Ioanna Kavvada, Esther Jung, Boom Sangveraphunsiri, Dokyun Kim, Kyoungtae Lee, Daewon Lee, Saleh Al-Beaik, Eric Choi, Andrea Medina, Jeremy Halpern, Jonghae Suh, Hyokyung Henry Ryu, Tahirih Brown, Daphne Huang, Michael Shin, Sooyeon Bae-Park, John Jin, Jinhyo Yoo, Kyeong-a Jung, Heejin Jung, Yoojin Chae, Eunhye Kim, and Koohong Jung. I also received a tremendous amount of love and support from Korea, and I thank Jiwon Shin, Hanyoung Kim, Lucy Shin, Sungjin Choi, Heesun Shin, Hyunkyoung Lee, Heemin Yoo, Soomin Ham, Heejeong Kim, Sehyun Tak, and Professor Jinwoo Lee.

Everything I have achieved in my life is due to my family - Jonggyu Woo, Kyeongsun Jeon, Jimin Woo, Seungmin Woo, Myeongja Na, Jongae Jo, and my grandparents in heaven. My parents raised me to believe in who I am and what I can be. They showed me the worth of hard work and being loving to others. I thank my sisters and grandparents for always being proud of me and encouraging my career. I love you all. Last but not least, I express my gratitude for the constant support and care from Jesse Park and Cola.

Chapter 1

Introduction

1.1 Background

According to one study [1], the number of vehicles in the world has almost doubled every 20 years since 1976. At the end of 2016, it was estimated that there were 1.3 billion vehicles in the world. With the ever-growing population of vehicles, however, came many problems. First, transportation has caused severe damage to the environment. The transportation sector contributed 28.6% to the total greenhouse gas emissions in the United States in 2019 [2], as shown in Figure 1.1. Over 90% of the fuel burned in transportation is based on petroleum, i.e., gasoline and diesel [2]. The transportation sector exacerbates climate change, inefficiently using non-renewable energy sources that are not sustainable. Second, though the safety on the road is improving, the transportation system is still unsafe. For instance, there were 36,096 motor vehicle traffic fatalities, and the fatality rate was 1.10 fatalities per 100 million VMT in the United States in 2019 [3], as seen in Figure 1.2. To combat these issues from transportation, great innovations have been made on vehicle technology via electrification, automation, and communication.

Vehicle electrification can reduce the pollution from the transportation sector by producing no greenhouse gas emissions at their pipes [5]. Initially, electric vehicles (EVs) have been lagging in the market adoption due to the range anxiety issues [6], and a lack of reliable access to charging infrastructure [7]. However, the governments and industries have put a joint effort to stimulate the adoption of EVs [8], installing charging infrastructure [9], [10] and improving the charging performance and the driving range of EVs [11]. The EV adoption is growing and will continue to grow. From 2013 to 2019, the number of passenger EVs grew globally, largely contributed by China [4], as seen in Figure 1.3. By 2032, '30% of all passenger cars worldwide are predicted to be EVs' that may reduce the greenhouse gas emissions with cleaner energy generation [12].

Also, vehicles have automated with advanced driving technologies and communication capabilities. For example, Cooperative Adaptive Cruise Control (CACC) is an emerging vehicle technology that brings the promise of greater road capacities without investing in

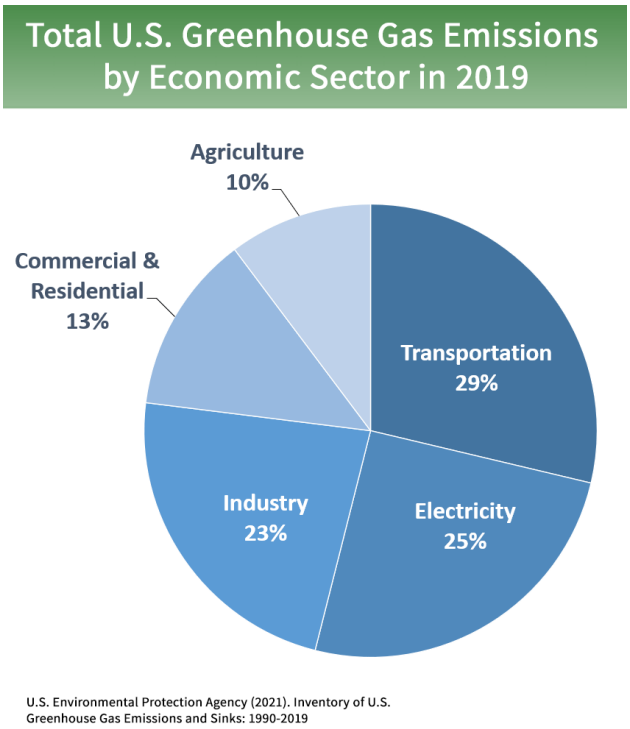

Figure 1.1: Total U.S. Greenhouse Gas Emissions by Economic Sector in 2019, from [2]

the road infrastructure, such as additional lanes or ramp metering controllers [14]. It can also improve fuel efficiency [15], [16], safety [17] and driver comfort [18]. A vehicle with Adaptive Cruise Control (ACC) senses the relative speed and gap with its leader vehicle and automatically adjusts its acceleration and speed to keep a safe gap. Vehicles with Connected Adaptive Cruise Control (CACC), in addition to the ACC capability, can communicate in real-time and high frequency with one another. Driving decisions, such as acceleration and deceleration, are shared and executed automatically, which may avoid human error in perception and reaction time. More importantly, this enables a reduction in headway between CACC vehicles and allows them to form platoons that are tighter than humanly possible, as shown in Figure 1.4. The reduction in headway will result in a higher capacity of road network [13], as shown in Figure 1.5. We will call vehicles equipped with CACC as Connected Automated Vehicles (CAVs).

However, vehicles are closely related to other urban systems, such as the energy grid, the charging infrastructure, and the traffic network, as shown in Figure 1.6. Although electrification and automation technologies can solve many problems, they can create unintended problems if we neglect their impact on the connected systems. In the following, we motivate some specific research questions.

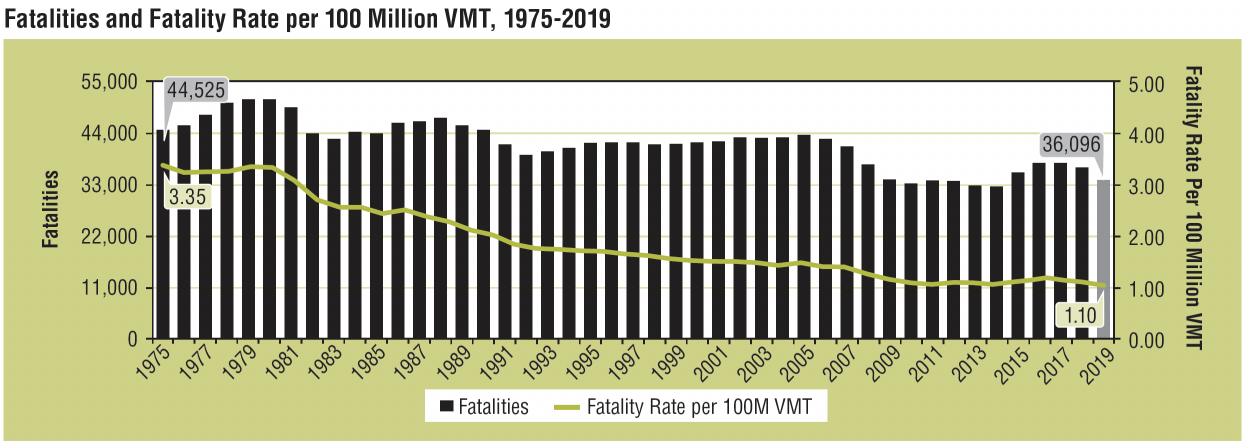

Figure 1.2: Fatalities and Fatality Rate per 100 Million VMT, 1975-2019, from [3]

1.2 Motivation

One problem that may arise from vehicle electrification is the increasing burden on the electrical grid operation. More EVs increase not only the total demand to the electrical grid but also the evening peak demand that ramps up quickly when the drivers charge their EVs at home after work [20]. In California, an additional burden from the EV charging load may be critical to the grid operation, which has a severe ramping not only from a surge of demand but also an abrupt drop of solar generation in the evening, as shown in Figure 1.7. It is often costly to upgrade the electrical grid infrastructure, and the grid operators face challenges with the EV charging load, such as the congestion in generation and transmission, the poor power quality with violation of voltage limits, the heavy loading on the network assets, and more emissions from using fossil fuels [21]–[23].

Vehicle electrification can also add challenges in planning a charging infrastructure, which must satisfy the demand of the increasing EVs, subject to the pricing schemes of the electrical grid. To manage the extreme ramping of demand, the electrical grid operators give incentives and penalties to their customers. They charge cheap Time-of-Use costs to encourage electricity consumption during the low demand and impose demand charges to discourage consumption during the high demand. However, these economic measures create challenges in building and operating an EV charging infrastructure. To satisfy a peak demand to charge EVs, a facility needs to build a large and expensive capacity to supply sufficient energy to the EVs. Subject to the pricing by the grid, the facility needs to pay a high price to purchase the necessary energy [24], [25]. Alternatively, a facility can build a smaller charging capacity and use less electricity during the peak. However, this can result in an unreliable charging service to the EVs as the facility may not satisfy the charging needs.

In addition, automating vehicles can create problems in the traffic network. The CAVs can form a platoon with short headways, promising the benefits to the traffic flow capacity,

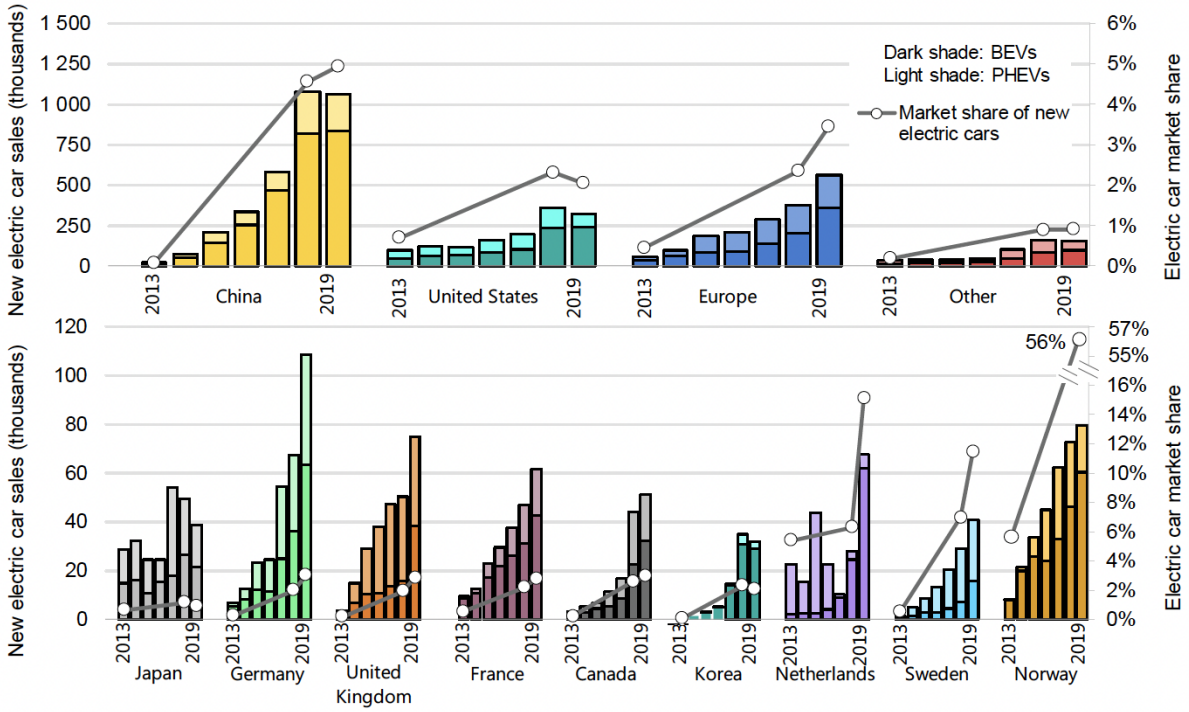

Figure 1.3: Passenger electric car sales and market share in selected countries and regions, 2013-19 from [4]

energy efficiency, or driver comfort. However, at low CAV penetration, the CAVs will be sparsely distributed on the road and diminish the probability of forming long platoons. Therefore, the promised benefits are likely to be small. For instance, Figure 1.5 shows that the flow capacity will increase at a slow rate up to the penetration rate of around 40%. Many researchers propose to solve this issue by *platoon organization* strategies, where the CAVs search for other CAVs on the road and change lanes if necessary to form longer platoons [26], [27]. However, the induced lane changes can potentially disrupt the traffic flow and cause more congestion [28]–[31]. In other words, a poorly designed operation strategy of the CAVs can cause problems to the traffic flow.

1.3 Research Objective

The goal of this dissertation is to better understand several unintended consequences of electrification and automation of mobility infrastructure and how to resolve these issues via connectivity, modeling, and control from an economic and environmental perspective.

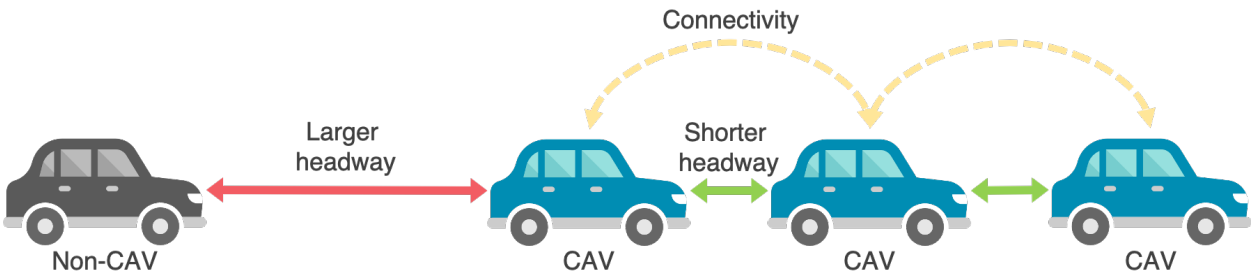

Figure 1.4: Illustration of the Connected Automated Vehicles (CAVs) driving in a platoon of shorter headways

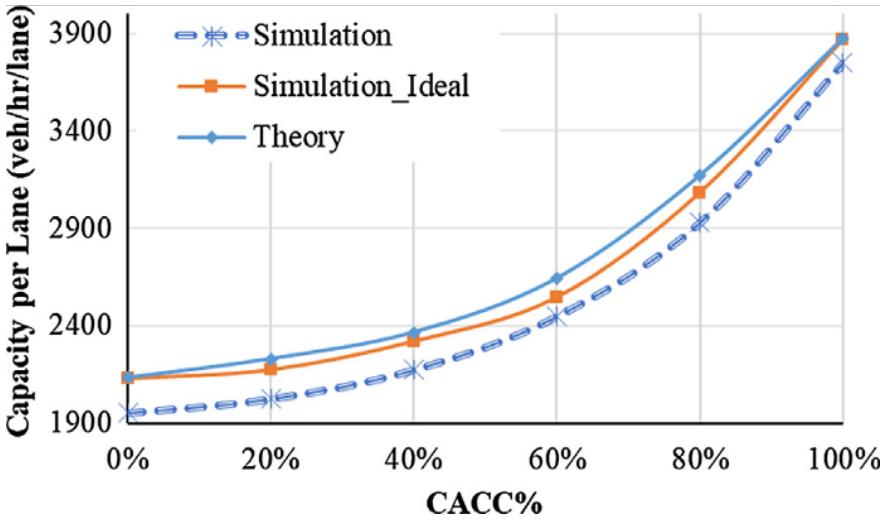

Figure 1.5: Capacity Improvement with Increasing Penetration of CAVs from [13] (Vehicles equipped with Cooperative Adaptive Cruise Control, or CACC, are CAVs)

1.4 Research Challenges

There are challenges in modeling and control of the mobility infrastructure with vehicle electrification and automation due to the following reasons:

- Mobility infrastructure involves many factors, such as drivers, charging infrastructure, energy grid, and traffic network. It requires an expert insight into the planning and operation of the mobility infrastructure to identify the unintended problems of vehicle electrification and automation.

- It is complex to model an optimization problem of multiple vehicles to improve the infrastructure performance because each system is governed by its own physics. One

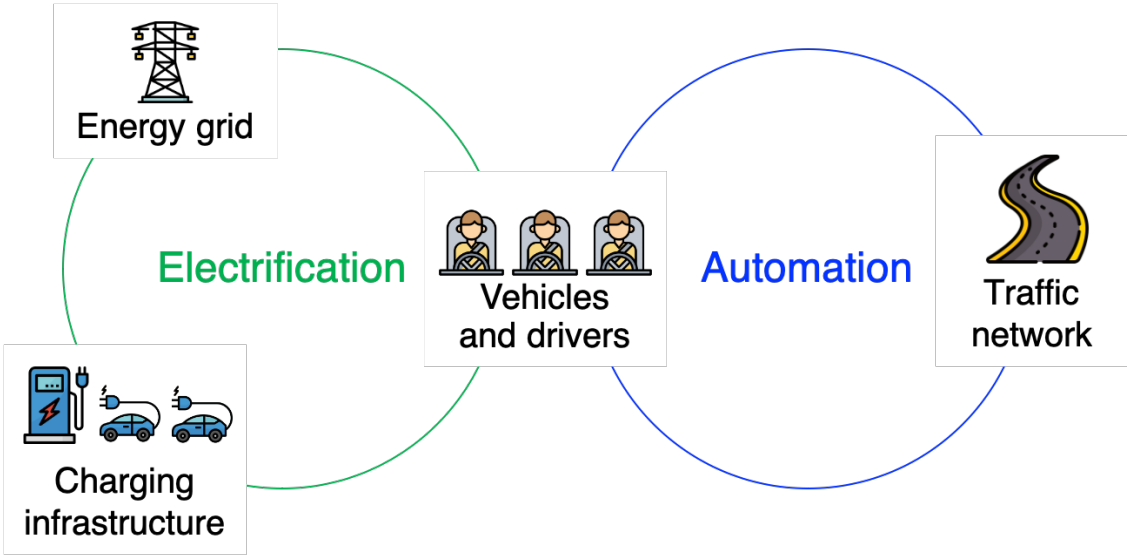

Figure 1.6: Example of Interconnected Urban Systems with Vehicles

must carefully design the problem with appropriate assumptions, a meaningful objective function, precise decision variables, relevant parameters, and accurate physical relationships.

- It is challenging to analyze the optimal result of controlling many agents in a large system. A clear understanding of the relevant physical models is required to interpret the results and discover meaningful findings.

1.5 Novel contributions

In this dissertation, a collection of research findings contributes to the current literature as the following.

Pareto optimal planning of an EV charging facility (Chapter 2)

This chapter focuses on the facility manager's perspective on an EV charging facility with a given electrical grid and the random charging demand of EVs.

- We identify the trade-off between the quality of service in charging EVs and the planning and operation costs. For the first time in the literature, we resolve this problem by planning a facility that achieves Pareto optimality with a high quality of service at a low cost.

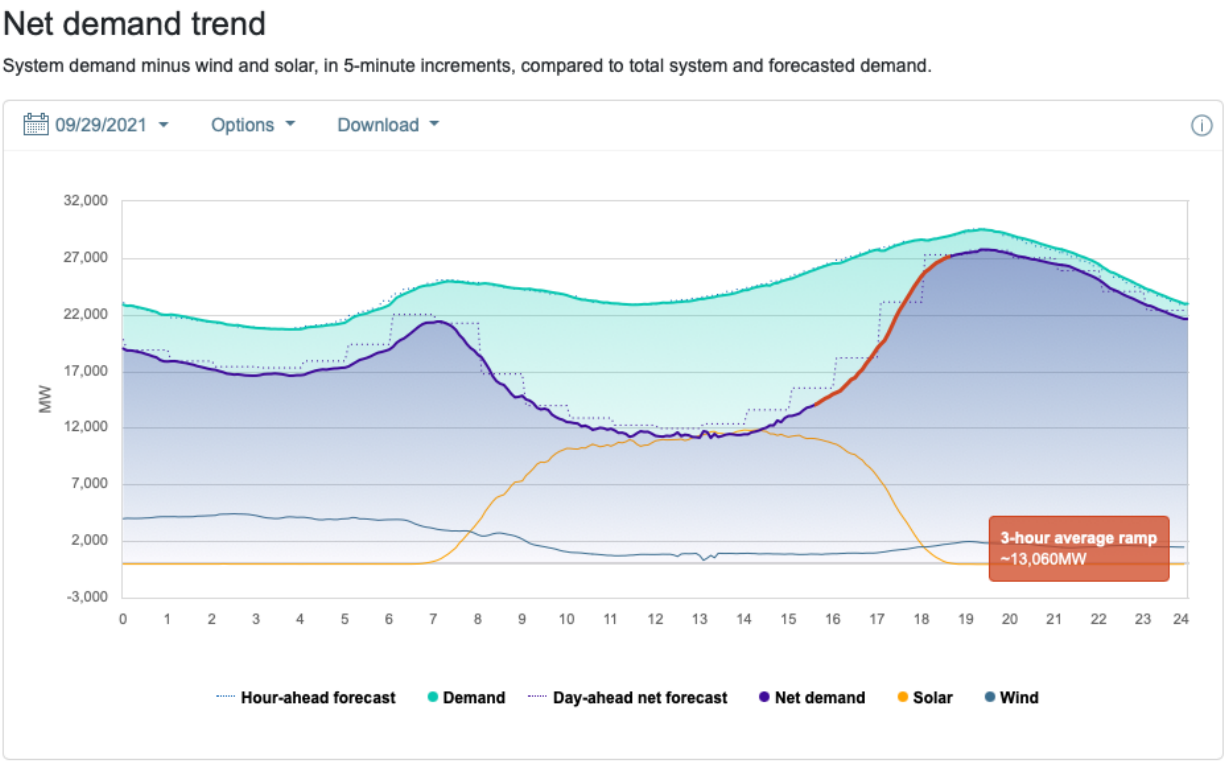

Figure 1.7: An Example of Severe Ramping to a Peak Electricity Demand in California ISO, Showing the Net Demand on September 29th, 2021 [19]. The figure shows a 3-hour average ramp in the evening by about 13,060 Mega Watts, due to the peak demand and reduction in the solar energy generation.

- We analyze the mechanism of demand management strategies, such as installing an energy storage system and rescheduling the EV charging sessions, in achieving the Pareto optimality.
- We model a robust optimization problem to plan an EV charging facility that considers the stochasticity of charging demand.

Economic and environmental benefits of optimal EV charging to the electricity grid (Chapter 3)

This chapter considers a fleet of EVs and their consumption in the energy grid on a large regional scale.

- We optimally schedule the charging of EV fleet in terms of both the time and location, for the first time in literature. The scheduling improves the electrical grid operation in

terms of the operation cost, the renewable energy mix, and greenhouse gas emissions.

- We overcome the limitations of the current literature that heavily depend on the simulated and aggregate data of EV charging demand by using the real driving and charging data of individual EVs and the real grid operation data in California.
- We estimate the maximum potential gains and recommend an optimal scheduling model for the best performance of the electrical grid operation.

Operation of CAV platoons for maximal traffic flow (Chapter 4)

This chapter studies the impact of a CAV operation strategy on traffic network performance.

- For the first time in the literature, we verify that the CAVs can disrupt the traffic flow and create unnecessary congestion in mixed traffic with human-driven vehicles if they follow a poor operation strategy to change lanes and form longer platoons with other CAVs.
- We propose a CAV operation strategy with an awareness of the current traffic flow that forms longer CAV platoons but prevents unnecessary congestion. We validate that the proposed strategy can form longer platoons while ensuring a maximal traffic flow.

Chapter 2

Planning of an Electric Vehicle charging facility with Pareto Optimality in Cost and Service Quality

This chapter is based on the previously published article: Woo, S., Bae, S., & Moura, S. J. (2021). Pareto optimality in cost and service quality for an Electric Vehicle charging facility. *Applied Energy*, 290(116779), 116779, https://doi.org/10.1016/j.apenergy.2021.116779.

This chapter examines the problem of planning an Electric Vehicle (EV) charging facility that provides a high quality of service in charging EVs and incurs a low cost to the facility manager. This problem is challenging because a facility with a larger charging capacity (hence better service quality) can be more expensive to build and operate. This chapter contributes to the literature by planning an EV charging facility that overcomes this trade-off and achieves Pareto optimality, i.e. a facility with a higher quality of service but at a lower cost. We propose an optimization model to size an EV charging facility that minimizes the facility cost and guarantees a high quality of service. To reduce the cost further and negate the cost increase from quality service quality, we adopt demand management strategies. Two strategies are explored, namely Stationary Demand Management (a local energy storage system) and Mobile Demand Management (rescheduling charging sessions of EVs). The proposed model produces a facility that guarantees a high quality of service in charging EVs at a minimal cost. Stationary Demand Management can reduce the cost similarly to Mobile Demand Management, while the latter can be more challenging in practice due to the compliance issues and demand uncertainty of the drivers.

Nomenclature

ESS Energy Storage System

EV Electric Vehicle

EV Electric Vehicle

LMP Locational Marginal Price

MDM Mobile Demand Management

MER Marginal Emission Rate

RE Renewable Energy

SDM Stationary Demand Management

$C_{\mathrm{LMP}}(t, x)$ Locational marginal price at time t and node x in USD/kWh

$C_{\mathrm{MER}}(t)$ Marginal emission rate at time t in tons]of CO_2E/kWh

$C_{\mathrm{RE}}(t)$ Renewable energy ratio at time t, unitless

$E_{b,i}$ Battery capacity in energy for vehicle i in kWh

E_f Final condition on the energy level required for vehicle i in kWh

$E^c_{i,k}$ Energy consumption for the trip departing from the destination node k for vehicle i in kWh

$E^{des}_{i,k}$ Desired charging energy at the destination node k for vehicle i in kWh

$E_{ini,i}$ Initial energy level in the battery of vehicle i in kWh

E_{max} Maximum level of energy required for vehicle i in kWh

$E_{min,i}$ Minimum level of energy required for vehicle i in kWh

K_i Number of locations that vehicle i visits over the optimization time horizon

N_{EV} Sample size of EVs

$P_{r,i}$ Rated charging power of vehicle i in kW

$S_i(t)$ Parking status of vehicle i at time t, which equals 1 if parked and 0 otherwise

$T^a_{i,k}$ Arrival time to the destination node k for vehicle i

$T^d_{i,k}$ Departure time from the destination node k for vehicle i

Δt Discrete time interval in hours

$\hat{x}_i(t)$ The electrical grid node that the location of vehicle i belongs to

i Vehicle index, $i \in [1, N_{EV}]$

k Destination index, $k \in [1, K_i]$

n Number of EV chargers

b Scale factors for ESS units [scale]

$P_c(i,t)$ Charging power for vehicle i at time t in kW

$\widehat{J_{\text{agg, LMP}}}$ The total LMP cost from the LMP-minimizing solution for aggregate EVs

$\widehat{J_{\text{agg, MER}}}$ The total MER from the MER-minimizing solution for aggregate EVs

$\widehat{J_{\text{agg, RE}}}$ The total RE from the RE-maximizing solution for aggregate EVs

$P_{\text{EV}}(\tau)$ Charging power to aggregate EVs [kW]

$P_{\text{B,C}}(\tau)$ Power charged to ESS [kW]

$P_{\text{B,D}}(\tau)$ Power discharged from ESS [kW]

$P_{\text{G,I}}(\tau)$ Power imported from the grid [kW]

$P_{\text{G,D}}$ Power used for demand charge calculation [kW]

$E_{\text{EV}}(\tau)$ Time-cumulative energy charged to aggregate EVs [kWh]

$E_{\text{B}}(\tau)$ Energy level of ESS [kWh]

$P^{\star}_{\text{EV,min}}(\tau)$ Power demand in charging EV aggregates, minimum to be satisfied [kW]

$E^{\star}_{\text{EV,min}}(\tau)$ Time-cumulative energy demand in charging EV aggregates, minimum to be satisfied [kWh]

$P^{\star}_{\text{L}}(\tau)$ Power demand from the building use [kW]

$P^{\star}_{\text{EV, min, MDM}}(\tau)$ Power demand in charging EV aggregates with mobile demand management, minimum to be satisfied [kW]

$E^{\star}_{\text{EV, min, MDM}}(\tau)$ Time-cumulative energy demand in charging EV aggregates with mobile demand management, minimum to be satisfied [kWh]

$\overline{P_L(\tau)}$ Expected value of $P^{\star}_{\text{L}}(\tau)$

$\sigma^2_{P_L}(\tau)$ Variance of $P^{\star}_{\text{L}}(\tau)$

$\mathcal{F}_{E,\tau}(z)$ Empirical cumulative distribution of $E^{\star}_{\text{EV, min, MDM}}(\tau)$

$\mathcal{F}_{P,\tau}(z)$ Empirical cumulative distribution of $P^{\star}_{\text{EV, min, MDM}}(\tau)$

$\mathcal{F}^{-1}_{E,\tau}(\tau)(\alpha_{EV})$ The inverse of $\mathcal{F}_{E,\tau}(z)$ at significance level α_{EV}, i.e., the aggregate EV charging energy demand at α_{EV}-th percentile at time τ

$\mathcal{F}^{-1}_{P,\tau}(\tau)(\alpha_{EV})$ The inverse of $\mathcal{F}_{P,\tau}(z)$ at significance level α_{EV}, i.e., the aggregate EV charging power demand at α_{EV}-th percentile at time τ

$P_{\text{EV,test,j}}(\tau)$ EV charging power demand for operation simulation date i [kW]

$P_{\text{L, test,j}}(\tau)$ Power demand from the building use for operation simulation of date i [kW]

b_{opt} Optimized scale factors for ESS units [scale]

n_{opt} Optimized number of EV chargers

$E_{B,\text{max}}$ Nominal ESS energy capacity per unit of ESS [14.0 kWh]

$P_{\text{EV, R}}$ Rated power of EV charger [2.33kW]

$P_{\text{G,I,max}}$ Power capacity for grid import [2000.0kW]

$P_{B,\text{max}}$ Nominal ESS power capacity per unit of ESS [5.0 kW]

α_{EV} The percentile value of the EV charging energy, at which the EV charging facility must satisfy [0.95]

$\alpha_{\text{G, l}}$ The probability of the grid import power is above minimum, 0kW [0.95]

$\alpha_{\text{G,u}}$ The probability of the grid import power is below the capacity, $P_{G,I,\text{max}}$ [0.95]

$\beta_{\text{B,i}}$ Initial ESS energy level ratio, [0.5%]

$\eta_{\text{B,C}}$ ESS charging efficiency, [0.98%]

$\eta_{\text{B,D}}$ ESS discharging efficiency, [0.98%]

η_{EV} EV charging efficiency [0.89%]

$b_{\max}$ ESS scale maximum limit [scale/kWh]

c_{B} Daily cost per energy storage system unit [0.066 USD /day/kWh]

c_{EV} Daily cost of an EV charger [0.274 USD/day]

$c_{\mathrm{G,D}}$ Demand charge cost, [19.0/30 USD/kW/day]

$c_{\mathrm{I}}(\tau)$ Time-of-Use electricity cost for time τ [USD/kWh]

dt Time interval, [1 hour]

τ Time step $\in [1, T]$ [hour]

T Number of time steps in a day [24 hours]

N_{cross} Sample size for cross validation [100 samples]

N_{test} Number of dates tested for operation simulation [71 dates]

f_{CC} Daily capital cost ($/day)

f_{OC} Daily operation cost ($/day)

f_{TC} Daily total cost ($/day)

f_{QoS} Performance metric of quality of service in charging EVs (kW)

2.1 Introduction

Vehicle electrification is a potential solution to reduce greenhouse gas emissions from the transportation sector [5]. To increase the market adoption of Electric Vehicles (EVs), it is crucial to build EV charging infrastructure and supply the growing demand on EV charging energy [9], [10], [32]. For instance, California needs to build around 78,000 Level 2 public chargers by 2025 to meet their goal on zero emission vehicles [10]. There are two aspects to consider in building EV charging infrastructure. On the one hand, the facility can be planned to minimize the capital and operation costs. On the other hand, the facility can be planned to achieve high quality of service in charging EVs and help alleviate the range anxiety of drivers [7]. In this study, we define quality of service in terms of satisfying the charging demand. The quality of service can be high when the facility has a sufficient charging capacity to supply the stochastic charging demand in a robust fashion. For instance, the EV charging demand can surge occasionally and a large capacity (with more chargers and/or at higher charging power) to charge will be needed for a high service quality. However, achieving these two goals may be challenging because a facility with a larger charging capacity (hence better

service quality) can be more expensive to build and operate [24], [25], [33]. In other words, a trade-off exists between cost and service quality.

To the best of authors' knowledge, no study has examined and mitigated this trade-off. Many solve the sizing problem of one or multiple EV charging facilities and analyze the cost reduction from managing the energy demand; however, they do not investigate how to reduce the cost while improving the quality of service [24], [25], [33]–[40]. To manage the energy demand, some literature study the coordination of the EV charging schedule [33], [36], [39], [40]. A paper [33] shows that the sizing cost is reduced by controlling the EV charging schedule. In [36], the authors also show that the coordination reduces cost, while satisfying the same charging demand. Similar results are shown in [39], where a penalty for incomplete charging demand is included in the sizing problem. The authors in [40] confirm that the control of charging schedule reduces cost in the real operation settings.

Some literature experiment with the plug-in states of EVs to chargers [34], [35] to manage the energy demand and reduce cost, though missing analysis on quality of service. A paper [34] analyzed the cost reduction with an 'interchange' algorithm to unplug the EVs that are finished charging and use the available chargers for other demanding EVs. Another paper [35] explores the probability of EVs leaving soon after charging completion and argues that increasing the utilization rate of chargers lowers the facility cost. Some literature reduce the facility cost by not only controlling the charge schedule but also using an energy storage system to control the purchasing times of electricity [37], [38].

Despite the lack of research in enhancing quality of service with cost reduction, there are a few papers that recognize the trade-off problem of cost and service quality [24], [25], [33]. These papers measure the quality of service differently. In [24], the researchers showed that unsatisfied charging load can be reduced with increasing planning costs. A paper [25] showed the longer the time drivers spend for charging, the lower the cost, due to longer trips to reach a charging facility and/or lower charging power. The authors in [33] show that the controlled charging schedule can reduce the driver's waiting time for charger availability and the excess charging time over parking time, at lower cost in some cases.

The state-of-art literature does not investigate the problem of increasing cost with higher service quality or suggest how a facility planner may achieve higher quality of service at lower cost. This chapter contributes to the literature by 1) analyzing the Pareto frontiers that quantity the trade-off between cost and quality of service and 2) identifying how demand management shifts the frontiers towards lower cost and higher quality of service. We provide an insight to facility planners to select demand management strategies that best meet their needs on cost and quality of service.

In the following, we develop an optimization model to plan an EV charging facility that minimizes the cost and guarantees a high service quality in charging EVs. The results show that the proposed model can plan a facility with a high service quality to charge random demand in a robust fashion. The results also show that increasing quality of service increases the facility cost at optimum. So we analyze the Pareto frontiers in cost and quality of service and test the impact of demand management strategies on these frontiers. We learn that demand management reduces the optimal cost further at a given quality of service,

by purchasing grid electricity at cheaper times, reducing the peak power of grid electricity purchase, and building less chargers. With demand management strategies, a facility achieves a higher service quality at a lower cost compared to a facility without the strategies.

The paper is organized as follows. Section 2.3 develops a robust sizing model to plan an EV charging facility. Section 2.4 describes the research methodology for the performance analysis of the robust sizing model and for the sensitivity analysis of demand management strategies. Supplementary algorithms are proposed in this section, such as the baseline sizing model to compare the robust model to and the simulation model of the facility operation. Section 2.5 describes the data used in this chapter. Section 2.6 provides the results on the robust planning model and on the sensitivity analysis with demand management. This chapter is concluded with Section 2.7.

2.2 Context of EV Charging Facility

We focus on a single facility that provides charging service through multiple chargers, as well as the building energy load. We explore two strategies of demand management:

- Stationary Demand Management (SDM) leverages the grid import cost with an Energy Storage System (ESS). The ESS is strategically charged (from the grid) and discharges to deliver electricity to minimize the electricity cost [37], [38], [41]. The discharging is based on time-variant electricity tariffs, i.e., charging when the tariff is low and supplying when the tariff is high, as well as on the demand charge, i.e. discharging when the power demand is at its peak.

- Mobile Demand Management (MDM) leverages the EV charging load with flexibility in charging schedule. While plugged in, EVs can be charged at any time until it is unplugged, as long as the charging demand is met. Instead of charging immediately upon arrival, an EV charging session may be deferred to alternative times with low electricity tariff and/or at off-peak power demand. This can distribute the charging sessions more evenly across time, which reduces the number of chargers to build as well as the operation cost to charge, but remains at the same quality of service [33], [36], [39], [40]

The aforementioned strategies help reduce both the operation cost with cheaper electricity and the capital cost by installing fewer chargers.

Figure 2.1 illustrates the components of an EV charging facility considered in this chapter, with arrows indicating the energy flow. The energy flow is balanced by the system operator that connects the facility components. The facility draws energy from the grid and supplies energy for the building load and the EV charging demand. The ESS stores energy and discharges it to supply when needed. The system minimizes the capital cost by finding the most economic sizing of the facility, while monetizing the unsatisfied demand. The capital cost is reduced further when EVs are charged flexibly via MDM and require less chargers

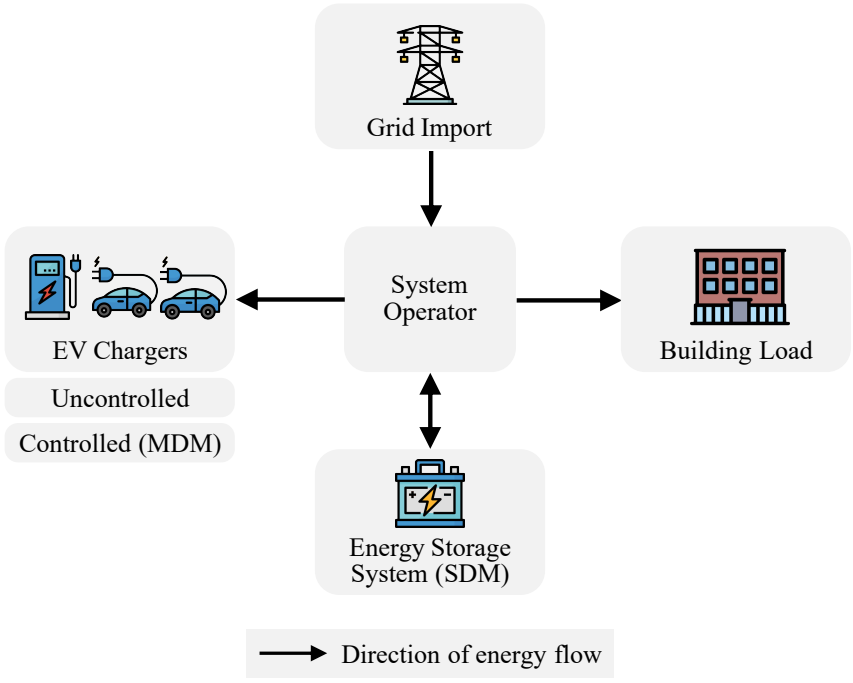

Figure 2.1: Illustration of an EV Charging Facility

to build. The system also minimizes the operation cost by finding the optimal schedule to import energy from the grid. The operation cost is reduced further by leveraging the ESS and charging flexibility, i.e. SDM and MDM.

The grid electricity import is subjected to the Time-of-Use (TOU) tariff and a constant demand charge. EV chargers are installed at a fixed rated power. EV chargers are assumed not to collect profit from charging EVs in this study to isolate the potential over-estimation of profit in the planning process. In other words, the facility is planned conservatively, not over-sizing for a potential charging demand that may lead to a large profit. An onsite ESS is installed and its capacity degradation is not considered. The EVs do not discharge their energy back to the facility. The facility does not export ESS energy to the grid.

2.3 Robust Sizing of an EV Charging Facility

From the system operator's perspective, the primary goal of an EV charging facility is to secure a high service quality by providing charging EVs as much as needed. However, excessive installation of EV chargers may result in the unnecessary expenditure of capital cost without enhancing the service quality. Therefore, it is important to estimate the level of EV charging demand and decide how much of the demand the charging facility must be designed for. In the following, we define the optimization variables and parameters, state

the statistical assumptions, and develop a robust optimization model to find the facility size, including the number of chargers and the battery size of local ESS.

Optimization Variables and Parameters

Recall that the system operator targets to minimize the capital and operation costs. Hence, the optimization variables are those that that affect the capital investment and the facility operations, colored in blue. The optimization variables include number of EV chargers n, number of ESS units to be installed b, charging power to aggregate EVs $P_{\mathrm{EV}}(\tau)$, ESS charging power $P_{\mathrm{B,C}}(\tau)$, ESS discharging power $P_{\mathrm{B,D}}(\tau)$, grid import power $P_{\mathrm{G,I}}(\tau)$, maximum of grid import power used for demand charge calculation $P_{\mathrm{G,D}}$, time-cumulative charging energy to EV aggregates $E_{\mathrm{EV}}(\tau)$, and energy level of ESS $E_{\mathrm{B}}(\tau)$.

The random parameters (colored in red and notated with *) are given, including the minimum charging power to EV aggregates $P^\star_{EV,\min}(\tau)$, the minimum time-cumulative charging energy to EV aggregates $E^\star_{EV,\min}(\tau)$, and the building load $P^\star_L(\tau)$. The deterministic parameters are given, such as costs (c_{EV}, c_B, $c_I(\tau)$, $c_{G,D}$), power efficiency (η_{EV}, $\eta_{B,C}$, $\eta_{B,D}$), ESS unit capacity ($E_{B,\max}$, $P_{B,\max}$), rated power of EV charger ($P_{EV,R}$, grid power limits ($P_{G,I,\max}$), ESS installment limits ($b_{\max}$), and levels of significance for statistics of random variables (α_{EV}, $\alpha_{G,l}$, $\alpha_{G,u}$).

Statistical Assumptions

We explain the statistical assumptions for the random parameters that will be used in the proposal of a robust sizing model. The random power demand from the building, $P^\star_L(\tau)$, is assumed to follow a normal distribution, defined independently for each time step τ.

$$P^\star_L(\tau) \sim \mathcal{N}(\overline{P_L(\tau)}, \sigma^2_{P_L}(\tau)) \qquad \forall\tau, \tag{2.1a}$$

$$P^\star_L(\tau_1) \perp P^\star_L(\tau_2) \qquad \forall\tau_1 \neq \tau_2. \tag{2.1b}$$

The random demands of EV charging power and energy, $P^\star_{EV,\min}(\tau)$ and $E^\star_{EV,\min}(\tau)$ respectively, are assumed to follow empirical distributions. Their cumulative distributions are defined respectively as $\mathcal{F}_{P,\tau}$ and $\mathcal{F}_{E,\tau}$, independently for each time step τ.

$$P^\star_{EV,\min}(\tau) \sim \mathcal{F}_{P,\tau}(z) = Pr(P^\star_{EV,\min}(\tau) \leq z) \qquad \forall\tau, \tag{2.2a}$$

$$E^\star_{EV,\min}(\tau) \sim \mathcal{F}_{E,\tau}(z) = Pr(E^\star_{EV,\min}(\tau) \leq z) \qquad \forall\tau, \tag{2.2b}$$

$$P^\star_{EV,\min}(\tau_1) \perp P^\star_{EV,\min}(\tau_2) \qquad \forall\tau_1, \neq \tau_2 \tag{2.2c}$$

$$E^\star_{EV,\min}(\tau_1) \perp E^\star_{EV,\min}(\tau_2) \qquad \forall\tau_1 \neq \tau_2. \tag{2.2d}$$

For simplicity, it is also assumed that $P^{\star}_{L}(\tau)$ is independent to the EV charging demand.

$$P^{\star}_{L}(\tau) \perp P^{\star}_{EV,\min}(\tau) \qquad \forall \tau, \tag{2.3}$$

$$P^{\star}_{L}(\tau) \perp E^{\star}_{EV,\min}(\tau) \qquad \forall \tau. \tag{2.4}$$

Model Derivation

We derive our robust planning model for an an EV charging facility in the following. We first describe the model with an objective function and constraints with uncertain variables, but this form is unsolvable. Therefore, we use the statistical distribution from the previous section to derive an expected value function for the objective function and second-order cone expressions for the constraints with uncertain variables. The final solvable model is given in Algorithm 1.

Objective Function

The objective of our sizing model is to minimize the expected value of the total cost, including the capital cost of EV chargers and ESS and the operation cost, such as electricity cost and demand charge. The cost is calculated in terms of a daily cost. The demand charge is calculated base on the maximum power over 15-minute period. For simplicity, no interest or present value is considered. Formally:

$$J = c_B b + c_{EV} n \tag{2.5a}$$

$$+ \sum_{\tau=1}^{T} [c_I(\tau) P_{G,I}(\tau)] dt \tag{2.5b}$$

$$+ c_{G,D} P_{G,D}, \tag{2.5c}$$

where (2.5a) represents the capital cost for EV charger and ESS installations, (2.5b) for grid import cost, and (2.5c) for demand charge cost.

Constraints and Reformulations

The objective function J in (2.5) is linear with respect to the decision variables (b, n, $P_{G,I}(\tau)$, $P_{G,D}$). However, the grid import power $P_{G,I}(\tau)$ is coupled with the building load $P^{\star}_{L}(\tau)$ (which is a random parameter) due to the power balance between supply and demand. The power balance equation can be expressed as:

$$P_{B,D}(\tau) + P_{G,I}(\tau) = P^{\star}_{L}(\tau) + P_{B,C}(\tau) + P_{EV}(\tau), \tag{2.6}$$

where the left hand side shows the power supply from the ESS discharging and the grid import, and the right hand side shows the power demand from the building load, the ESS

charging, and the EV charging. The objective function (2.5) remains mathematically intractable, due to its coupling to the power balance (2.6) with stochasticity.

The grid import $P_{G,I}$ is lower and upper bounded by its physical limitation by $[0, P_{G,I,\max}]$:

$$0 \leq P_{G,I}(\tau) \leq P_{G,I,\max}, \tag{2.7}$$

but this constraint is also intractable due to its coupling to the power balance (2.6) in the current form.

Therefore, we reformulate the power balance (2.6) and the coupled equations (2.5) and (2.7) to make them tractable. We use the chance-constraint method in [42], given the statistical distributions of random parameters described in Section 2.3. We denote level of confidence on the grid import $P_{G,I}(\tau)$ as $\alpha_{G,l}$ for the lower bound and $\alpha_{G,u}$ for the upper bound. The level of confidence values represent the probability that the grid import power is above 0kW and below the grid capacity of $P_{G,I,\max}$, respectively. Note that due to the coupling of grid import power $P_{G,I}(\tau)$ to EV charging power $P_{\mathrm{EV}(\tau)}$ shown in (2.6), the EV charging power $P_{\mathrm{EV}(\tau)}$ can be limited by the grid capacity, $P_{G,I,\max}$.

The normal distribution of $P_L^\star(\tau)$ is transformed into a cumulative standard normal distribution, Φ. Re-expressing (2.6) in terms of $P_{G,I}(\tau)$ and taking the upper and lower statistical bounds using the level of significance gives (2.8) and (2.9).

$$\Phi^{-1}(\alpha_{G,l}) \cdot \sqrt{\sigma^2_{P_L}(\tau)} \leq P_{B,C}(\tau) + P_{EV}(\tau) + P_{G,E}(\tau) - P_{B,D}(\tau) + \overline{P_L}(\tau), \tag{2.8}$$

$$\Phi^{-1}(\alpha_{G,u}) \cdot \sqrt{\sigma^2_{P_L}(\tau)} \leq P_{G,I,\max} - P_{B,C}(\tau) - P_{EV}(\tau) - P_{G,E}(\tau) + P_{B,D}(\tau) - \overline{P_L}(\tau). \tag{2.9}$$

The objective function takes an expected total cost, by taking the expected value of grid import $P_{G,I}(\tau)$ in (2.6):

$$\begin{aligned} J =& c_B \cdot b + c_{EV} \cdot n \\ &+ \sum_{\tau=1}^{T} c_I(\tau)[P_{B,C}(\tau) + P_{EV}(\tau) + P_{G,E}(\tau) - P_{B,D}(\tau) + \overline{P_L}(\tau)]dt \\ &+ c_{G,D} \cdot P_{G,D}. \end{aligned} \tag{2.10}$$

In addition to the power balance in (2.8) and (2.9), constraints on the power dynamics, capacity limitation, and sizing variables are formulated:

$$E_B(\tau+1) = E_B(\tau) + \left[\eta_{B,C} \cdot P_{B,C}(\tau) - \frac{1}{\eta_{B,D}} P_{B,D}(\tau)\right]dt, \tag{2.11}$$

$$E_B(0) = \beta_{B,i}[bE_{B,\max}], \tag{2.12}$$

$$E_B(T) = E_B(0), \tag{2.13}$$

$$0 \leq E_B(\tau) \leq b \cdot E_{B,\max}, \tag{2.14}$$

$$0 \leq P_{B,C}(\tau) \leq b \cdot P_{B,\max}, \tag{2.15}$$

$$0 \leq P_{B,D}(\tau) \leq b \cdot P_{B,\max}, \tag{2.16}$$

where (2.11) describes the power dynamics of ESS units with efficiency factors for charging and discharging. Equation (2.12) and (2.13) define the boundary conditions to avoid a myopic use of ESS units in the optimization. Equation (2.14), (2.15) and (2.16) describe the energy capacity, charging power capacity, and discharging power capacity of ESS units respectively, in terms of the ESS sizing variable, b. Note we assume a fixed ratio between power capacity and energy capacity of ESS. The optimization variable b scales power and energy capacity relative to nominal values, while keeping the energy-to-power ratio fixed.

For the EV charging dynamics, we consider cumulative energy consumption as a linear function of charging power:

$$E_{EV}(\tau+1) = E_{EV}(\tau) + dt[\eta_{EV} \cdot P_{EV}(\tau)]. \tag{2.17}$$

Other constraints for EV charging are formulated as:

$$E_{EV}(0) = 0, \tag{2.18}$$
$$P^{\star}_{\mathrm{EV,min}}(\tau) \leq \eta_{\mathrm{EV}} P_{\mathrm{EV}}(\tau), \tag{2.19}$$
$$E^{\star}_{\mathrm{EV,min}}(\tau) \leq E_{\mathrm{EV}}(\tau), \tag{2.20}$$
$$0 \leq P_{\mathrm{EV}}(\tau) \leq n \cdot P_{\mathrm{EV,R}}, \tag{2.21}$$

where (2.18) sets the initial cumulative energy zero, (2.19) and (2.20) guarantee sufficient charging supply for the demand and (2.21) constraints the number of EV chargers n to meet the necessary EV charging power capacity. The parameter $P_{\mathrm{EV,R}}$ in (2.21) can be various charging powers, such as low-level chargers to fast chargers, expanding the range of charger types to be considered in the planning. Note, the random variables $P^{\star}_{EV,\mathrm{min}}(\tau)$ and $E^{\star}_{EV,\mathrm{min}}(\tau)$ make (2.19) and (2.20) difficult to solve. Therefore, we reformulate these equations as chance constraints.

With the empirical distributions (2.2a) and (2.2b), we can choose a level of significance to represent probable values of charging power and energy demands. At a level of significance $\alpha_{EV,\mathrm{lower}}$, the power and energy demands can be expressed as $\mathcal{F}^{-1}_{P,\tau}(\tau)(\alpha_{EV})$ and $\mathcal{F}^{-1}_{E,\tau}(\tau)(\alpha_{EV})$ respectively. We plan the facility to guarantee such demands, by constraining the lower bounds of power and energy delivery $P_{EV}(\tau)$ and $E_{EV}(\tau)$. Therefore, (2.19) and (2.20) can be replaced by (2.22) and (2.23), respectively. These constraints, together with (2.17) and (2.21), require the number of EV chargers to achieve a robust capacity to the random demand at a percentile of $\alpha_{EV,\mathrm{lower}}$.Note that (2.22) enforces the model to plan enough EV chargers to satisfy the EV charging demand at α_{EV}-th percentile all hours τ.

$$\mathcal{F}^{-1}_{P,\tau}(\tau)(\alpha_{EV}) \leq \eta_{EV} \cdot P_{EV}(\tau), \tag{2.22}$$
$$\mathcal{F}^{-1}_{E,\tau}(\tau)(\alpha_{EV}) \leq E_{EV}(\tau). \tag{2.23}$$

The power value to calculate the demand charge cost is given in (2.24). As the objective function considers an expected value of demand charge cost, (2.24) is similarly modified as (2.25) without the variable $P_{G,I}(\tau)$.

$$P_{G,D} \geq P_{G,I}(\tau), \tag{2.24}$$
$$P_{G,D} \geq P_{B,C}(\tau) + P_{EV}(\tau) + P_{G,E}(\tau) - P_{B,D}(\tau) + \overline{P_L}(\tau). \tag{2.25}$$

We consider a maximum limit for the ESS units to be built with a given parameter $b_{\max}$ as (2.26). The facility planner may use this parameter $b_{\max}$ to reflect the physical constraints for the ESS installment and the facility operator's preference.

$$0 \leq b \leq b_{\max}. \tag{2.26}$$

Complete Formulation

The final model for robust sizing of an EV charging facility is organized in Algorithm 1 for all $\tau = [1, ..., T]$. The number of EV chargers is a non-negative integer as (2.27) and (2.28). The proposed robust sizing in Algorithm 1 is a convex problem of Integer and Second-Order Cone Programming. The solution guarantees an optimal solution, if feasible.

Algorithm 1: Robust Sizing Model

Minimize (2.10),

Subject to (2.8), (2.9), (2.11), (2.12), (2.13), (2.14), (2.15), (2.16), (2.17), (2.18), (2.21), (2.22), (2.23), (2.25), (2.26),

$$0 \leq n, \tag{2.27}$$
$$n \in \mathbb{Z}. \tag{2.28}$$

2.4 Methodology

In this section, we describe how we evaluate the proposed sizing model for a robust EV charging facility. Supplementary models for this evaluation are provided, such as a baseline sizing model and the simulation model for the facility's operation. We also describe how we conduct the sensitivity analysis of energy demand management on the facility performance, giving us a clue how to overcome the trade-off between the cost and quality of service. We explain how the Mobile and Stationary Demand Management strategies are implemented and analyzed.

Performance of the Robust Sizing Model

The proposed robust sizing model is evaluated in comparison to a baseline sizing model that optimizes based on the expected values of random parameters. Since it is impractical to test the performance of sizing models in the field, a simulation model is used to emulate the daily operation of the facility. For brevity, a facility planned by the proposed robust model and the baseline model are termed 'robust facility' and 'baseline facility', respectively. The metrics on cost and quality of service evaluate the performance of robust and baseline facilities. The results are cross-validated with 100 random samples of EV charging demand. In addition, sample trajectories of power and energy in the robust and baseline facilities are presented for detailed discussion.

We describe in the following the baseline sizing model, the operation simulation model, the performance metrics of an optimized facility, and the cross-validation process to compare between the robust and baseline sizing models.

Baseline Sizing Model

Algorithm 2 describes the baseline sizing model, which uses the expected values of the random parameters. This model is inspired by the work in [43], which considers the operation scenarios to plan a facility, for example the input data for energy use will take 3-day samples each month. This model is applied in the open-source program, called Distributed Energy Resources Customer Adoption Model (DER-CAM) from Lawrence Berkeley Lab. The building power demand $P^{\star}_{L}(\tau)$, minimum EV charging power $E^{\star}_{EV,\min}(\tau)$, and minimum EV charging energy $P^{\star}_{EV,\min}(\tau)$ are represented with their average values with $\overline{P_L}(\tau)$, $\mathcal{F}^{-1}_{P,\tau}(\tau)(\alpha_{EV}=0.5)$, and $\mathcal{F}^{-1}_{E,\tau}(\tau)(\alpha_{EV}=0.5)$, respectively. The algorithm is expressed for all $\tau=[1,...,T]$. The proposed baseline sizing in Algorithm 2 is a convex problem of Linear Integer Programming. The solution guarantees an optimal solution, if feasible.

Algorithm 2: Baseline Sizing Model

Minimize (2.5),

Subject to (2.11), (2.7), (2.12), (2.13), (2.14), (2.15), (2.16), (2.17), (2.18), (2.21), (2.24), (2.26), (2.27), (2.28),

$$P_{B,D}(\tau)+P_{G,I}(\tau)=\overline{P_L}(\tau)+P_{B,C}(\tau)+P_{EV}(\tau), \quad (2.29)$$

$$\mathcal{F}^{-1}_{P,\tau}(\tau)(\alpha_{EV}=0.5)\leq \eta_{EV}\cdot P_{EV}(\tau), \quad (2.30)$$

$$\mathcal{F}^{-1}_{E,\tau}(\tau)(\alpha_{EV}=0.5)\leq E_{EV}(\tau). \quad (2.31)$$

Operation Simulation Model

Algorithm 3 describes the simulation model for an EV charging facility's operation. Given the ESS units and the number of EV chargers, b_{opt}, n_{opt}, the total daily cost is minimized by controlling the operation variables for each day in the testing data set. The facility supplies EV charging demand as much as the charging capacity allows without a cost-minimizing behavior. When the demand exceeds the charging capacity, the EV charging demand is unsatisfied and lost without queuing. The proposed baseline sizing in Algorithm 3 is a convex problem of Linear Integer Programming. The solution guarantees an optimal solution, if feasible.

Algorithm 3: Daily Operation Simulation Model

$$\textbf{Minimize} \quad c_B \cdot b_{\text{opt}} + c_{EV} \cdot n_{\text{opt}} + \sum_{\tau=1}^{T} dt[c_I(\tau) \cdot P_{G,I}(\tau)] + c_{G,D} \cdot P_{G,D}, \tag{2.32}$$

$$\begin{aligned}
\textbf{Subject to} \quad & (2.7), (2.11), (2.13), (2.17), (2.18), (2.24), && (2.33)\\
& P_{B,D}(\tau) + P_{G,I}(\tau) = P_{L,\text{test},j}(\tau) + P_{B,C}(\tau) + P_{EV}(\tau), && (2.34)\\
& E_B(i,0) = \beta_{B,i}[b_{\text{opt}} \cdot E_{B,\max}], && (2.35)\\
& 0 \le E_B(\tau) \le b_{\text{opt}} \cdot E_{B,\max}, && (2.36)\\
& 0 \le P_{B,C}(\tau) \le b_{\text{opt}} \cdot P_{B,\max}, && (2.37)\\
& 0 \le P_{B,D}(\tau) \le b_{\text{opt}} \cdot P_{B,\max}, && (2.38)\\
& P_{EV}(\tau) = \min(\eta_{EV}^{-1} \cdot P_{EV,test,j}(\tau), n_{\text{opt}} \cdot P_{EV,R}). && (2.39)
\end{aligned}$$

Cross-Validation Process

The robust and baseline facilities are compared with cross-validation. The total dates of EV charging demand data are randomly split into a sizing set (training) and a simulation set (testing) in a 7:3 ratio, 100 times. For each training set, empirical distributions of the EV charging demand is calibrated, i.e. (2.2a) and (2.2b). The robust and baseline models use these distributions to find the optimal sizing of the facility. The charging demand of multiple dates in the testing sets are used to simulate the robust facility and the baseline facility. Algorithm 4 gives a pseudo-code for the cross-validation of robust and baseline sizing. Note that for cross-validation, the maximum ESS units is set as $b_{\max} = 2$.

Algorithm 4: Cross-Validation of Robust and Baseline Sizing Models

Result: Power and Energy Trajectories of Simulated Operation, Total Daily Costs, and QoS values

for $i = 0;\ i < N_{cross};\ i = i + 1$ **do**
  Optimize a robust facility with Algorithm 1 as sample i ;
  Optimize an baseline facility with Algorithm 2 as sample i ;
  for $j = 0;\ j < N_{test};\ j = j + 1$ **do**
    Simulate the robust facility for date j with Algorithm 3 ;
    Simulate the baseline facility for date j with Algorithm 3 ;
  end
  Evaluate the robust facility of sample i with (2.42) and (2.43) ;
  Evaluate the baseline facility of sample i with (2.42) and (2.43) ;
end

Performance Metrics

From the operation simulation results, the facility performance is evaluated on the daily operation cost, daily capital cost, total daily cost and the quality of service in charging EVs as f_{OC} (\$/day), f_{CC} (\$/day), f_{TC} (\$/day) and f_{QoS} (kW), given in (2.40), (2.41), (2.42) and (2.43), respectively.

$$f_{\text{OC}} = \frac{1}{N_{\text{test}}} \sum_{j=1}^{N_{\text{test}}} \left[\sum_{\tau=1}^{T} c_I(\tau) P_{G,I,j}(\tau) dt + c_{G,D} P_{G,D,j} \right], \tag{2.40}$$

$$f_{\text{CC}} = \frac{1}{N_{\text{test}}} \sum_{j=1}^{N_{\text{test}}} \left[c_B b_{\text{opt}} + c_{EV} n_{\text{opt}} \right], \tag{2.41}$$

$$f_{\text{TC}} = f_{\text{OC}} + f_{\text{CC}}. \tag{2.42}$$

Equation (2.42) calculates the average daily cost, including the capital cost, electricity cost and demand charge cost, over the simulated dates in the testing set.

$$f_{\text{QoS}} = \frac{1}{N_{\text{test}}} \sum_{j=1}^{N_{\text{test}}} \left[1 - \frac{\max\limits_{\tau \in [1,T]} [P_{EV,\text{test},j}(\tau) - P_{EV,j}(\tau)]}{\max\limits_{\tau \in [1,T]} [P_{EV,\text{test},j}(\tau)]} \right]. \tag{2.43}$$

Equation (2.43) for f_{QoS} calculates the quality of service, by measuring how much charging power is not satisfied by the facility's physical capacity. Since the EV charging demand can fluctuate largely throughout the day, it is crucial for the metric to capture the unsatisfied

demand at its maximum. Equation (2.43) uses time variables, simulation date $j \in [1, N_{\text{test}}]$ and hour $\tau \in [1, T]$ for each date j. The fraction expression has two maximum expressions. The maximum expression in denominator finds the maximum power demand in charging over all τin j, i.e. the hourly peak power demand of the date j. The maximum expression in the numerator finds the maximum unsatisfied power demand in charging over hours all τ in date j, i.e. the largest difference between the demand and supply of charging power during the day. Therefore, the fraction evaluates the ratio of the maximum unsatisfied power to the maximum charging demand. By subtracting 1 by this fraction, the expression inside the sum measures the satisfaction of charging demand, i.e. the quality of service. The measurements are averaged over all j.

Sensitivity Analysis on Demand Management

We explore the energy demand management strategies to reduce the facility cost (especially the demand charge cost), while maintaining a level of service quality. Traditionally, the utility companies impose a demand charge cost on the customers to reduce the demand peaks, economize their grid operations, and improve the grid service quality. However, the EV charging demand can surge during the day [44] without consideration to the power peaks in grid import because the demand charge is not internalized to the EV drivers. Therefore, we target to manage the peak in grid import and reduce the cost. In the following, we describe the two strategies for demand management to experiment in this chapter.

Stationary Demand Management (SDM)

Stationary Demand Management (SDM) installs ESS units that decouple the facility's energy demand peak and the grid import peak. Regardless of the energy demand, the ESS units can store energy from the grid when it is cheap and flexibly discharge it to supply the demand. The facility can use the stored energy instead of grid import energy during the demand peak and reduce the demand charge cost. The effect of SDM is observed by comparing different maximum limits for the ESS, $b_{\max} = [2, 10]$

Mobile Demand Management (MDM)

Mobile Demand Management (MDM) flattens the peak of total EV charging demand by rescheduling the individual charging sessions. This can achieve a similar effect of the grid network flattening the demand peak with the demand charge ,i.e. the facility can reduce the operation cost from power surge and avoid building an excessive charging capacity. [45].

We use a heuristic model to reschedule individual EV's charging demand. When a subject EV arrives at the charging facility, its charging session is scheduled based on its known departure time, charging power, energy demand, and the current total demand on charging power at the facility. The charging demand of other EVs in the future is assumed unknown. The subject EV is scheduled to charge when the current total demand so far is the smallest

within its parking duration, but it is scheduled to charge its desired energy by its departure. The total demand accumulates with this decision. Once a vehicle starts charging, there is no break in charging within the charging session. The power demand with MDM is the total charging demand after rescheduling for all EVs that arrive at the facility in a day, notated as $P^{\star}_{EV,min,MDM}(\tau)$. This is integrated and cumulatively summed to produce the cumulative energy demand, $E^{\star}_{EV,min,MDM}(\tau)$. Note that only the EV charging demand is rescheduled, not the building energy demand. The effect of MDM is observed by comparing different EV charging demands, i.e. $[P^{\star}_{EV,\text{min}}, E^{\star}_{EV,\text{min}}]$ or $[P^{\star}_{EV,min,MDM}, E^{\star}_{EV,min,MDM}]$.

Sensitivity Analysis

To evaluate the effect of SDM and MDM on facility sizing performance, three parameters are explored as a sensitivity analysis. First is the maximum ESS units allowed to build, which helps evaluate the effect of SDM, $b_{\text{max}} = [2, 10]$. Second is the EV charging demands for MDM, $[P^{\star}_{EV,\text{min}}, E^{\star}_{EV,\text{min}}]$ or $[P^{\star}_{EV,min,MDM}, E^{\star}_{EV,min,MDM}]$, which helps evaluate the effect of MDM. Third is the level of significance in EV charging demand, $\alpha_{EV} = [0.05, 0.10, ..., 0.90, 0.95]$, which results in different qualities of service in charging EVs. The resulting facility sizing is evaluated via the operation simulation in Algorithm 3 with a high level of EV charging demand at 95th percentile.

2.5 Data

We consider a workplace EV charging facility. We use real-world data on workplace EV charging demand, office building energy demand, and electricity tariff for businesses. We describe the data in the following and other parameters are provided in the Nomenclature.

EV Charging Demand

The EV charging demand is represented by the Adaptive Charging Network data from January 1st 2019 to September 9th 2019, collected from the California Institute of Technology (CalTech) campus garage in Pasadena, California [46]. The data describes individual EVs in terms of their time of connection and disconnection to the charger and the total energy delivered. We process the data to aggregate the total power and cumulative energy delivered to the EVs in 15-min increments with an assumption of constant charging power. From this original demand, rescheduled charging demand with MDM is produced.

Figure 2.2 shows the original data and the rescheduled data with MDM in terms of the aggregate power at 15-min intervals. Each line represents each date in the sample. We observe that MDM reduced the peak of power demand with a flatter trend throughout the day. The MDM algorithm does not change the total energy demand.

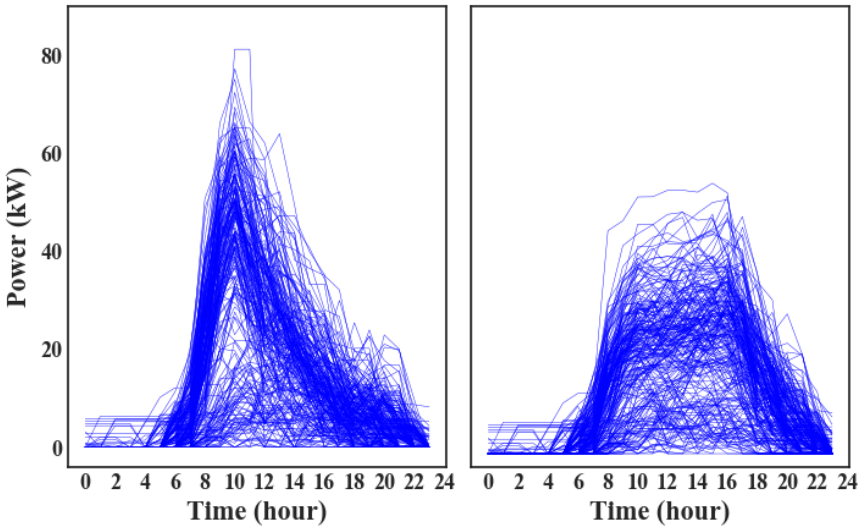

(a) Original Demand (b) Demand with MDM

Figure 2.2: EV Charging Demand Trajectories for Sample Dates (California Institute of Technology (CalTech) Campus Garage in Pasadena, California, from 2019/1/1 to 2019/9/9): the left plot shows the original demand and the right plot shows the result from mobile demand management on the original demand

Building Energy Demand

The building energy demand is represented by the data from Lawrence Berkeley Lab Building 74 in California from January 1st to September 9th, 2014 [47]. Figure 2.3 shows the mean daily power use plus and minus one standard deviation.

Electricity Cost

We consider a Time-of-Use energy tariff and a demand charge on peak power. The Time-of-Use energy tariff, $c_I(\tau)$ (USD/kWh), is represented by the rates for businesses in summer from PG&E in California as shown in Fig. 2.4 [48]. The demand charge is assumed as a constant, $c_{G,D} = 19.0$ USD/kW per month.

2.6 Results

In this section, we evaluate the performance of the robust sizing model compared to the baseline sizing model. The results show that the robust facility produces a higher quality of service than the baseline facility, but incurs in a larger cost due to constructing and operating a larger charging capacity. To overcome this trade-off, we analyze how demand management

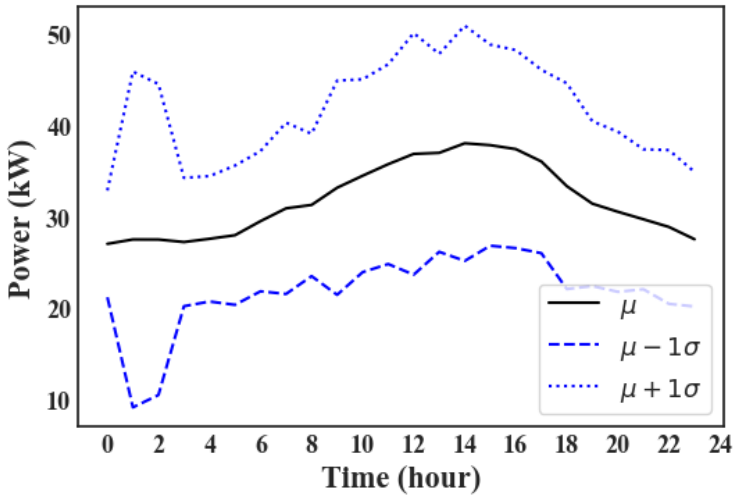

Figure 2.3: Building Energy Demand from Sample Dates (Lawrence Berkeley Lab Building 74, California, from 2014/1/1 to 2014/9/9): μ denotes the mean value and σ denotes the standard deviation

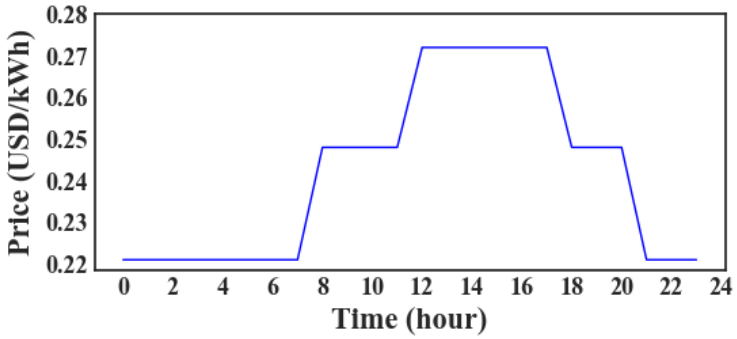

Figure 2.4: Time-of-Use Electricity Price

strategies impact the planning and operation of an EV charging facility. The results show that when Stationary and Mobile Demand Managements are applied to a robust facility, it overcomes the trade-off and achieves a higher quality of service at a lower cost, compared to a robust facility without these strategies.

Performance of the Robust Sizing Model

Table 2.1 shows the sizing and operation results of the robust and baseline sizing models, averaged over the cross validation sample of size $N_{\text{cross}} = 100$. The robust facility builds more chargers (shown with n_{opt}) than the baseline facility, ensuring a larger capacity to supply

Table 2.1: Cross Validation Results of Optimal Sizing and Operation Simulation (Note f_{OC}, f_{CC}, and f_{CC} are in units of ($/day))

Model	Average over N_{cross} samples					
	n_{opt}	b_{opt}	f_{OC}	f_{CC}	f_{TC}	f_{QoS}
Robust	31.5	2	257.1	7.0	264.1	0.9963
Baseline	20.5	2	254.0	4.6	258.6	0.9054

the random EV charging demand. For both robust and baseline facilities, the ESS units are planned at the maximum limit, $b_{\text{opt}} = b_{\max} = 2$, because ESS units facilitate flexible grid import and reduce cost. The robust facility has a larger operation cost than the baseline facility because more chargers satisfy more demand, importing more energy for the EVs. With the capital cost of a larger facility, the robust facility has a larger total cost (shown with f_{TC} computed in (2.42)) than the baseline facility. However, we observe that the daily operation cost (shown with f_{OC}) is much larger than the daily capital cost (shown with f_{CC}). In other words, operation is the major component (above 95 %) of the total cost. This validates the need to economize the facility operation, as we will achieve with SDM and MDM in the following section.

The quality of service in charging EVs, f_{QoS}, is larger in the robust facility than the baseline facility. Therefore, f_{QoS} of the robust facility is around 9% higher than that of the baseline facility. To visualize why this occurs, please refer to Fig. 2.5 with sample trajectories of power and energy during simulated operation. The left column shows the robust facility and the right column shows the baseline facility. The top figures show that the robust facility satisfies most of the EV charging demand, whereas the baseline facility cannot satisfy some EV demand due to its limited charging capacity (around 40kW).

Note that the operation simulation does not allow charging demand to queue, i.e. when demand cannot be served immediately, then it is considered lost. So the charging demand in the baseline facility becomes unsatisfied; as shown with unsatisfied cumulative energy indicated by the gap between the two curves in the right middle figure of Fig. 2.5. Therefore, f_{QoS} of the baseline facility is often lower than that of the robust facility, as shown in Fig. 2.6.

The trade-off between quality of service and increasing cost is illustrated by the bottom row in Fig. 2.5. If a small capacity ESS is installed, then both facilities have no choice but to import grid power following the peak of EV charging demand, indicated by $P_{G,I,j}(\tau)$. However the grid import peaks higher for the robust facility than the baseline facility, resulting in a larger demand charge on top of the larger energy cost. Moreover, we realize that the peak charging demand only lasts a short period of time. This means that for the robust facility, much of the charging capacity is not used most of the day. Instead of supplying energy simply as demanded, if the facility can be proactive in managing the demand and make the planning and operation more economical, the trade-off with increasing cost may be reduced. The next section analyzes the impact of demand management strategies on an

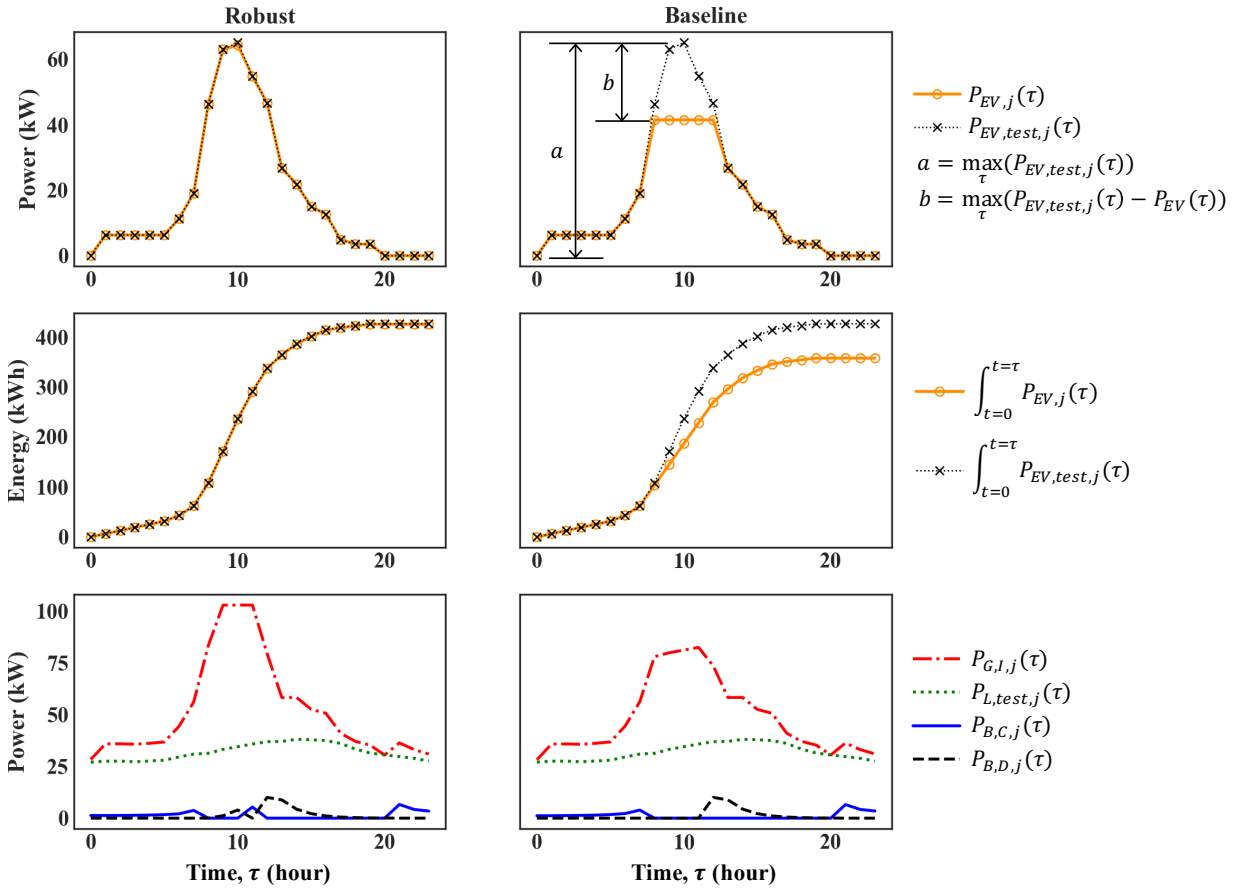

Figure 2.5: Sample Trajectory of EV Charging Operation with Robust and Baseline Sizing (Note: $f_{\text{QoS}} = \sum_{j=1}^{N_{\text{test}}}[1 - \frac{b}{a}]$)

EV charging facility.

Sensitivity Analysis on Demand Management

Figure 2.7 presents how a robust facility with demand management strategies perform better than a facility without strategies, in terms of both the cost and quality of service. The total cost as f_{TC} is on the x-axis and the quality of service as f_{QoS} on the y-axis. Four scenarios of demand management are evaluated. "None" indicates the scenario with original EV charging demand and the maximum ESS units allowed to be built as $b_{\max} = 2$. "MDM" indicates the scenario with rescheduled EV charging sessions (therefore with flattened charging demand as in the right figure of Fig. 2.2). "SDM" indicates the scenario with a larger maximum ESS units allowed to be built as $b_{\max} = 10$. "MDM and SDM" indicates the scenario with both rescheduled EV charging sessions and a larger maximum ESS size allowed to be built. Each

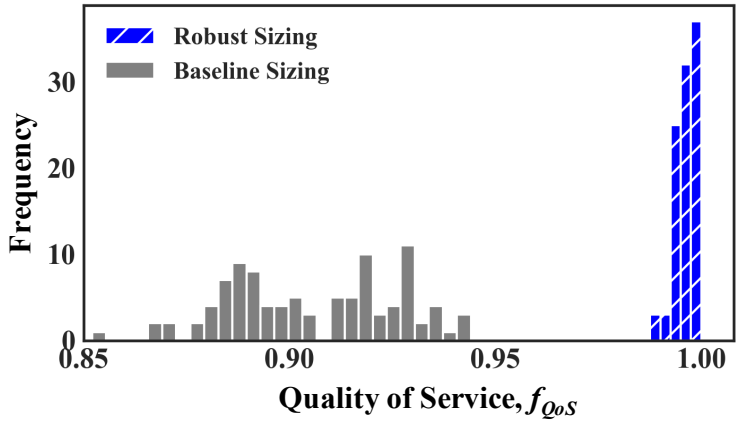

Figure 2.6: Quality of Service (Cross-Validation of 100 samples with unique demand scenarios)

data point shows the results of varying levels of significance, α_{EV}. A facility sized with a smaller α_{EV} (from (2.22) and (2.23)) yields a smaller f_{QoS}, so the left-most point in each scenario is the result with $\alpha_{EV} = 0.05$ and the right-most point is the result with $\alpha_{EV} = 0.95$. Note the result with $\alpha_{EV} = 0.5$ with scenario "None" is approximates of the baseline sizing model in Table 2.1, which is based on average values of EV charging demand. The result with $\alpha_{\text{EV}} = 0.95$ in scenario "None" corresponds to the robust sizing result in Table 2.1.

First from the graph we notice that the facility improves the quality of service with a larger cost. Moreover, increasing the cost has an increasing marginal return on the quality of service, i.e. the quality of service improves at an increasing rate as the cost increases. This means that the trade-off between the cost and quality of service is in the favor to build a larger facility. Second, a facility implemented with both MDM and SDM achieves the highest quality of service at a given cost, i.e. the "MDM and SDM" scenario has Pareto optimality to any other scenario in terms of cost and quality of service. Implementing no demand management has the poorest quality of service at a given cost. It is interesting that at a high service quality, the SDM scenario and MDM scenario have similar costs and service qualities. This means that the system operator may choose any of the two strategies to enjoy a similar cost reduction at high service quality. When it is difficult to reschedule EV charging sessions due to issues in driver compliance [49] and uncertain mobility demands, a larger ESS can be installed to result in a similar cost reduction. The capital investment of ESS (SDM) poses a solution to potential issues in operational investment of rescheduling EV charging (MDM). Also, if it is challenging to install ESS units (SDM) for instance due to limited physical space, rescheduling EV charging (MDM) can result in a similar cost reduction.

In addition to the finding above, Figure 2.7 also exemplifies how the proposed algorithm can help the facility planner to finalize the facility size by selecting the level of significance in charging demand α_{EV}. With the figure's visualization of facility performance, the facility

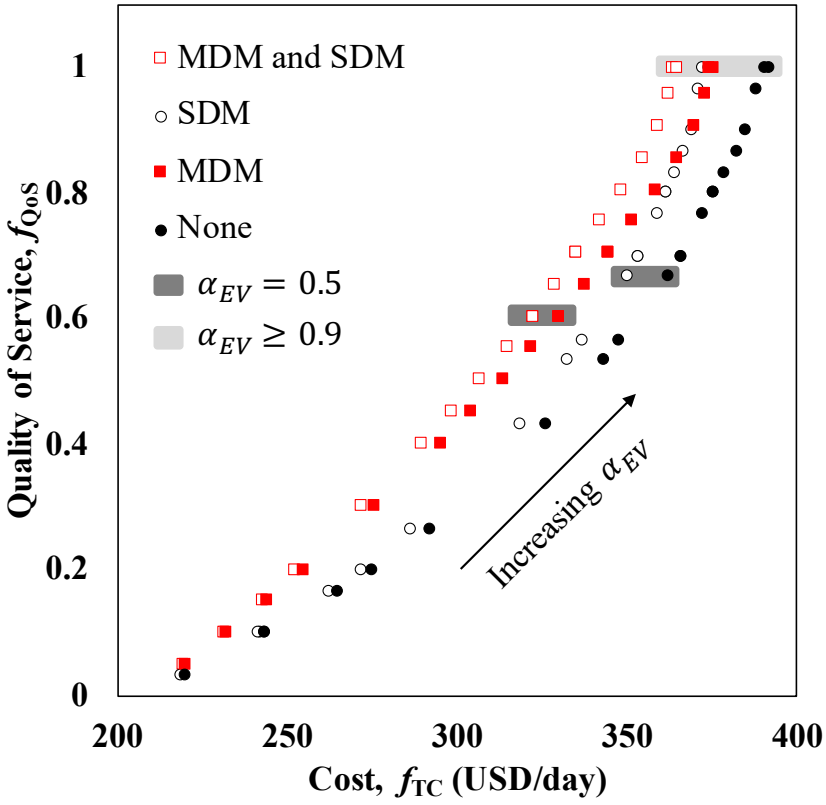

Figure 2.7: Pareto Curves of Cost and Quality of Service

operator can choose the level of significance that best suits her business needs. For instance, it is possible that a charging facility is in high competition with neighboring facilities and the operator desires an expensive but a high-quality facility. The facility operator may choose a sizing result with a high level of significance that corresponds to a desired level of service quality and cost.

Also, we see that the finding from Section 2.6 agrees with the results in Fig.2.7, i.e., a robust facility builds a larger charging capacity, increasing the quality of service and the cost. Please refer to Table 2.2, which supplements Fig.2.7. For each demand-management scenario, the robust sizing with $\alpha_{\text{EV}} = 0.95$ results in more chargers and larger f_{QoS} and f_{TC} than the baseline sizing approximated with $\alpha_{\text{EV}} = 0.5$. Therefore, Fig.2.7 show the results with $\alpha_{\text{EV}} = 0.95$ to be higher in f_{QoS} and f_{TC} than the results with $\alpha_{\text{EV}} = 0.5$ in Fig.2.7. Note that for all scenarios and sizing models, the optimal solutions produce the ESS units to be built at the maximum limit, $b_{\text{opt}} = b_{\text{max}}$, where $b_{\text{max}} = 2$ for cases without SDM and $b_{\text{max}} = 10$ for cases with SDM.

Table 2.2: Baseline and Robust Sizing Results with Stationary and Mobile Demand Management Strategies

Item	Sizing [1]	Demand Management Scenario			
		None	MDM	SDM	MDM and SDM
n_{opt}	B	21	12	21	12
	R	32	21	32	21
b_{opt} [2]	B	2	2	10	10
	R	2	2	10	10
f_{QoS}	B	0.7	0.6	0.7	0.6
	R	1.0	1.0	1.0	1.0
f_{TC} (\$/day)	B	365.5	329.5	352.8	321.8
	R	390.0	373.9	372.4	362.9

To further explore how SDM and MDM reduce the cost, sample power trajectories over a day are analyzed; refer to Fig. 2.8. The four columns show the trajectories for the scenarios of "None", "SDM", "MDM", and "SDM and MDM" as explained above, respectively. The top figures show the input data of EV charging demand for planning, indicated by $P_{EV,test,j}(\tau)$. For scenarios with MDM, the charging demand has a reduced peak power but same total energy. Since this figure shows robust facilities planned with $\alpha_{\text{EV}} = 0.95$, almost all EV charging demands are met, indicated by coinciding lines of $P_{EV,test,j}(\tau)$ and $P_{EV,j}(\tau)$. The bottom figures show trajectories of operation power.

Compared to the scenarios without any demand management ("None"), both SDM and MDM similarly reduce the peak of grid import power (shown with $P_{G,I,j}(\tau)$). The scenario with SDM shows that the grid import peak is reduced by discharging the ESS, shown with $P_{B,D,j}(\tau)$. The scenario with MDM shows that the grid import peak is reduced by flattening the peak of EV charging demand, shown shown with $P_{EV,test,j}(\tau)$ on the top. Although the total energy of grid import is the same, both SDM and MDM reduce the demand charge by reducing the peak power import from the grid. Moreover, both SDM and MDM avoid high Time-of-Use tariff and reduce the energy cost by discharging the ESS energy or removing the charging sessions, respectively. Although SDM and MDM use inherently different mechanisms, they both reduce demand charge and energy cost and result in similar cost reductions as seen in Fig. 2.7. Note that the last column in Fig. 2.8 shows that implementing both

[1] B: Baseline sizing approximated with $\alpha_{EV} = 0.5$, R: Robust sizing with $\alpha_{EV} = 0.95$

[2] The optimal solutions produce b_{opt} at the maximum limit, $b_{\max}$ for all results, i.e., ($b_{\max} = 2$ without SDM and $b_{\max} = 10$ with SDM)

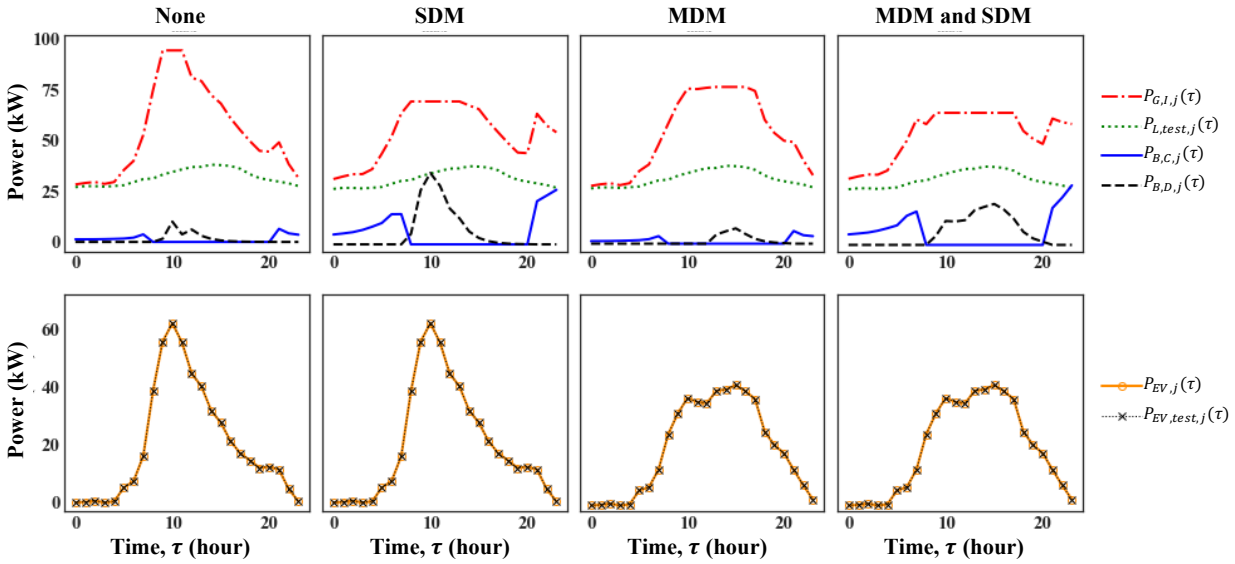

Figure 2.8: Sample Operation Trajectory with Mobile and Stationary Demand Management ($\alpha_{EV} = 0.95$)

SDM and MDM decreases the grid import peak the most, reducing the cost the most.

In addition, we find that a facility with MDM uses the chargers more efficiently than without MDM, which is intuitive as they satisfy the charging demand with less number of chargers. Fig. 2.9 shows sample trajectories of the charging capacity sitting idle without charging EVs as $P_{\text{idle}}(\tau) = n_{\text{opt}} P_{\text{EV,R}} - P_{\text{EV}}(\tau)$. The solid line is the idle capacity without MDM ("None") and the dotted line shows one with MDM. The facility without MDM has a larger charging capacity (74.56kW $= P_{\text{EV,R}} \cdot 32$ chargers) than a facility without MDM (48.93kW $= P_{\text{EV,R}} \cdot 21$ chargers), where we assumed $P_{\text{EV,R}} = 2.33kW$. However, the facility without MDM uses its capacity only for a short period of time and most capacity is idle for a longer period of time, compared to the facility with MDM.

2.7 Conclusion

To increase the market adoption of electric vehicles, it is critical to plan an EV charging facility that provides energy to EVs at a low cost with high quality of service. An EV charging facility can be planned with a larger capacity for high quality of service; however, this increases cost. To overcome this trade-off between the cost and quality of service, We propose a solution to plan an EV charging facility that achieves high quality of service at a reduced cost. This chapter proposes a robust optimization model to minimize the cost and guarantee high quality of service. To reduce the cost further, two strategies of demand management are explored - namely Stationary Demand Management (installing ESS) and

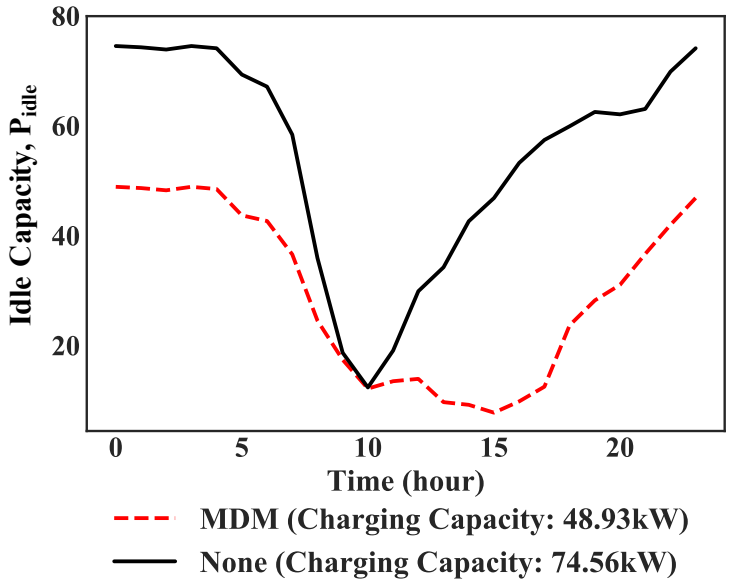

Figure 2.9: Efficient Use of Charger Capacity with MDM

Mobile Demand Management (rescheduling EV charging sessions).

The findings of this chapter are highlighted as follows. The proposed robust model for facility sizing guarantees high quality of service in charging EVs at a minimal cost. A facility with demand management strategies achieves high quality of service but at a lower cost, achieving Pareto optimality to a facility without demand management strategies. A facility with either ESS units or rescheduled EV charging demand can reduce the cost similarly at high quality of service. If it is challenging to reschedule the EV charging sessions in practice, the system operator can install a larger ESS to enjoy a similar cost reduction to rescheduling the charging demand. Similarly, if it is technically difficult to install an ESS, the facility operator can reschedule the EV charging sessions instead.

To improve this research further, the planning and operation simulation models can be modified to consider the EV charging demand in individual vehicle level, instead of an aggregate level. For instance, we can model the queuing process of EVs arriving, waiting for an available charger, charging, and leaving. This may optimize the number of chargers more accurately. Also, the analysis on demand management strategies can be more comprehensive. For the impact of SDM on the facility, we explored only two values for the maximum ESS units to be built $b_{\max} = [2, 10]$. However, it is possible that the cost does not decrease further with an ESS sizing above a certain level and this cut-off point for the diminishing return may depend on how the EVs shift their charging (MDM) [37]. Future research can explore the impact of SDM on the facility sizing in more detail by experimenting various values of $b_{\max}$.

For MDM, we assume perfect success of rescheduling EV charging sessions. In reality,

MDM can have numerous challenges to reschedule with issues in compliance, awareness, uncertainty, and incentives. In addition, rescheduling of charging sessions may influence the facility performance. Rescheduling EV charging sessions can be modeled as a coupled problem with the facility planning problem for better rescheduling, facility sizing, and operation. Therefore, the effect of SDM and MDM on the facility must be thoroughly investigated for optimal and practical application. Other possible improvements on the planning model include the consideration of ESS degradation, maintenance costs of the facility, and various charger models with different charging power rates.

Chapter 3

Economic and Environmental Benefits for Electricity Grids from Spatiotemporal Optimization of Electric Vehicle Charging

This chapter is based on the previously published article: Woo, S., Fu, Z., Apostolaki-Iosifidou, E., & Lipman, T. E. (2021). Economic and environmental benefits for electricity grids from spatiotemporal optimization of electric vehicle charging. *Energies*, 14(24), 8204, https://doi.org/10.3390/en14248204.

In this chapter, we address the problem of estimating the potential economic and environmental gains for utility grids of shifting the electric-vehicle (EV) charging time and location. The current literature on shifting EV charging loads has been limited by real-world data availability and has typically therefore relied on simulated studies. Collaborating with a large automobile company and a major utility grid operator in California, we use actual EV operational data and grid-operation data including locational marginal prices, marginal grid emission rate data, and renewable energy generation ratio information. With assumptions about the future availability of EV charging stations, we estimate the maximum potential gains in the economic and environmental performance of the electrical-grid operation by optimizing the time and location of EV charging. For the problem of rescheduling the charging sessions, the optimization models and objective functions are specifically designed based on the information available to the energy system operators that influence their economic and environmental performance like grid congestion, emissions, and renewable energy. The results present the maximum potential in reducing operational costs and marginal emissions and increasing renewable energy use in the utility grid by rescheduling the EV charging load with respect to its time and location. The analysis show that the objective functions of minimizing the marginal cost or the marginal emission rate performed the best overall.

Nomenclature

ESS Energy Storage System

EV Electric Vehicle

EV Electric Vehicle

LMP Locational Marginal Price

MDM Mobile Demand Management

MER Marginal Emission Rate

RE Renewable Energy

SDM Stationary Demand Management

$C_{\text{LMP}}(t, x)$ Locational marginal price at time t and node x in USD/kWh

$C_{\text{MER}}(t)$ Marginal emission rate at time t in tons]of CO_2E/kWh

$C_{\text{RE}}(t)$ Renewable energy ratio at time t, unitless

$E_{b,i}$ Battery capacity in energy for vehicle i in kWh

E_f Final condition on the energy level required for vehicle i in kWh

$E^c_{i,k}$ Energy consumption for the trip departing from the destination node k for vehicle i in kWh

$E^{des}_{i,k}$ Desired charging energy at the destination node k for vehicle i in kWh

$E_{ini,i}$ Initial energy level in the battery of vehicle i in kWh

E_{max} Maximum level of energy required for vehicle i in kWh

$E_{min,i}$ Minimum level of energy required for vehicle i in kWh

K_i Number of locations that vehicle i visits over the optimization time horizon

N_{EV} Sample size of EVs

$P_{r,i}$ Rated charging power of vehicle i in kW

$S_i(t)$ Parking status of vehicle i at time t, which equals 1 if parked and 0 otherwise

$T^a_{i,k}$ Arrival time to the destination node k for vehicle i

$T^d_{i,k}$ Departure time from the destination node k for vehicle i

Δt Discrete time interval in hours

$\hat{x}_i(t)$ The electrical grid node that the location of vehicle i belongs to

i Vehicle index, $i \in [1, N_{EV}]$

k Destination index, $k \in [1, K_i]$

n Number of EV chargers

b Scale factors for ESS units [scale]

$P_c(i,t)$ Charging power for vehicle i at time t in kW

$\widehat{J_{\text{agg, LMP}}}$ The total LMP cost from the LMP-minimizing solution for aggregate EVs

$\widehat{J_{\text{agg, MER}}}$ The total MER from the MER-minimizing solution for aggregate EVs

$\widehat{J_{\text{agg, RE}}}$ The total RE from the RE-maximizing solution for aggregate EVs

$P_{\text{EV}}(\tau)$ Charging power to aggregate EVs [kW]

$P_{\text{B,C}}(\tau)$ Power charged to ESS [kW]

$P_{\text{B,D}}(\tau)$ Power discharged from ESS [kW]

$P_{\text{G,I}}(\tau)$ Power imported from the grid [kW]

$P_{\text{G,D}}$ Power used for demand charge calculation [kW]

$E_{\text{EV}}(\tau)$ Time-cumulative energy charged to aggregate EVs [kWh]

$E_{\text{B}}(\tau)$ Energy level of ESS [kWh]

$P^{\star}_{\text{EV,min}}(\tau)$ Power demand in charging EV aggregates, minimum to be satisfied [kW]

$E^{\star}_{\text{EV,min}}(\tau)$ Time-cumulative energy demand in charging EV aggregates, minimum to be satisfied [kWh]

$P^{\star}_{\text{L}}(\tau)$ Power demand from the building use [kW]

$P^{\star}_{\text{EV, min, MDM}}(\tau)$ Power demand in charging EV aggregates with mobile demand management, minimum to be satisfied [kW]

$E^{\star}_{\text{EV, min, MDM}}(\tau)$ Time-cumulative energy demand in charging EV aggregates with mobile demand management, minimum to be satisfied [kWh]

$\overline{P_L(\tau)}$ Expected value of $P^{\star}_{\text{L}}(\tau)$

$\sigma^2_{P_L}(\tau)$ Variance of $P^{\star}_{\text{L}}(\tau)$

$\mathcal{F}_{E,\tau}(z)$ Empirical cumulative distribution of $E^{\star}_{\text{EV, min, MDM}}(\tau)$

$\mathcal{F}_{P,\tau}(z)$ Empirical cumulative distribution of $P^{\star}_{\text{EV, min, MDM}}(\tau)$

$\mathcal{F}^{-1}_{E,\tau}(\tau)(\alpha_{EV})$ The inverse of $\mathcal{F}_{E,\tau}(z)$ at significance level α_{EV}, i.e., the aggregate EV charging energy demand at α_{EV}-th percentile at time τ

$\mathcal{F}^{-1}_{P,\tau}(\tau)(\alpha_{EV})$ The inverse of $\mathcal{F}_{P,\tau}(z)$ at significance level α_{EV}, i.e., the aggregate EV charging power demand at α_{EV}-th percentile at time τ

$P_{\text{EV,test,j}}(\tau)$ EV charging power demand for operation simulation date i [kW]

$P_{\text{L, test,j}}(\tau)$ Power demand from the building use for operation simulation of date i [kW]

b_{opt} Optimized scale factors for ESS units [scale]

n_{opt} Optimized number of EV chargers

$E_{B,\text{max}}$ Nominal ESS energy capacity per unit of ESS [14.0 kWh]

$P_{\text{EV, R}}$ Rated power of EV charger [2.33kW]

$P_{\text{G,I,max}}$ Power capacity for grid import [2000.0kW]

$P_{B,\text{max}}$ Nominal ESS power capacity per unit of ESS [5.0 kW]

α_{EV} The percentile value of the EV charging energy, at which the EV charging facility must satisfy [0.95]

$\alpha_{\text{G, l}}$ The probability of the grid import power is above minimum, 0kW [0.95]

$\alpha_{\text{G,u}}$ The probability of the grid import power is below the capacity, $P_{G,I,\text{max}}$ [0.95]

$\beta_{\text{B,i}}$ Initial ESS energy level ratio, [0.5%]

$\eta_{\text{B,C}}$ ESS charging efficiency, [0.98%]

$\eta_{\text{B,D}}$ ESS discharging efficiency, [0.98%]

η_{EV} EV charging efficiency [0.89%]

$b_{\max}$ ESS scale maximum limit [scale/kWh]

c_{B} Daily cost per energy storage system unit [0.066 USD /day/kWh]

c_{EV} Daily cost of an EV charger [0.274 USD/day]

$c_{\text{G,D}}$ Demand charge cost, [19.0/30 USD/kW/day]

$c_{\text{I}}(\tau)$ Time-of-Use electricity cost for time τ [USD/kWh]

dt Time interval, [1 hour]

τ Time step $\in [1, T]$ [hour]

T Number of time steps in a day [24 hours]

N_{cross} Sample size for cross validation [100 samples]

N_{test} Number of dates tested for operation simulation [71 dates]

f_{CC} Daily capital cost ($/day)

f_{OC} Daily operation cost ($/day)

f_{TC} Daily total cost ($/day)

f_{QoS} Performance metric of quality of service in charging EVs (kW)

3.1 Introduction

Electric vehicles (EVs) are now proliferating in major automobile markets around the world. Despite the environmental benefits of EVs for air quality, greenhouse-gas emissions, and human health [50], EVs can add significant electrical loads and cause potential negative impacts for electrical-grid operations, such as grid congestion, violations of voltage limits, and heavy loading of network assets (e.g., distribution transformers) [21], [22]. EV load is not characterized only by the time of the day that takes place but also by geographical location and the specific section of the distribution grid where the load is connected. Therefore, EV charging solutions that are based on both time and location can be important to potentially reducing the impacts of EVs on the grid. Managing the timing and location of EV charging is becoming increasingly possible as the battery capacity of EVs grows larger, and also because personal vehicles including EVs spend most of the time parked and have large time windows in which to charge. In this study, we address the problem of estimating the maximum potential gains in terms of economics, the integration of renewable energy sources, and greenhouse-gas emission reductions for electrical-grid operators in shifting the time and

location of charging EVs based on a real-world study. For background, there is a large body of research that optimizes EV charging to improve the performance of electrical-grid operation. Optimal charging schedules for EVs can improve various aspects of grid operations, such as reducing costs, emissions, peak loads, power losses, and integration of renewable energy sources [51], [52]. However, there can be trade-offs between improving one aspect at the expense of another. For instance, EV-charging schedules that target nighttime charging to reduce electricity costs can result in higher emissions of carbon dioxide [53]. Additionally, attempts to optimize overnight EV charging with respect to a time-of-use pricing regime can increase the curtailment of renewable energy [23]. In the current literature, it is not clearly identified which performance metric of the grid operation one must target in optimizing the EV charging so that the grid performance improves holistically without foregoing another.

In addition, some studies use performance metrics that are not easily measurable or directly useful on the grid operators. For instance, Kara et al. [54] optimized EV charging by shaving the peak demand; Tarroja et al. [55] shifted the charging load to hours with high renewable generation; and Jian et al. [56] filled the valley and shaved the peak of the energy demand. However, managing EV charging with these objectives may not lead directly to cost reduction, emission reduction, or an increase in renewable energy use. These performance metrics will be easier to use in practice if the values are easily measurable and immediately useful to the grid operator.

Additionally, most of the literature has been limited in studying optimal charging at fixed locations, i.e., changing the charging time or charging power within each plug-in session to improve the operation of the electrical grid [23], [52], [54]–[59]. However, there is a significant benefit to relocating charging sessions as well, for example, from the home to the workplace so that EVs charge midday and use solar energy [44]. Szinai et al. [23] also found that there is only little value in smart charging at fixed locations at workplaces because people often charge at home. Therefore, we investigate the benefit of optimal EV charging by not only shifting the time of charging within each plug-in session but also choosing the charging location across the places that the vehicle visits. Expanding the solution space of charging decisions in both time and space allows us to enhance the benefits in optimal charging.

With EV-charging control, many studies attempt to estimate potential improvements to electrical-grid operation. However, most studies depend only on aggregated or simulated data on the driving and charging demand of EVs because real data for individual EVs are scarce. Examples of studies that use aggregate data include the work by Kara et al. [54], which uses the aggregate charging demand of the EVs and the "load flexibility" of EVs, i.e., the ratio of charging time to the parking time, to estimate the maximum benefit in shaving the demand peak. Similarly, Teng et al. [57] used an aggregate EV-charging demand and aggregate flexibility to estimate the reduction in grid operation cost, though the demand and flexibility values were calculated from individual EVs and their mobility constraints.

Examples of studies that simulate the driving and charging of EVs based on the United States National Household Travel Survey include the work by Tarroja et al. [55], which calculated the reduction in emissions and fuel for the vehicles on the road and estimated the increase in renewable energy use. Forrest et al. [58] used the survey data to simulate

EVs and estimate the economic and environmental value of renewable-energy integration. Van Triel and Lipman [52] simulated EVs and grid operation based on the survey data and calculated the reduction in renewable energy curtailment and consequently avoided installment of the energy storage system. Other interesting examples of simulation studies include Jian et al. [56], who simulated the charging load of millions of EVs and estimated the peak energy demand with EV charging management. Szinai et al. [23] simulated the detailed travel and charging demand of EVs with an agent-based model called BEAM and a grid-operation model called PLEXOS and estimated the maximum benefit in reducing the cost and the renewable energy curtailment with EV-charging management.

In this chapter, we present an analysis based on the actual driving and charging behavior of hundreds of EVs operating in the San Francisco Bay Area in California. We collaborate with an automobile company (BMW North America LLC, Woodcliff Lake, NJ, USA), a grid operator (Pacific Gas and Electric Company or PG&E, San Francisco, CA, USA), a grid-services company (Olivine Inc. Berkeley, CA, USA), and an energy data-analytics company (Kevala Analytics, San Francisco, CA, USA). We combine grid data for corresponding locations and times, along with the real-world data for driving and charging individual EVs. With this rich set of data, we estimate the electrical grid benefit from optimal charging as realistically as possible. The grid data include the locational marginal price (LMP), the marginal-emission rate (MER), and the renewable-energy (RE) ratio, which are measurable to grid operators. The data used in the analysis are explained in more detail in Section 3.3.

Our contribution to the current knowledge in EV charging and its benefit to the electrical-grid operation is threefold. First, we identify and recommend an objective function to optimize EV-charging sessions so that the grid operation can improve holistically in terms of operation costs, greenhouse-gas emissions, and renewable energy integration. These objective functions are developed based on measurable and immediately useful values to the grid operator. Second, we develop an algorithm that optimizes both the time and location of charging individual EVs to enhance electrical-grid operation. With assumptions on charging compliance, data availability, and perfect knowledge, we estimate the maximum benefit that the algorithm can bring in reducing the operation cost, reducing the greenhouse gas emissions, and increasing the renewable energy usage. Third, we overcome the limitations in simulating and aggregating the behavior of EVs by using the real driving and charging data of individual EVs and grid-operation data in California. This allows us to realistically estimate the benefit of optimal charging to the grid operation.

Our research is presented as follows. In Section 3.2, we describe three performance metrics of electrical-grid operation based on the LMP, the MER, and the RE ratio, for which EV charging was optimized. We propose two optimization models: (1) a fixed-Location model to schedule only the time to charge EVs and (2) an inter-location model to schedule both the time and location to charge EVs. These two models can solve objective functions for the three performance metrics. We also describe how we evaluated the performance of the optimization models. In Section 3.3, we describe the real data from California used in this research, namely, the telematics data of individual EVs on driving and charging and the operational data for the local electrical grid. We also briefly explain how the data

were processed for this research. In Section 3.4, we verify the fixed-location model and the inter-location model with sample trajectories of charging power for individual vehicles and validate the model performance in terms of the electrical-grid operation for charging a fleet of EVs. We estimate the maximum gain to electrical-grid operation from controlling EV charging time and location, in terms of cost savings, emission reductions, and renewable-energy usage. Finally, we compare the performance of six cases (two optimization models and three objective functions) and recommend a policy that can reduce grid operation cost and greenhouse gas emissions and increase the usage of renewable energy. Future work is described in Section 3.5 and the chapter is concluded in Section 3.6.

3.2 Methodology

We propose two optimization models to schedule the charging time and location of EVs and explain how we evaluate the performance of optimization models in generating benefits to the electricity-system operator. We first describe three metrics, namely, the locational marginal price (LMP), the emission rate, and the renewable-energy ratio, to reflect the economic and environmental performance of the local electrical grid. We use these metrics to develop the objective functions and propose two optimization models to solve them. These are the fixed-location model and the inter-location model. We then describe the methodology to conduct a case study of real EV drivers in California to evaluate the potential benefits to the system operator in optimizing the EV charging schedule.

Performance Metrics of Electrical Grid

We choose the LMP, the MER, and the RE percentage to evaluate grid performance because they are measurable values by the grid operator. We use the LMPs as defined by the transmission system operator of California, the California Independent System Operator (CAISO). LMP is the marginal cost of delivering the energy in units USD per MWh, commonly understood as the wholesale electricity cost, and it is used to control electricity grid congestion and to optimize power flow [60]. CAISO sets LMPs at nodes, including scheduling points, and aggregated pricing nodes. The distance between the nodes can be from less than a mile to several miles. The LMP value changes for each node and each time interval and shows inter-location variations based on the marginal cost of energy, power losses, and grid congestion. In this study, the LMP metric is used independently of the distribution grid and its components (distribution transformers). An example of an hourly LMP trend at a node is shown in Figure 3.1. The figure shows that there is a sharp increase in pricing in the morning before work hours and in the afternoon when people return home. We define a parameter for LMP, $C_{\mathrm{LMP}}(t, x)$, as the locational marginal price at time t and node x, converted to USD per kWh.

For the emission rate, we use the MER of greenhouse gases in California. The MER is the rate of emissions that are produced when additional load is added and new generation

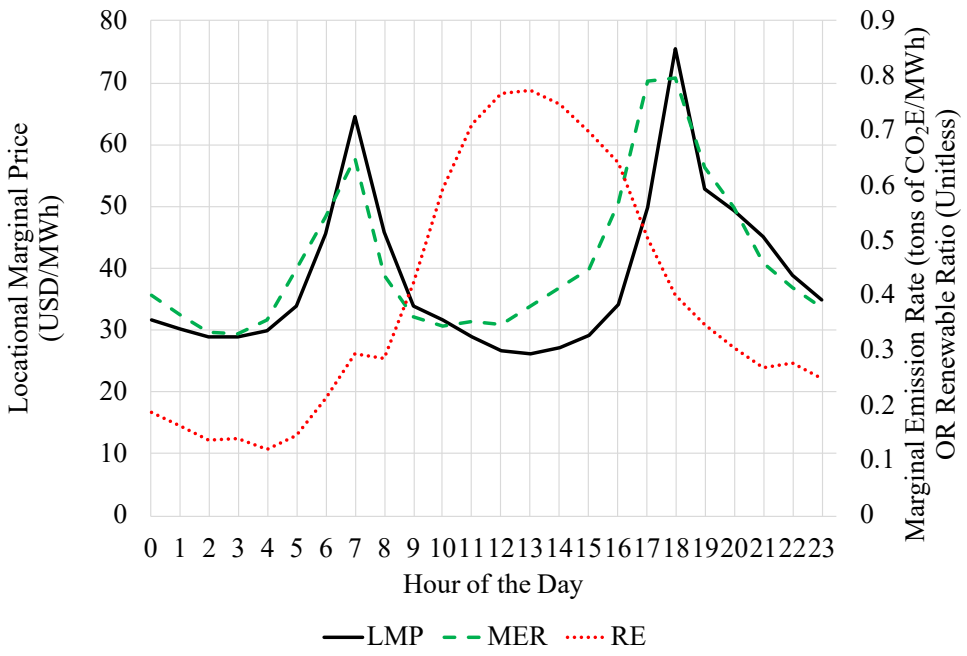

Figure 3.1: Example of locational marginal pricing, the marginal-emission rate, and the renewable ratio (2017/11/2, LMP node ID: BAYSHOR2-1-N001, SubLAP: PGSF).

subsequently comes online. The MER is expressed as the marginal emissions in units of tons of CO_2E/MWh. This greenhouse-gas-intensity metric was extracted from the 2019 avoided-cost calculator (ACC) model, developed by E3 consulting. Figure 3.1 shows an example of the MER values; these change over time and location. However, we assume these are independent of the location due to the data availability. Similar to the trend of LMP, there are two peaks: one in the morning and another in the afternoon. We define $C_{\text{MER}}(t)$ as the marginal emission rate at time t, converted to tons of CO_2E/kWh.

As for the renewable energy (RE) ratio, we use the data provided by PG&E indicating the unitless ratio of the generated RE. This provides the RE ratio for each hour that does not change with location within the PG&E service territory. An example of the hourly RE ratio is shown in Figure 3.1. The RE ratio has a different trend from LMP and MER, with one peak that appears around noon through early afternoon when solar energy is largely generated. The RE ratio is low during the evening and before sunrise. We define $C_{\text{RE}}(t)$ as the RE ratio at time t, without units.

Note that in the following formulation of the optimization models, we assume the knowledge of values for $C_{\text{LMP}}(t, x)$, $C_{\text{MER}}(t)$, and $C_{\text{RE}}(t)$ at all times and locations, where vehicles are present over the optimization time window.

Optimization Models

In this section, we first describe the vehicle, time, and location notation. We propose the fixed-location model and the inter-location model to schedule the charging of individual EVs, as well as the three objective functions for each model. We also explain the evaluation method of the proposed models.

Notation

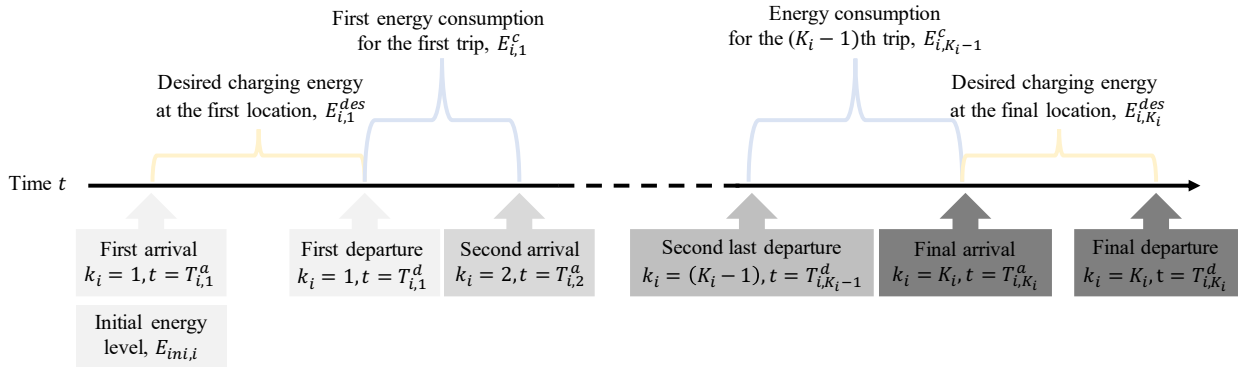

Nomenclature

- $i \in [1, N_{EV}]$: vehicle index, where N_{EV} is the sample size of EVs
- $k_i \in [1, K_i]$: destination index of i-th vehicle, where K_i is the total number of destinations of the vehicle
- $T^a_{i,k}, T^d_{i,k}$: i-th vehicle's arrival time to the k-th destination and departure time from the k-th destination, respectively
- $E_{ini,i}$: i-th vehicle's initial energy level
- $E^{des}_{i,k}$: i-th vehicle's desired charging energy at the k-th destination
- $E^c_{i,k}$: i-th vehicle's energy consumption in the trip from the k-th destination

Figure 3.2: Notations to Describe the Multiple Destinations for a Vehicle

We define vehicle index $i \in [1, N_{EV}]$, where N_{EV} is the sample size of EVs. We define the destination index that vehicle i visits as $k \in [1, K_i]$ over the optimization time horizon. For each vehicle i, its battery capacity in energy is assumed as $E_{b,i}$. For each destination k, a tuple of parameters are known: $(T^a_{i,k}, T^d_{i,k}, E^{des}_{i,k}, E^c_{i,k})$, which are the arrival time to the node, the departure time from the node, the desired charging energy at the node, and the energy consumption for the trip departing from the node, respectively. These notations are shown in Figure 3.2 with arrivals and departures of a vehicle i over time t. Note that the energy consumption to the first location in the sample is disregarded, and the initial energy level $E_{ini,i}$ is evaluated at the arrival of the first location. Note that we assume the parameter tuples shown in the graph to be known. If there is no information of final departure, we assume that its time coincided with the final arrival and that the final desired charging energy is zero.

In addition, we define a binary parameter to indicate the known information on the parking status as $S_i(t)$, which equals 1 if the vehicle i is parked at time t and 0 otherwise. Additionally, for each time step t, the electrical grid node that the vehicle's location belongs to is expressed as $\hat{x}_i(t)$. We assume that only $S_i(t) \cdot \hat{x}_i(t)$ is known; in other words, we know the grid node that the vehicle is connected to, only if it is parked.

Fixed-Location Charging Optimization

The fixed-location model schedules the charging time of an individual EV at a given location, by exploiting the variation in the LMP, the MER, and the RE ratio over time. The model assumes that the EV can charge at various power levels under its physical capacity once it is plugged in. The EV may not start to charge immediately upon plugging in, but it can also defer its charging during the plugging session. The model requires the provision of the demanded energy at each destination. The model is applied for all destinations of all EVs in the sample, and the total gains in the LMP, the MER, and the RE were computed for the aggregate EVs.

Three optimization problems are given below. We minimized the LMP cost in units of USD as shown in (3.1a), minimized the MER metric in units of tons of CO_2E as shown in (3.1b), and maximized the RE in units of MWh as shown in (3.1c). The optimization variable is the charging power at each time step, $P_c(i,t)$ for vehicle i in units of kW. The optimization time t ranges over $[T^a_{i,k}, T^d_{i,k}]$ with a discrete interval of $\Delta t = 1$ hour.

$$\min_{P_c(i,t)} \; J_{\text{LMP,i,k}}, \qquad \text{where} \;\; J_{\text{LMP,i,k}} = \Delta t \sum_{t=T^a_{i,k}}^{T^d_{i,k}} P_c(i,t) \cdot C_{\text{LMP}}(t, \hat{x}_i(t)), \tag{3.1a}$$

$$\min_{P_c(i,t)} \; J_{\text{MER,i,k}}, \qquad \text{where} \;\; J_{\text{MER,i,k}} = \Delta t \sum_{t=T^a_{i,k}}^{T^d_{i,k}} P_c(i,t) \cdot C_{\text{MER}}(t), \tag{3.1b}$$

$$\max_{P_c(i,t)} \; J_{\text{RE,i,k}}, \qquad \text{where} \;\; J_{\text{RE,i,k}} = \Delta t \sum_{t=T^a_{i,k}}^{T^d_{i,k}} P_c(i,t) \cdot C_{\text{RE}}(t). \tag{3.1c}$$

To constrain the physical charging capacity of vehicles, we constrain the charging power, $P_c(i,t)$ by the rated charging power of the vehicle i, $P_{r,i}$. We also model the desired charging energy, $E^{des}_{i,k}$, during the stay at location k. The constraints for the fixed-location optimization are given below:

$$0 \leq P_c(i,t) \leq P_{r,i}, \tag{3.2}$$

$$E_{i,k}^{des} \leq \Delta t \sum_{t=T_{i,k}^{a}}^{T_{i,k}^{d}} P_c(i,t). \tag{3.3}$$

As a simplification, we assume there is negligible energy loss in charging. Since the optimization problem is linear and convex, the optimization result is globally optimal. We use the constraints (3.2) and (3.3) to solve three optimization problems in terms of LMP, MER, and RE, by choosing (3.1a), (3.1b), or (3.1c), respectively. We apply this optimization problem to each parking instance of individual EVs in an optimization horizon. The performance of the fixed-location model can be expressed as the following:

$$\widehat{J_{\text{agg, LMP}}} = \sum_{i=1}^{N_{\text{EV}}} \sum_{k=1}^{K_i} J_{\text{LMP,i,k}} \Big(\underset{P_c(i,t)}{\text{argmax}}\, J_{\text{LMP, i,k}} \Big), \tag{3.4a}$$

$$\widehat{J_{\text{agg, MER}}} = \sum_{i=1}^{N_{\text{EV}}} \sum_{k=1}^{K_i} J_{\text{MER,i,k}} \Big(\underset{P_c(i,t)}{\text{argmax}}\, J_{\text{MER, i,k}} \Big), \tag{3.4b}$$

$$\widehat{J_{\text{agg, RE}}} = \sum_{i=1}^{N_{\text{EV}}} \sum_{k=1}^{K_i} J_{\text{RE,i,k}} \Big(\underset{P_c(i,t)}{\text{argmax}}\, J_{\text{RE, i,k}} \Big), \tag{3.4c}$$

where (3.4a), (3.4b) and (3.4c) evaluate the total minimized LMP cost, the total minimized MER, and the total maximized RE ratio, respectively, on aggregate EVs over a given optimization horizon. We assume that the change of charging schedule in individual EVs do not affect the LMP, MER, and RE.

Inter-location Charging Optimization

The inter-location model expands the feasible solution set from the fixed-location model by scheduling not only when to charge but also where to charge among the locations that the EV parks. This model assumes that, in the future, every destination that an EV visits has a charger available to use. The inter-location model exploits the LMP, MER, and RE values that vary over time across multiple locations that the vehicle visits. This model finds the optimal time and location to charge, while satisfying the energy needs to drive between the locations, a minimum and maximum energy level for each vehicle, and a final condition for the battery state-of-charge level at the end of the optimization horizon. The model is applied for all EVs in the sample and the total gains in the LMP, the MER, and the RE are computed for the aggregate EVs.

Three objective functions are proposed. We minimize the LMP cost in USD as shown in (3.5a), minimize the greenhouse gas emission in unit of tons of CO_2E as shown in (3.5b),

and maximize the RE ratio of energy generation provided to charge the vehicle as shown in (3.5c).

$$\min_{P_c(i,t)} \; J_{\text{LMP,i}}, \qquad \text{where} \;\; J_{\text{LMP,i}} = \Delta t \sum_{t=T^a_{i,1}}^{T^d_{i,K_i}} P_c(i,t) \cdot C_{\text{LMP}}(t, \hat{x}_i(t)), \tag{3.5a}$$

$$\min_{P_c(i,t)} \; J_{\text{MER,i}}, \qquad \text{where} \;\; J_{\text{MER,i}} = \Delta t \sum_{t=T^a_{i,1}}^{T^d_{i,K_i}} P_c(i,t) \cdot C_{\text{MER}}(t), \tag{3.5b}$$

$$\max_{P_c(i,t)} \; J_{\text{RE,i}}, \qquad \text{where} \;\; J_{\text{RE,i}} = \Delta t \sum_{t=T^a_{i,1}}^{T^d_{i,K_i}} P_c(i,t) \cdot C_{\text{RE}}(t). \tag{3.5c}$$

The optimization problems in (3.5) are similar to those in (3.1); however, they are different in the optimization time range. The inter-location problem spans multiple locations that each vehicle visits, i.e., for vehicle i, the optimization searches a solution from the arrival time at the first location, $T^a_{i,1}$ until the departure time of the final (or K_i-th) location, T^d_{i,K_i}. The optimization variable is the charging power at each time step t for vehicle i, $P_c(i,t)$.

The inter-location model limits the charging power by the rated charging power, $P_{r,i}$, and also by its parking status $S_i(t)$. Refer to (3.6) below where the charging power is forced to be zero when the vehicle is on the move, i.e. $S_i(t) = 0$.

$$0 \le P_c(i,t) \le S_i(t) \cdot P_{r,i}. \tag{3.6}$$

The model also develops a schedule to satisfy the necessary energy for the trips and to maintain the energy level of EV to being within in a given range, $[E_{min,i}, E_{max,i}]$. We assume $E_{min,i} = 0.10 \cdot E_{b,i}$ and $E_{max,i} = E_{b,i}$, respectively. At arrival to each destination after the first destination, we check that the vehicle's initial energy level $E_{ini,i}$ and the cumulative charging energy satisfy the cumulative energy consumption as shown in (3.7). For all $q = 2, ..., K_i - 1$,

$$E_{min,i} \le E_{ini,i} + \Delta t \sum_{t=T^a_{i,1}}^{T^a_{i,q}} P_c(i,t) - \sum_{p=1}^{q-1} E^c_{i,p} \le E_{max,i}. \tag{3.7}$$

This constraint provides a minimum energy to the vehicle for the duration of the upcoming trip. For instance, at arrival to the second destination ($q = 2$), the sum of initial energy level, the cumulative charging energy at the first location, and the energy consumption to the second location must be within the range, $[E_{min,i}, E_{max,i}]$.

Energy level is also checked at all departures; refer to (3.8). For all $q = 1, ..., K_i - 1$,

$$E_{min,i} \leq E_{ini,i} + \Delta t \sum_{t=T^a_{i,1}}^{T^d_{i,q}} P_c(i,t) - \sum_{p=1}^{q-1} E^c_{i,p} \leq E_{max,i}. \tag{3.8}$$

This constraint prevents the vehicle from charging over its battery capacity. For instance, at departure from the first destination ($q = 1$), the sum of initial energy level and the cumulative charging energy at the first destination must be in range $[E_{min,i}, E_{max,i}]$ as $E^c_{i,0} = 0, \forall i$. At departure from the second destination ($q = 2$), the sum of initial energy level, the cumulative charging energy, and the cumulative energy consumption to the second location must be in range $[E_{min,i}, E_{max,i}]$.

We also enforce a final condition for the battery energy level to be at least 50%, i.e., $E_f = 0.50 \cdot E_{b,i}$, to prevent the solution from depleting the EV energy by the final time step, as below:

$$E_{ini,i} + \Delta t \sum_{t=T^a_{i,k}}^{T^d_{i,K_i}} P_c(i,t) - \sum_{k=1}^{K_i} E^c_{i,k} \leq E_f. \tag{3.9}$$

Here again, we assume there is negligible energy loss in charging. Since the optimization problem is linear and convex, the optimization result is globally optimal. We use the constraints (3.6), (3.7), (3.8) and (3.9) to solve three optimization problems in terms of LMP, MER, and RE, by choosing (3.5a), (3.5b), or (3.5c), respectively. We apply these optimization problems to each individual EV over a time period, such as one month. In other words, we optimize from the arrival time at the first destination to the departure time from the last destination within a month for each vehicle. The performance of the inter-location model can be expressed as the following:

$$\widehat{J_{\text{agg, LMP}}} = \sum_{i=1}^{N_{\text{EV}}} J_{\text{LMP, i}} \Big(\underset{P_c(i,t)}{\text{argmin}}\, J_{\text{LMP, i}} \Big), \tag{3.10a}$$

$$\widehat{J_{\text{agg, MER}}} = \sum_{i=1}^{N_{\text{EV}}} J_{\text{MER, i}} \Big(\underset{P_c(i,t)}{\text{argmin}}\, J_{\text{MER, i}} \Big), \tag{3.10b}$$

$$\widehat{J_{\text{agg, RE}}} = \sum_{i=1}^{N_{\text{EV}}} J_{\text{RE, i}} \Big(\underset{P_c(i,t)}{\text{argmax}}\, J_{\text{RE, i}} \Big), \tag{3.10c}$$

where (3.10a), (3.10b) and (3.10c) evaluate the total minimized LMP cost, the total minimized MER, and the total maximized RE ratio, respectively, on aggregate EVs. We assume that the change of charging schedule in individual EVs do not affect the values of LMP, MER, and RE.

Performance Evaluation

We have thus proposed two optimization models and three objective functions to solve for each model. We first present the detailed results of each model in minimizing the LMP cost, i.e., solving (3.1a) and (3.5a). We validate each model with the sample trajectories of charging power for an individual vehicle. We evaluate the performance of both models by analyzing the EV sample size (veh), the total parking hours (veh-hrs), the total charging hours (veh-hrs), the total hours with change in charging status (hrs), the total change in the LMP cost (USD), and the average change in the LMP cost (USD/veh-hr).

The total parking (or charging) hours are computed as the sum of parking (or charging) hours of all vehicles in the sample. We use the term "idle" to describe the charging status of vehicle that is parked but not charging. The total hours with the change in charging status calculates the sum of hours such that the vehicle's charging status is different in the optimization result from the actual data. For instance, there is a 1-hour change in status if a vehicle was charging from 8:00 a.m. to 8:30 a.m. (or up to 9:00 a.m.) in the actual data, but the optimization result recommends it to be "idle." The total change in the LMP cost is the optimized LMP cost (the values of (3.4a) or (3.10a)), subtracted by the total LMP cost in actual data. The total change in the LMP cost is negative when LMP costs are saved with optimization. The average change in the LMP cost is the total change in the LMP cost, divided by the total parking hours in the actual data.

Additional analysis is performed for the inter-location model results by grouping them based on various destinations. These include anonymized home locations, "away" locations (destinations other than the home locations), and two regional units called sub-load aggregation Points (SubLAPs). The SubLAP regions are defined by CAISO to aggregate demand response and other distributed sources and to define a basis for congestion revenue and capacity planning [61]. The SubLAP map of California can be found in [62]. With the analysis of SubLAPs, we show the load shifting potential and benefits based on the local aggregation areas. The results for LMP savings are further analyzed for the hourly variation in a day.

Next, we analyze the performance of different objective functions by comparing the results of the fixed-location model to solve the three problems in (3.1) and the results of the inter-location model to solve the three problems in (3.5). We analyze the total LMP cost ((3.4a) and (3.10a)), the total MER ((3.4b) and (3.10b)), and the total RE ((3.4c) and (3.10c)) and recommend an objective to implement in more generally optimizing EV charging in electricity system operation.

Please note that the proposed optimization models are solved in Python, using an open-source modeling package called CVXPY [63].

3.3 Data

The main project data consist of actual vehicle telematics data from EVs, along with operational data for the electrical grid in California and the PG&E service territory. This

allows us to estimate the economic and environmental benefits of load shifting in an ideal case, despite the strong assumptions of optimization, such as knowledge of vehicle arrivals, departures, and energy demand. Below, we describe the vehicle telematics data and the grid operational data, such as the LMP, the MER, and the RE, and we also briefly explain the pre-processing of the vehicle data.

Data Description

We use telematics data from approximately 300 BMW electric and hybrid vehicles, whose drivers participated in this phase of the research project. The individual EV data describe the following anonymized types: the vehicle ID, the vehicle model, timestamps (for parking/charging events), the state of charge in the battery, the connection status of the vehicle to a charger, the vehicle location, and the odometer reading. The time period of data used for this analysis was from 10 November 2017 to 30 November 2017. BMW provided the information for battery capacity and the rated charging power for each vehicle model, as well as the anonymized home locations for each vehicle ID. The sample vehicles included BMW models i2, i8, and iPerformance, whose nominal rated charging powers ranged from 3.6 to 7.4 kW. The histogram for the actual charging power from the data is shown in Figure 3.3. The actual charging power deviates from the nominal charging power value; however, we used the nominal values for the rated charging power in (3.2) and (3.6).

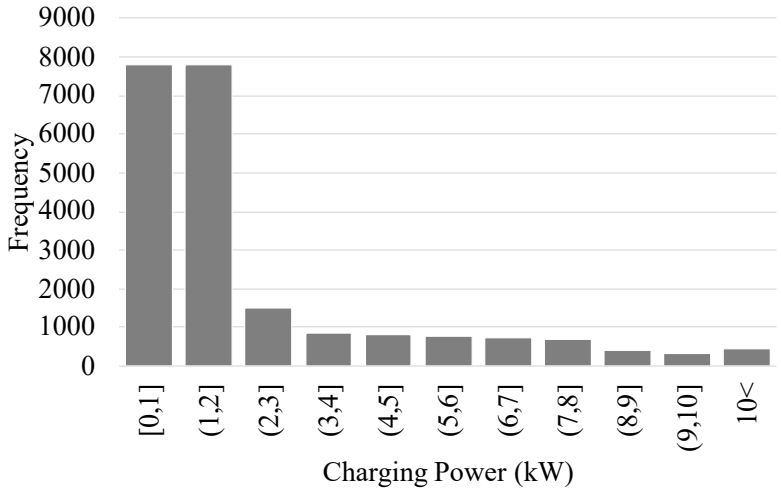

Figure 3.3: Histogram of Actual Charging Power in the Sample

We obtained the day-ahead prices for the LMP data for the locations and times of parking sessions in the EV data. Each vehicle location given in latitude and longitude is matched to an LMP zone, the regional unit for which the LMP value is defined. The matching and gathering of LMP data were processed with an application programming interface tool by

Kevala Analytics. Since LMP zones represent much larger geographic regions than the point values of latitude and longitude, the proposed models require much less precision for the location data. This may alleviate the privacy and accessibility issues with vehicle-location data for this type of analysis.

Due to data constraints, we obtained data of the MER and the RE ratio in different years to the driving data and the LMP data. We obtained the MER prediction values for every hour in 2019 from the ACC model. Data for the RE ratio for the total generated energy for every hour in 2018 were obtained from PG&E. The MER and the RE ratio do not include geographical information. Though it is possible that the MER and the RE ratio values may change in trend, we tried our best to match the time periods of the driving data and LMP data by using the time period from 10 November 2019 to 30 November 2019 for MER and the time period from 10 November 2018 to 30 November 2018 for the RE ratio.

Data Processing

The actual EV telematics data include anomalies, such as departure time before arrival time and negative values for the charging energy. These data, as well as data for vehicles that left California for any or all of the time period used, were excluded from the analysis. The percentage of the raw data that passed these criteria was 69.3%, i.e., the total vehicle-hours observed in the raw data and the processed data were 135,075 veh-hours and 93,576 veh-hours, respectively. For the fixed-location model, the desired energy at destination k, $E_{i,k}^{des}$, was the actual charging energy at destination k in the data.

However, this actual charging energy was not used for the inter-location model. Instead, the energy consumption from the k-th destination to the next destination, $E_{i,k}^{c}$, was used. For the inter-location model, we processed the data to only contain the vehicles that have state-of-charge values at arrival always less than or equal to the state of charge values at the time of the previous departure. This is because if the state of charge is higher at arrival than at the previous departure, the charging energy demand is calculated as negative.

This anomaly can occur because some charging sessions are missing in the data. Not all parking instances are collected in the data, since the GPS tracking devices turn off when vehicles are on the move, and the vehicles may park inside some parking structures, where the GPS readings are unavailable. It is also possible that some plug-in hybrid EVs are charged during driving due to using gasoline and powering the vehicle generator. After this cleaning criteria, a data set with parking hours of 63,411 veh-hours was available for the inter-location model.

Data Flow

Based on the proposed models and the real data of the EV telematics and the utility grid operation, we optimize the time and location of the EV charging sessions through the data flow shown in Figure 3.4. First, the EV telematics data are processed to meet the optimization model requirements as described in Section 3.3, based on the EV parameters, such as

the rated charging power and battery capacities for each vehicle model. This processing outputs the clean data of parking and charging instances that can be used for the optimization with information on the time, the location, the battery state of charge, the original charging power and energy, and the transmission node connected to the parking location.

Second, the utility grid data on the LMP, the MER, and the RE are filtered according to the time and transmission nodes of the parking and charging instances. This helps reduce the memory required for computation because only a small subset of the available grid data can cover the times and locations present in the telematics data. Third, the parking and charging instances and the filtered grid data are used to solve the optimization problems proposed in (3.1) or in (3.5). Finally, the optimal results were outputted in terms of the optimal charging time, power, and energy. For the inter-location model, the charging location was also found. The final result also included the optimal grid performance for the aggregate EVs.

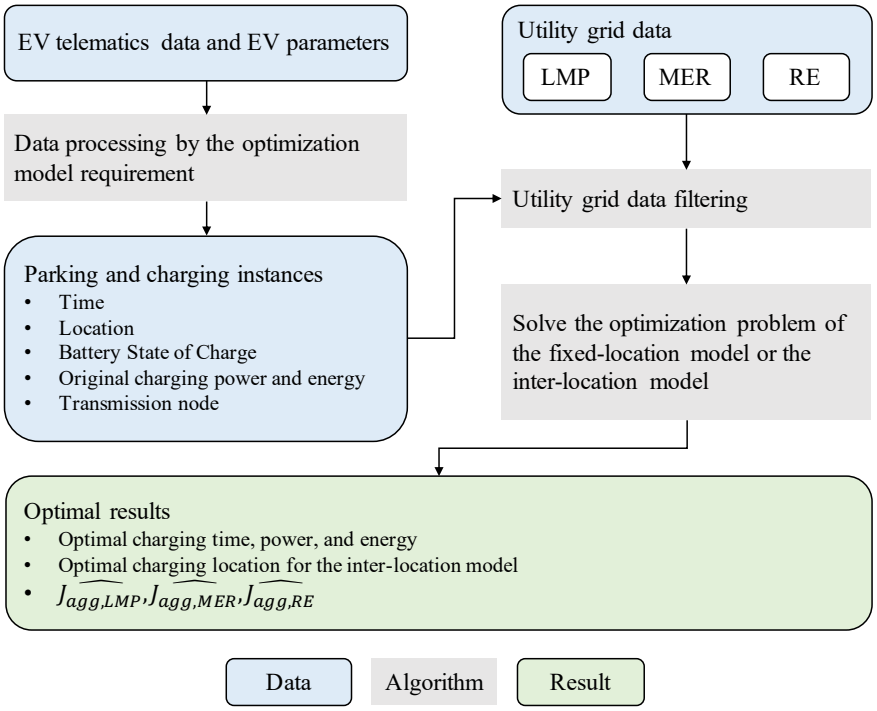

Figure 3.4: Data flow of the EV-charging optimization.

3.4 Results

In this section, we verify the fixed-location and inter-location models with sample trajectories of charging power of individual vehicles. We evaluate the two models based on the resulting locational marginal price cost, marginal emission rate, and renewable-energy ratio and show

that the inter-location model brings greater benefit to the electricity system operator than the fixed-location model. Additionally, we analyze the optimization performances among three objective functions and make a recommendation for the energy system operator to use.

Fixed-Location Model of Charging Optimization

We verify the optimization results of the fixed-location model, as shown in Figure 3.5, which shows the sample trajectories of charging powers of one vehicle in the actual data and the optimization result. The x-axis shows time; the left y-axis shows the charging power in kW; and the right y-axis shows the given LMP values in USD per MWh. The red dotted line plots the actual charging power in the data; the red continuous line plots the LMP-minimizing charging power; and the blue thick line plots the actual LMP values at the vehicle's current node during those hours $C_{\text{LMP}}(t, \hat{x}_i(t))$. The figure shows one parking session in the optimized result, which lasted from 2 November 2017 12:00 a.m. to 11:00 p.m.. In the actual data, the vehicle charged from midnight to 7:00 a.m. at 1.75 kW, though the LMP increased sharply in the morning around 5:00 a.m.. The optimization result recommends charging at hours with low LMP values, this being early in the morning around 2:00 to 3:00 a.m. and around 11:00 a.m. to 5:00 p.m. The total charging energy in the optimal solution is the same as the actual charging schedule.

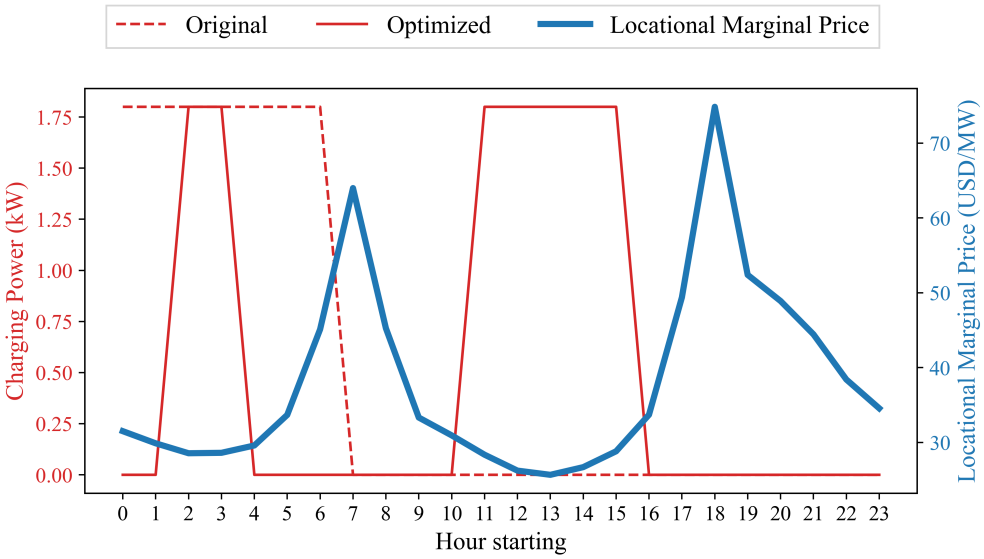

Figure 3.5: Sample Trajectories of Charging Powers in the Original Data and the Fixed-Location Model Solution

Table 3.1 presents the statistics of fixed-location results with LMP minimization, in terms of the total, home locations, and "away" locations. The statistics on total parking hours and

Table 3.1: Fixed-location Result with LMP Minimization

Item	Total	Home	Away
EV Sample Size (veh)	245	196	138
Total parking hours (veh-hr)	93,576	72,170	21,406
Total parking hours, where charging occurred (veh-hr)	55,819	48,099	7,720
Total charging hours (veh-hrs)	15,383	12,867	2,516
Total hours with a change in charging status due to optimization (veh-hrs)	12,374	10,608	1,766
Total change in LMP cost (US dollars, optimal - actual cost) for 30 days of sample	-236.8	-205.8	-31.1
Average change in LMP cost [1] (US dollars/veh-hr)	-0.0025	-0.0029	-0.0015

total charging hours are the same in the original data and optimal results, as only the charging hours within each parking session are altered. Note that, on average, vehicles charge only 8.7% of the time in a day ($15,383$ veh-hrs divided by 245veh·24h/day·30days). Only 27.6% of the parking hours was used for charging (15,383 veh-hrs divided by 55,819 veh-hrs). This shows that there is ample flexibility for the EV drivers to choose the charging schedule; however, the vehicles mostly charge outside the optimal hours. The optimal charging schedule is different from the actual data by 12,374 veh-hrs, which constitutes 80.4% of the total charging hours of the vehicles.

By significantly adjusting the charging hours, the LMP cost is reduced by USD 236.8 dollars for the fleet over a month. This is a significant savings, considering the relatively small level of the LMP cost (generally less than USD 100 per MW) and the small fleet size (245 vehicles in this case). This monthly savings can scale up directly if the number of participating EVs grows, where there are already more than 1000 times this many EVs in California with 256,000 registered in 2018 [64]. The LMP saving can also be calculated as USD 0.0025 /veh/hr on average; in other words, there is an average gain of USD 0.0025 in LMP savings for each hour that one vehicle staid in the system (or USD 0.06 for each day of one vehicle).

Analyzing the results in home and away locations separately, we see that the majority of the LMP cost reduction occurs at home, contributing to around 86.9% of the savings. One reason for this is because the vehicles park and charge more at home than away, so more adjustments are made to the charging schedule at home. Another reason is because the LMP peaks in the morning and the afternoon when people are primarily at home, so rescheduling charging powers at home brings benefits at a greater margin than at other locations.

[1] The denominator is the total parking hours, for instance 93,576 veh-hrs for the total.

Inter-location Model of Charging Optimization

We verify the optimization result of inter-location model with Figure 3.6, which shows the actual and optimal charging power levels and LMP values for two consecutive parking events of one EV. The vehicle parks from 7PM to 6AM in the first parking session as shown on the top graph, drives for two hours, and parks from 8AM to 4PM in the second parking session as shown in the bottom graph. The axes and legends are similar to Figure 3.5.

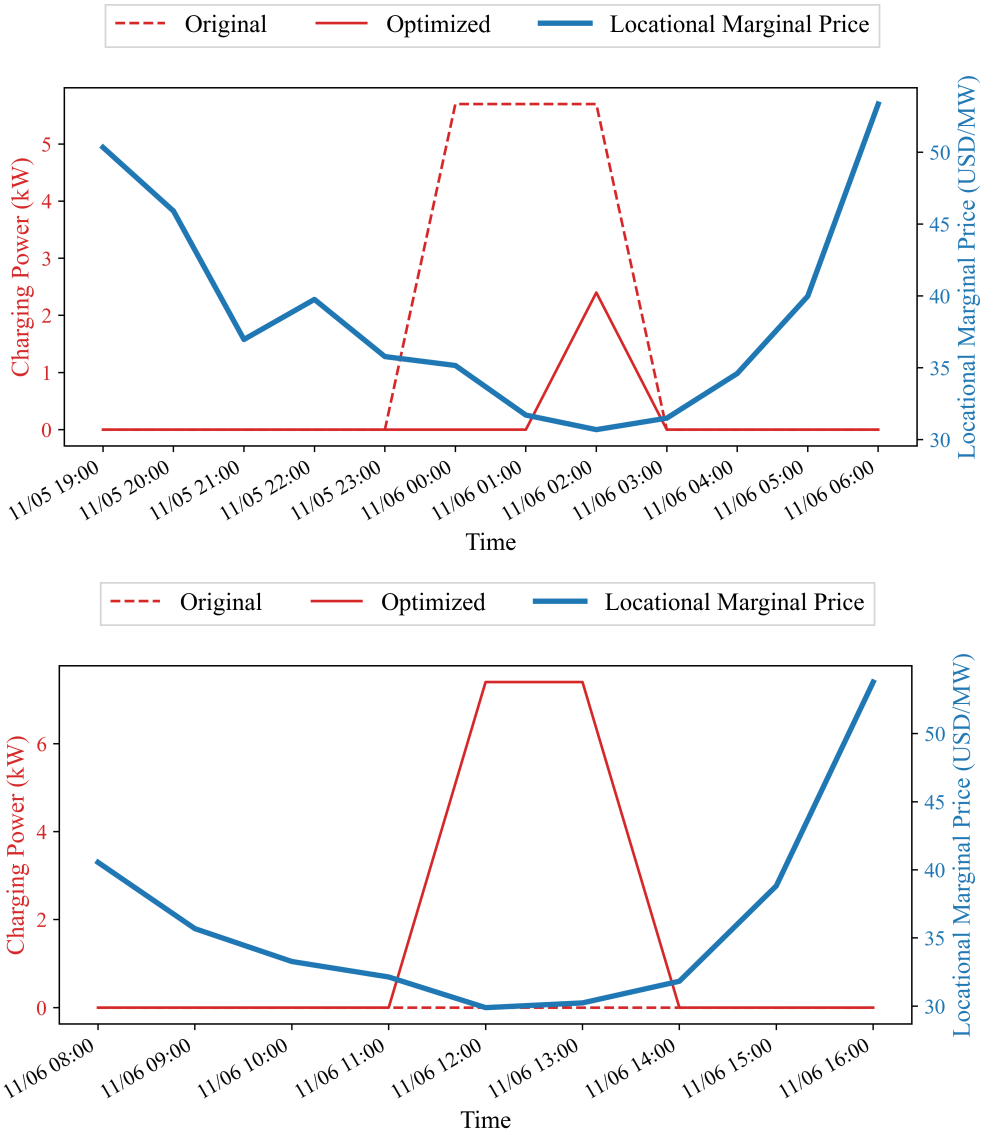

Figure 3.6: Sample Trajectories of Charging Powers in the Original Data and the Inter-Location Model Solution

Table 3.2: Inter-location Result with LMP Minimization

Item	Total	Home	'Away'	PGP2[2]	PGSI[3]
EV sample size (veh)	224	173	211	109	4
Total parking hours actual data (veh-hrs)	63,411	48,522	14,889	21,429	577
Total charging hours, actual data / optimized result (veh-hrs)	10,456 / 3,812	8,605 / 2,644	1,851 / 1,168	3,833 / 1,208	42 / 44
Total charging events, actual data / optimized result (events)	2,277 / 1,818	1,706 / 1,151	571 / 667	752 / 584	12 / 17
Average charging power, actual data / optimized result (kW)	2.3 / 5.6	2.1 / 5.6	3.4 / 5.7	1.9 / 5.5	6.8 / 6.2
Total hours with change in charging status due to optimization (veh-hrs)	12,944	10,309	2,635	4,621	86
Total change in LMP cost (US dollars, optimal cost - actual cost)	-369.5	-325.4	-44.1	-117.4	-7.1
Average change in LMP cost[4] (US dollars/veh-hrs)	-0.0059	-0.0067	-0.0030	-0.0055	-0.0123 [5]

We see that the inter-location model can schedule charging across multiple parking locations and hours, potentially recommending charging at locations and hours for lower LMP values. As seen in the top graph, the vehicle originally charged from midnight to 3:00 a.m., when the LMP cost was low. However, the model recommends that the vehicle be charged only shortly to exploit the lowest LMP cost at 2:00 a.m. in the first parking location, shifting the rest of the charging demand to the second parking location from 11:00 a.m. to 2:00 p.m., where the LMP cost was even lower for a longer period of time. Note that the optimization model has a hard constraint to meet the driver mobility needs. The model also ensures that the vehicle's state of charge is above a minimum level, $E_{min,i}$, at all times.

Table 3.2 presents the statistics for the inter-location model results with LMP minimization. The results are presented for the total, home locations, away locations, and two SubLAP regions. First, in total, we see that we had a smaller sample size of data for the inter-location model than for the fixed-location due to the data processing explained in Section 3.3. This suggests that, in practice, inter-location optimization will be more challenging

[2]Sublap example 1: Peninsula and Bay Area (PGP2)

[3]Sublap example 2: Sacramento and Sierra (PGSI)

[4]The denominator is the total parking hours in actual data, for instance 63,411 veh-hrs for the total.

[5]Though this result is presented for completeness, note that the sample size is only 4 vehicles and this result does not carry statistical significance.

than fixed-location optimization because of the data requirements for sequential and multi-location data. Additionally, the optimal solution charges vehicles at a lower number of hours and charging sessions, and the average charging power increases, compared to the actual behavioral data. This is because the optimization attempts to exploit lower-cost LMP hours by using its maximal charging power and avoids higher-cost LMP hours by reserving from charging. Therefore, the optimization result tends to decrease the total charging hours with more frequent charging instances and a higher average charging power.

Similar to the fixed-location model, the results shows a significant need to reschedule the charging sessions for better operation of the grid. The charging status changed from "idle" to "charging" or vice versa by the amount of 12,944 veh-hrs, which is even greater than the original charging duration of 10,456 veh-hrs. With this impact, the average LMP cost can be reduced by USD 369.5 dollars in total for 224 vehicles in a month, or USD 0.0059 per veh-hr. On average, the inter-location model produces about 2.36 times more LMP savings than the fixed-location model. This is because the inter-location model gives more freedom to reschedule the charging sessions and explore lower-cost LMP periods. In this model, the vehicles are recommended to change the charging hours, as well as the charging locations.

The results are compared for the home and 'away' locations in the third and fourth columns of Table 3.2. Since the drivers tend to park and charge longer at home, the total parking and charging hours are much larger at home than away, as well as the number of total charging events. However, the optimal solution reduces charging hours and charging sessions more significantly at home than away, possibly because the vehicles are located away from home (such as workplaces), when the LMP values are low during the day. We see that there is a larger LMP saving at home than 'away', first because there are originally more charging loads at home but also because the charging load is removed from home and added to the 'away' locations.

Different SubLAPs also experience different results from optimization, as exemplified in the last two columns of Table 3.2. Among the 12 SubLAPs, PGP2 is a SubLAP around the San Francisco Peninsula area with the largest reduction in LMP cost and PGSI is a SubLAP around Sacramento, California, with the smallest reduction of LMP cost. Though the LMP values are not significantly different among the SubLAPs at the same hours, the total charging load can be very different among the SubLAPs. For instance, the actual charging energy is 7,418.6kWh in PGP2, much larger than 285.9kWh in PGSI, during the optimized time period. A larger LMP savings is expected to occur in regions with larger charging loads.

The hourly variation in LMP savings is depicted in Figure 3.7. The LMP cost in the optimal solution is larger than in the actual data from 9:00 a.m. to 2:00 p.m., because the charging load is in these hours with low LMP values (California has high solar-energy generation and relatively low LMP costs in this period). The optimal solution suggests suppressing the charging of EVs when drivers are home from 3:00 p.m. to 8:00 a.m. the next day, and the LMP cost is greatly reduced in the afternoon. As a net outcome, the LMP saving from 3:00 p.m. to 8:00 a.m. is larger than the LMP increase from 9:00 a.m. to 2:00 p.m.

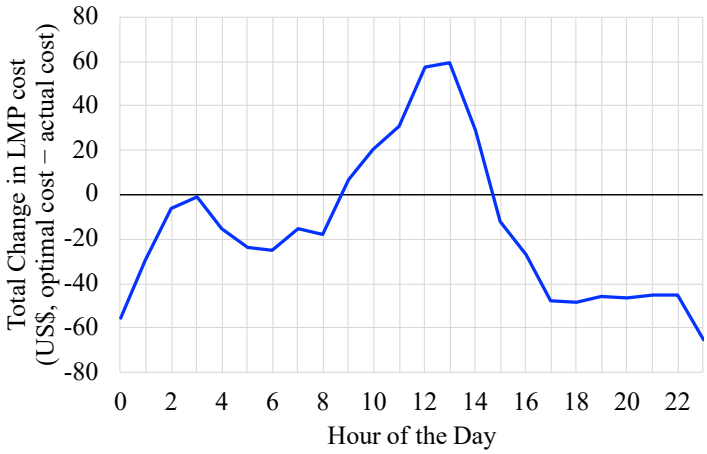

Figure 3.7: Hourly Variation in Total Change in LMP Cost

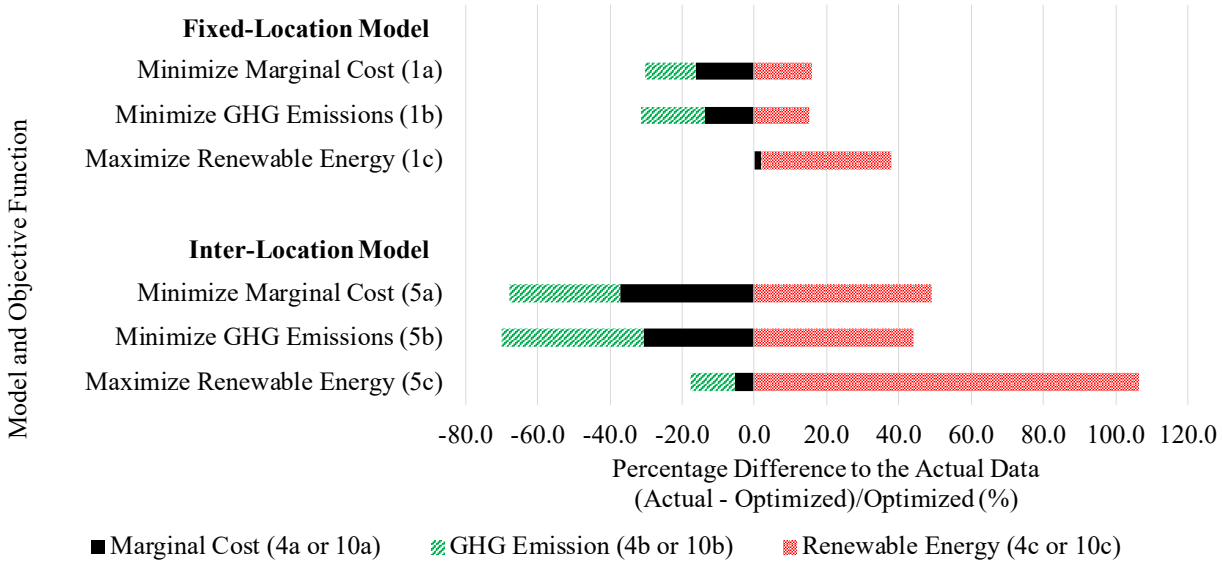

Figure 3.8: Comprehensive Comparison of Optimization Models and Objective Functions on their Economic and Environmental Performance (Percentage Difference)

Optimization With Various Objectives

We present a comprehensive analysis of the proposed models and objective functions to reschedule EV charging sessions and to improve electricity system operation. Figure 3.8 shows the results of the fixed-location and inter-location models with the three objective functions. (For the detailed results, refer to Table 3.3 in the Appendix The results are

shown as a percentage difference relative to the actual data. For instance, the percentage difference of the actual data from the LMP optimized result was calculated as (3.11), where $J_{\text{actual, LMP}}$ is the actual total LMP cost in the data.

$$\Delta_{\text{LMP}} = \frac{\widehat{J_{\text{agg, LMP}}} - J_{\text{actual, LMP}}}{J_{\text{actual, LMP}}} \cdot 100\% \tag{3.11}$$

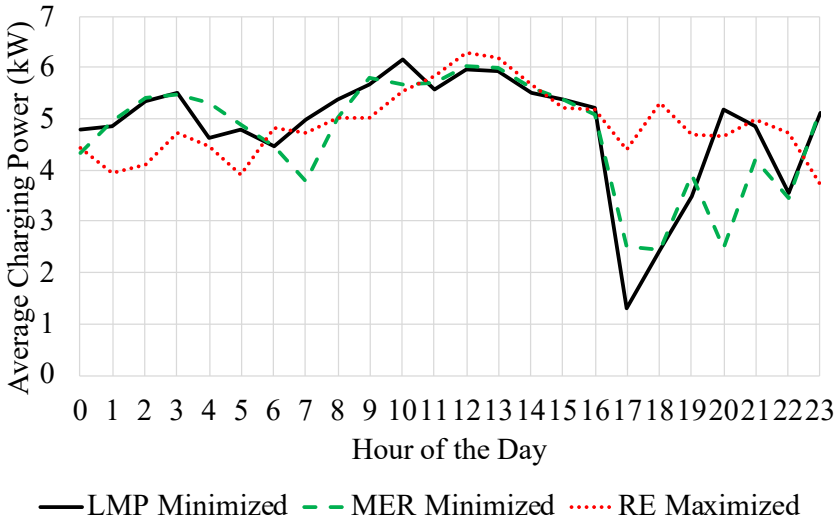

Figure 3.9: Optimal Charging Power of Various Objective Functions (Inter-location Model)

Next, we extend the comparison of the fixed-location and inter-location models from the previous section to two additional objective functions, i.e., minimizing the MER and maximizing the RE. Figure 3.8 shows that the inter-location model reduced the MER and increased the RE to a greater extent compared with the fixed-location model. However, the inter-location model will be more challenging to implement in practice than the fixed-location model because the inter-location model makes more assumptions, such as the availability of sequential data for a vehicle's multiple destinations, accurate prediction of the vehicle's energy consumption, and successful relocation of charging sessions. Though the fixed-location model brings a smaller benefit than the inter-location model in theory, its easier implementation may result in better performance than the inter-location model in real-world settings.

We also compare the performance of the LMP, MER, and RE objective functions. For each optimization model, we observe that minimizing the LMP and the MER resulted in a similar performance in the LMP, the MER, and the RE. This is understandable from Figure 3.1, where the LMP and the MER have a very similar pattern over a sample day. Note that the RE value is relatively high at the start of the evening peak for LMP and MER. For instance,

the RE ratio is around 0.3 to 0.6 from around 4:00 to 6:00 p.m. when the LMP and MER values are rapidly increasing. Therefore, maximizing the RE induces a substantial charging load during the peak hours of the LMP and the MER. Additionally, we see from Figure 3.8 that the RE-maximized solution increases the RE more than other solutions but does not largely improve the LMP or MER. This is understandable by observing Figure 3.9, where the optimal charging power to maximize the RE shows a different pattern to the charging powers to minimize the LMP or the MER. For instance, the RE-maximizing charging power is high at around 5 kW on average from 5:00 to 7:00 p.m., and the LMP-minimizing and MER-minimizing charging powers are much lower at below 3 kW. The start of the evening peak is a conflicting period because RE usage can be maximized with more charging but at a higher cost with rapidly increasing LMP and MER values. We observe that the fixed-location result for maximizing the RE results in a small increase in the LMP cost and a negligible increase in the MER.

Policy Implications

Based on these results, we make a recommendation on the design of an EV-charging rescheduling program that improves electrical-grid performance. Currently the system operators for electricity generation, transmission, and distribution are subjected to various regulations and policies. For instance, California's Renewables Portfolio Standard (RPS) regulates the renewable energy procurement (in terms of delivered energy in watt-hours) to be at least 60% of the total energy by 2030 for "all electric load serving entities" [65]. Additionally, major electric power-generators in California must participate in California's Greenhouse Gas Cap-and-Trade Program to control their climate-related pollutants [66].

Among the various motivations for the grid-operators to optimize EV charging, we recommend programs for rescheduling EV charging focusing on grid congestion and cost (with respect to the LMP values) or to the emission level (with respect to the MER values) because they not only reduce marginal costs and emissions but also increase renewable usage. When renewable energy is maximized, it can induce more charging load at the start of peak hours with rapidly increasing demand, high grid congestion, and high marginal emission rates. Maximizing renewable energy in optimal EV charging can bring a substantial benefit to certain operators subjected to control their RE use; however, it can increase the burden on controlling grid congestion and emissions. Note that the renewable energy use can be increased with deployment of energy storage system, though it is more costly to upgrade grid infrastructure in this way than through controlled EV charging [23].

Assuming that the regional grid operation stays unaffected by the EV charging demand and rescheduling, we estimate the maximum improvements for the grid operation for about 250 EVs in Tables 3.1 and 3.2. As EV charging operation solutions scale much higher in the future, however, relative to the goal of California in deploying 5 million zero-emission vehicles by 2030 [67], the optimal EV charging can bring more benefits to the grid, but the large demand of charging will clearly affect grid operations, potentially in profound ways as highlighted by the large-scale simulation studies cited above. Extending this work to

use growing amounts of real-world data to further evaluations of mass-scale EV charging optimization for improving the grid performance is the subject of future work.

In addition, we note that the current time-of-use (TOU) rate for EVs provided by PG&E for residential customers is not perfectly aligned with various goals of grid operation, such as reducing cost, reducing emissions, and increasing the use of renewable energy. For instance, on the PG&E "EV-B" plan in April 2021 [68], the energy cost is most expensive during the peak period at USD 0.56 per kWh from 2:00 p.m. to 9:00 p.m. However, this period may overlap with some hours with relatively low marginal cost, low marginal emissions, and high renewable energy around 2:00 p.m. to 4:00 p.m. (shown in Figure 3.1). Under some conditions, grid operators may thus want to vary particularly the start time and also potentially the end times of peak TOU pricing periods during certain seasons with the potential to more fully maximize the benefits of EV charge timing to grid operations.

3.5 Future Work

Potential future work on this topic is as follows. First, this analysis does not explore the impact of shifting EV charging loads for the residential and workplace utility customer bills. For instance, utility demand charges (peak usage charges applied to commercial customers) can be impacted for EV-charging facility operators when loads are shifted across time and space. It is possible that the peak power and demand charges would increase due to a higher peak power of charging facilities, making the facility operator worse off, while the energy system operator is made better off. A potential negative effect on the electrical grid customers must be evaluated and solved, possibly with adjustments to the TOU energy and power pricing from the utilities.

Second, the impact of optimal EV charging on the electrical grid from a mass-scale level of implementation is not analyzed here, though several other studies have done this with simulations of a large EV fleet projected in the future. Utility grid performance can be affected by shifting the charging loads of a large fleet of EVs, expected in the future where, for instance, California has a goal of achieving 5 million zero-emission vehicles by 2030 [67]. In future work, the sample of individual EVs can be increased to reflect larger EV populations in the future. The EV charging can be optimized, and the grid performance can be evaluated with electrical-grid-operation simulators such as PLEXOS at the transmission level and/or PyDSS at the distribution level, accounting for additional grid factors such as changes in generation dispatch and power-quality issues, related to the large amount of load that can then be shifted on a regional basis.

Third, the analysis estimates the upper bound on the benefits to the electrical grid, but the lower bound is also important to better understand and advertise an optimal EV charging program. In other work, we have analyzed cases with current constraints on away-from-home charging, but in the future we expect EV-charging availability in between the current levels and the ubiquitous availability of charging assumed here. Further, the various factors that influence the success rate of optimal EV charging can be analyzed, such as driver

compliance with the optimal charging schedule, uncertainty in driver response to their future trip plans, uncertain energy consumption during trips (due to speed, hills/grades, etc.), uncertain availability of chargers due to driver queuing, the potential impact of "power split" multi-port chargers, and mechanical or point-of-sale system failures. In future work, these factors can be parameterized to help further estimate the lower bound of the benefits. Behavioral surveys and focus groups and analysis of pilot studies on smart charging [69] can be used to better understand driver behavior and motivations in accepting a proposed optimal EV-charge-scheduling program. Additional key behavioral factors include driver adherence to planned departure times, driver propensity to plug in even when charging is not necessarily needed, and the statistical likelihood of sudden unplanned trips where the vehicles are unexpectedly disconnected.

3.6 Conclusion

In this research, we estimate the maximum potential gains to electrical-grid operators in shifting the time and location of charging a sample group of EVs. We fill a gap in the literature by proposing optimization models that schedule not only the time but also the location to charge the individual EVs among the locations that they visit. The models are applied to three objective functions, based on the easily measurable and immediately meaningful values to the grid operator, including the locational marginal price cost, the greenhouse-gas emission rate, and the renewable-energy ratio. This work overcomes the limitations of simulating or aggregating the driving and charging of EVs commonly found in the literature by using real data on a sample of individual, household-based EVs. Collaborating with an automobile company, a grid operator, and two grid-services and energy data-analytics companies, this research uses the driving and charging data of real individual EVs and the electrical grid data in the San Francisco Bay Area in California.

The results of the analysis shows a greater value in optimizing both the time and the location of charging EVs (inter-location model) than optimizing only the time of charging EVs (fixed-location model). However, the fixed-location optimal charging will be easier to implement in practice due to a simpler data requirement and a higher success rate from less uncertainty in trip demand and charging-schedule compliance. From the realistic estimation of the maximum benefits from optimal EV charging, it is recommended that grid operators consider the use of objective functions to reduce operational costs or marginal emission rates. These objective functions reduce grid operational costs and greenhouse-gas emissions, and they also increase renewable-energy usage. We do not recommend the maximization of renewable energy as a primary objective function as it can induce a higher load at the start of the evening peak, where renewable-energy generation is still high but where the energy load is ramping up with high marginal operation costs and emission rates. For the future work, the impact of shifting the EV-charging loads can be evaluated in terms of the residential and workplace utility bills for customers and the electrical grid performance. In addition, the lower bound of the benefits to the electrical grid from the optimal EV charging can be

Table 3.3: Comprehensive Comparison of Optimization Models and Objective Functions on their Economic and Environmental Performance

Model	Optimization	Performance Metric		
		Total LMP cost (US dollars)	Total MER (tons/kWh·kWh)[6]	Total RE (kWh)
Fixed Location	None (Actual Data)	1,892,127.3	22,851.2	18,540.4
	LMP Minimized	1,583,195.0 (-16.3%)	19,619.4 (-14.1%)	21,458.7 (15.7%)
	RE Maximized	1,928,675.7 (1.9%)	22,931.8 (0.4%)	25,156.9 (35.7%)
	MER Minimized	1,633,163.7 (-13.7%)	18,822.2 (-17.6%)	21,354.1 (15.2%)
Inter -Location	None (Actual Data)	1,211,738.6	14,492.2	11,987.8
	LMP Minimized	762,861.9 (-37.0%)	10,051.2 (-30.6%)	17,871.8 (49.1%)
	RE Maximized	1,146,037.2 (-5.4%)	12,728.3 (-12.2%)	24,745.9 (106.4%)
	MER Minimized	839,052.8 (-30.8%)	8,781.6 (-39.4%)	17,277.6 (44.1%)

estimated.

Appendix

Table 3.3 presents the detailed results of the fixed-location and inter-location models that optimize three objective functions, corresponding to Figure 3.8. Note that in the table, the performance metrics are the total resulting LMP cost, MER, and RE delivered. This result calculates the total values for optimizing the charging of approximately 250 EVs after a data cleaning process. To find the results per vehicle-hour, divide the results by the total parking hours of EVs in the data, which is 93,576 veh-hrs for the fixed-location results and 63,411 veh-hrs for the inter-location results.

[6]The MER parameter $C_{MER}(t)$ is given as rate in tons/kWh, which indicates how much tons of emission will be produced per kWh when an additional load is given to the system. We calculate the 'total MER' as the MER value multiplied by the charging energy in kWh. The limitation of this approach is the underestimation of marginal emission, as the MER value may increase as more load is given to the system.

Chapter 4

Flow-Aware Platoon Formation of Connected Automated Vehicles in a Mixed Traffic with Human-driven Vehicles

This chapter is based on the previously published article: Woo, S., & Skabardonis, A. (2021). Flow-aware platoon formation of Connected Automated Vehicles in a mixed traffic with human-driven vehicles. Transportation Research. Part C, Emerging Technologies, 133(103442), 103442, https://doi.org/10.1016/j.trc.2021.103442.

Connected Automated Vehicles (CAVs) bring promise of increasing traffic capacity and energy efficiency by forming platoons with short headways on the road. However at low CAV penetration, the capacity gain will be small because the CAVs that randomly enter the road will be sparsely distributed, diminishing the probability of forming long platoons. Many researchers propose to solve this issue by *platoon organization* strategies, where the CAVs search for other CAVs on the road and change lanes if necessary to form longer platoons. However, the current literature does not analyze a potential risk of platoon organization in disrupting the flow and reducing the capacity by inducing more lane changes. In this research, we use driving model of Cooperative Adaptive Cruise Control (CACC) vehicles and human-driven vehicles that are validated with field experiments and find that platoon organization can indeed drop the capacity with more lane changes. But when the traffic demand is well below capacity, platoon organization forms longer CAV platoons without reducing the flow. Based on this finding, we develop the *Flow-Aware platoon organization strategy*, where the CAVs perform platoon organization conditionally on the local traffic state, i.e., a low flow and a high speed. We simulate the Flow-Aware platoon organization on a realistic freeway network and show that the CAVs successfully form longer platoons, while ensuring a maximal traffic flow.

4.1 Introduction

Cooperative Adaptive Cruise Control (CACC) is a vehicle technology that brings promise of greater road capacities and improved energy efficiency without investing on the road infrastructure, such as additional lanes or ramp metering controllers. Vehicles equipped with this technology are henceforth termed Connected Automated Vehicles, or CAVs for short. These vehicles monitor their speeds and gaps relative to their lead vehicles, and automatically adjust their motions in response. Moreover, CAVs can communicate with others of their kind nearby in real time and at high frequencies. With this communication, vehicle accelerations, lane-change maneuvers and other driving decisions can be shared across vehicles without the perception errors and reaction times associated with human drivers. These capabilities enable smaller vehicle headways than were previously possible (and thus larger road capacities) [14] and smaller air drag, improving energy efficiency [15], [16], [31]. Note that the present research focuses on freeway setting to study the traffic impact of CAVs forming platoons without interruptions, such as signalized intersections.

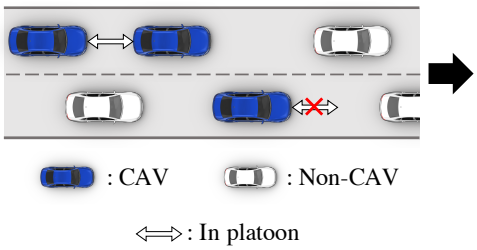

Figure 4.1: Challenges of CAVs at Low Penetration

Capacity gains are likely to be small, however, when the market penetration of CAVs is low in the early stage of implementation [13], [14], [70]. The sparse distribution of CAVs that randomly enter the road diminishes the probability of a CAV immediately following another of its kind, as shown in Figure 4.1. This introduces challenges when trying to form long platoons of CAVs so as to diminish the average headway in a traffic stream. To overcome this challenge, the CAVs can maneuver to organize the relative positions to each other on the road. The CAVs may have non-CAVs between them in the same lane or the CAVs may be in different lanes. A CAV can maneuver to follow another by accelerating, decelerating, or changing lanes. Then the gap between the consecutive CAVs must be reduced to form a platoon. In this present research, a term *platoon organization* is defined to describe the strategies for CAVs to maneuver on the road to form longer platoons.

Platoon organization has two potential impacts to the traffic. On the one hand, it can increase the number of CAVs in platoon, reducing the headways within the platoons and increasing the traffic capacity. On the other hand, it can induce more lane changes on the road that may disrupt the roadway flow [28]–[31]. In other words, it is possible to negate the gain in capacity from longer platoons by the flow disruption from the induced lane changes.

If platoon organization worsens capacity, it will be unfair for the society to suffer a lower capacity, while the drivers in CAVs enjoy the platooning benefits, such as fuel efficiency and driver comfort [15], [16], [31]. Unfortunately, no literature has analyzed the traffic capacity under platoon organization, considering the impact of lane changes.

Many researchers propose to promote CAVs to form longer platoons with dedicated lanes for CAVs, where only CAVs are allowed to travel in the designated lanes and increase the probability of forming a platoon. However, their results on capacity vary. Some argue that traffic capacity increases with platoon organization, but do not consider the realistic impact of lane changes [26], [27]. Ghiasi et al [26] analytically calculate that the capacity increases with dedicated lanes for CAVs, using a Markov Chain model. However, they assume that the CAVs enter the road already formed in longer platoons on the dedicated lanes and do not describe the impact of lane changes in capacity analysis. Hua et al [27] use Cellular Automata model to show that the traffic capacity increases for all levels of CAV penetration with dedicated lanes for CAVs, however the lane change model is simple and does not model its flow disruption.

Some do not model the disruptive impact of lane changes, but still show that the capacity can drop at low CAV penetration because the dedicated lanes for CAVs are under-saturated [71]–[74]. Talebpour et al [71] show that the throughput is smaller at low CAV penetration but higher at high CAV penetration, if the CAVs optionally use the dedicated lanes for CAVs. However, they use a game-theory based lane change model, which is to be calibrated in future research [75]. Chen et al [72] analytically calculate that the capacity decreases at low penetration with dedicated lanes for CAVs, but capacity increases if the dedicated lanes are optional for the CAVs. They use a formulation derived from a single-lane capacity, recommending a future study to consider the effect of lane changes in the formulation. Ye et al [73] show that throughput decreases in free-flow but increases in congestion at low CAV penetration, though their model does not describe the realistic impact of lane changes, such as the stochastic reaction of vehicles upstream of a lane-changing vehicle. Ma et al [74] show that the dedicated lanes for CAVs decrease capacity at low CAV penetration but increases it over 40% CAV penetration. However, they use modified Cellular Automata with a simple assumption for the CAVs to change lanes in a 'cooperative and instantaneous' manner.

Some model the impact of lane changes realistically, however do not analyze the traffic capacity under platoon organization [76], [77]. Zhong et al [76] use a CACC model (E-IDM) and a lane change model (MOBIL) that describe the flow disruption of lane changes. Xiao et al [77] implement an extensive model of lane change behavior [78], [79] and simulate a mixed traffic of CAVs and non-CAVs on a freeway network. However, the analysis on traffic capacity is missing. At low CAV penetration, both studies report poorer traffic performance with dedicated lanes for CAVs because those lanes are under-saturated. The dedicated lanes will be more saturated at higher CAV penetration, however both studies only use the same demand for all CAV penetration levels and do not analyze the traffic flowing at capacity at high CAV penetration. Note that Xiao et al [77] observed speed reduction in the dedicated lanes for CAVs due to the lane changes to enter and exit the dedicated lanes.

To the best of our knowledge, it is still unclear if and how platoon organization increases

or decreases the traffic capacity in a mixed traffic of CAVs and non-CAVs. To answer this question, we must analyze the traffic capacity, considering the impact of lane changes and using a platoon organization strategy that can saturate all lanes. Finally, it is necessary to design an operation strategy for CAVs to form longer platoons, while ensuring a maximal traffic flow.

In this chapter, we contribute to the current literature by revealing that platoon organization can reduce capacity and create congestion, by inducing lane changes that disrupt the flow. We use a driving model for CACC vehicle that is empirically verified from the real world data and conduct a sensitivity analysis on platoon organization at various traffic demands. We learn that when the demand is below capacity, platoon organization forms longer CAV platoons but does not reduce the flow. Based on this finding, we propose the *Flow-Aware strategy of platoon organization* that forms longer CAV platoons and ensures maximal traffic flow without a capacity drop. We validate the Flow-Aware strategy by simulating it on a realistic freeway network.

This chapter is structured as follows. In Section 4.2, we describe the microscopic traffic model to evaluate the traffic performance that considers the flow disruption of lane changes. We also propose a sample strategy of platoon organization that fully saturates all lanes at capacity. In Section 4.3, we present a preliminary study to validate that platoon organization can drop the traffic capacity with more lane changes. The main experiments include the sensitivity analysis on platoon organization at various flow levels and the validation of the performance of the Flow-Aware Platoon organization strategy. In Section 4.4, we describe the sensitivity analysis method, propose the Flow-Aware platoon organization strategy, and explain how we validate the Flow-Aware strategy on a freeway network. In Section 4.5, we present the results of the sensitivity analysis and show that the Flow-Aware strategy produces longer platoons without flow disruption. In Section 4.6, we highlight the findings and discuss the shortcomings of this chapter. Supplementary materials are given in the Appendix.

4.2 Research Approach

In this work, we will conduct experiments to evaluate the impact of CAVs under platoon organization on traffic capacity and develop CAV operation strategy that forms longer platoons and ensures a maximal traffic flow. Although the CAVs are not readily available in real settings, their driving behavior has been modeled via small scale experiments [80]–[83]. We will use the driving models to simulate the mixed traffic of CAVs and non-CAVs. The following describes four features of a traffic model that this research requires to emulate platoon organization in a mixed traffic with CAVs and non-CAVs. The traffic models from the current literature are classified based on the four features and we will select one model to be used in the present study. In addition, we develop a sample strategy of platoon organization that saturates all lanes at capacity at all CAV penetration rates, eliminating the factor on capacity drop from unsaturated lanes.

Table 4.1: Literature on Microscopic Simulation of Mixed Traffic

Publications	Mixed Traffic of CAVs and Non-CAVs	Microscopic Model	Lane Change Model	Calibration with CAV Experiments
[26], [72], [86], [87]	✓			
[88], [89]	✓	✓		
[90]	✓	✓	✓	
[13], [79]	✓	✓	✓	✓

Microscopic Traffic Model

We need four features in a traffic model to emulate platoon organization. First, the model needs to describe mixed traffic composed of CAVs and non-CAVs at various penetrations of CAVs. Second, the model needs to be microscopic so as to depict the detailed operation of platoon organization, such as the number of CAVs in platoon. Third, the model needs to describe the impact of lane changes on roadway flow. Fourth, the model needs to be calibrated with experiments involving CAVs.

The current literature on traffic models for the mixed traffic is organized according to the four features in Table 4.1. Among them, the model in [13], [79] for mixed traffic satisfies the model requirements of the present study. Note that this model was calibrated for human and automated driving behaviors in [80], [84] and the lane change model for human drivers was calibrated in [85]. This present work uses the model in [13] as it is an improved model from [79]. Table 4.2 provides a list of parameters to be used in simulations from the model in [13], used in the current study. In this chapter, we simulate the traffic using Aimsun with external behavior enabled by MicroSDK.

Note that in this model, simulated drivers in CAVs change lanes manually because we assume the CAVs are equipped with CACC, which automates the car-following maneuvers but not the lane-change maneuvers. The model assumes that CAVs have a weaker motivation for discretionary lane changes than human drivers do because the CAVs prefer to stay in a platoon than to seek higher speeds. Note that when the brake is applied manually, the automatic car-following mode of a CAV is deactivated immediately and reverts to the manual driving mode. Additional description of the model is given in the Appendix.

Platoon Organization Strategy

We develop a platoon organization strategy called pseudo dedicated (PD) lane, to avoid under-saturating a particular lane at high flow, which occurs with dedicated lanes for CAVs at low CAV penetration. Similar strategies have been proposed in the literature that allow both CAVs and non-CAVs on particular lanes [71], [72]. Figure 4.2 explains the PD lane strategy in comparison to the dedicated lane for CAVs.

Table 4.2: Microscopic Driving Parameters

Parameters	Non-CAV	CAV
Average Reaction Time	1.2s	0.4s
Average Headway	1.25s	0.6 - 1.1s [80]
Minimum Space Gap	1.5m	1.5m
Average Maximum Acceleration	-4m/s^2	-4m/s^2
Average Maximum Deceleration	1.5m/s^2	1.5m/s^2
Vehicle Length	4m	4m
Average of Maximum Desired Speed	110km/h	110km/h
Inter-platoon gap	NA	1.5s
Maximum Number of Vehicles in a Platoon	NA	10

The left figure shows the dedicated lane for CAVs, where only CAVs are allowed to travel on a dedicated lane. At low penetration, the dedicated lane will not be saturated and worsen capacity.[1] To isolate the effect of inefficient lanes in capacity estimation, the dedicated lane strategy is not used in this present study. In the pseudo dedicated (PD) lane strategy shown in the right figure, CAVs are motivated to maneuver into the PD lane for platoon organization, but non-CAVs are not banned from it. As the penetration increases, non-CAVs will naturally move away from the PD lane as more CAVs start to crowd it and travel slower than other lanes. We assume that due to the higher probability of forming long platoons, the CAVs have a stronger motivation to stay in the PD lane than the non-CAVs. This strategy thus guards against under-utilization of the lane at low market penetration of CAVs.

Throughout this study, we define *baseline capacity*, as the traffic capacity of a given penetration rate of CAVs that do not perform platoon organization. We assume that a CAV can change a lane when it is the leader of a platoon. If a follower in a platoon were to change a lane, it must brake and split from its present platoon before the lane change. When a CAV immediately follows another CAV, it automatically starts to form a platoon. Note that we acknowledge a potential error in simulating the platoon organization with an assumption that the CAVs change lanes manually by the human drivers. Future work to improve this issue is described in Section 4.6 Discussion.

[1]The dedicated lanes for CAVs also pose an equity issue because a portion of public road is allocated only to people who can afford expensive CAVs [76].

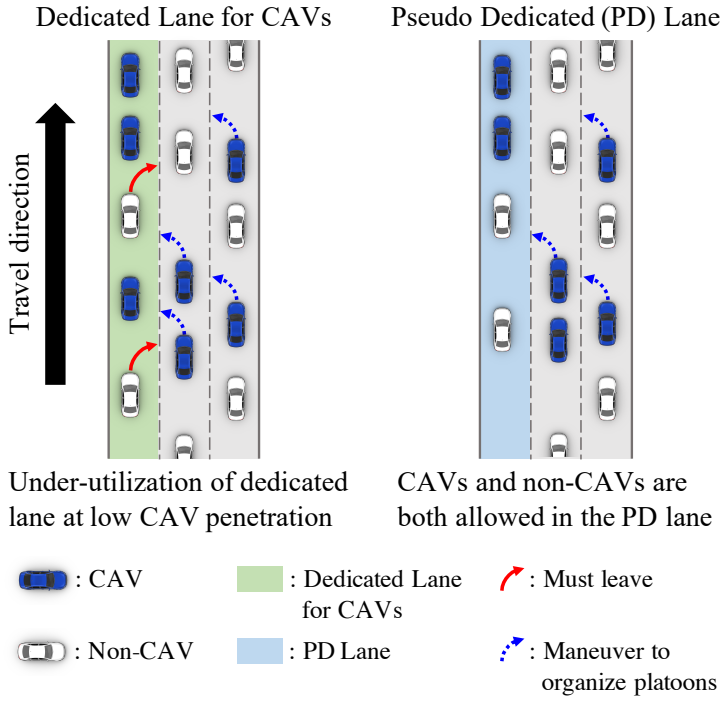

Figure 4.2: Pseudo Dedicated (PD) Lane

4.3 Preliminary Study: Capacity Drop with Platoon Organization

This section describes a preliminary study to test if platoon organization can drop capacity by inducing lane changes to disrupt the flow. We simulate the traffic on a homogeneous road segment, comparing the capacity with and without platoon organization. The results validate that when the CAVs change lanes to organize platoons, the traffic flow is reduced and the bottleneck capacity drops.

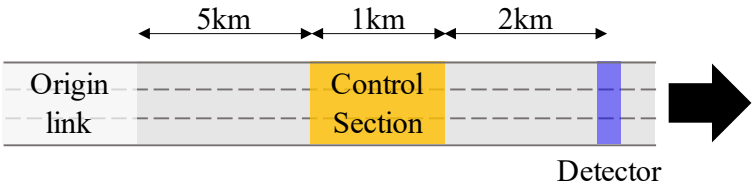

Figure 4.3: Homogeneous Road Segment

This simulation experiment uses a 3-lane homogeneous road segment; refer to Figure 4.3. After the first stretch of 5km, CAVs execute the PD lane strategy in the control section of 1km. As the PD lane strategy allows both CAVs and non-CAVs, the PD lane is not regulated by infrastructural measures (like egress and ingress points) but by the lane targeting behavior of the CAVs. In the control section, the CAVs in short platoons change lanes to the PD lane to form longer platoons. CAV penetration levels are tested from 0 to 100% at increments of 25%. Vehicles are generated according to a Poisson process of a traffic demand rate and vehicle types are decided with Bernoulli trials with the probability of CAV type as the CAV penetration.

The simulation procedure is as follows. First, the baseline capacity is estimated for each CAV penetration level without platoon organization. To estimate the baseline capacity, the traffic demand to the origin link as shown in Figure 4.3 is increased until a queue forms in the link. The baseline capacity is measured as the maximum sustained flow discharged from the queue over a 60-minute period, at the flow detector shown in Figure 4.3. Second, the capacity of a bottleneck that forms in the control section under the platoon organization strategy is estimated for each penetration level of CAVs. For one hour, an input flow that produces the baseline capacity flow is used. The first 20 minutes is used as a warm-up period to create a stationary flow. In the next 40 minutes, the PD lane strategy is implemented in the control section and a queue forms in the control section. The bottleneck capacity is measured after the warm-up period for the 40-minute period as the maximum sustained flow discharged from the queue, measured at the flow detector.

Figure 4.4 shows the capacity with and without platoon organization as functions of CAV penetration. The baseline capacity without platoon organization is shown in a black solid line, which increases slowly at low CAV penetration up to 50% and increases rapidly at higher penetration. We see that platoon organization worsens the capacity, as shown in a red dotted line. At 25% CAV penetration, the PD lane strategy produces a capacity (around 1800 vph/lane) even less than the baseline capacity at 0% penetration (around 2000 vph/lane). This means that capacity with CAVs under platoon organization can be worse than the capacity with no CAVs. At 50% CAV penetration, the PD lane results in a capacity around 2000 vph/lane, similar to the baseline capacity at 0% penetration. In other words, the PD lane can cancel the capacity improvement from having CAVs comprise half the vehicles on the road.

This negative effect of platoon organization on traffic capacity can be interpreted with queuing theory, which tells us that the output rate of a closed system is bounded by its input rate regardless of the dynamics in the system. We can define our closed system as the homogeneous road segment in Fig. 4.3, with one input and one output. Applying the theory to our experiment, it is impossible for the CAVs to increase the discharge flow (i.e., output rate) further than the input flow of baseline capacity (i.e., input rate), no matter how they maneuver on the road (i.e., platoon organization). Therefore, platoon organization cannot improve the capacity further than the baseline capacity. This must be true for any design of the closed system, whether it is a homogeneous road segment or a freeway network with multiple entrances and exits. Furthermore, the theory explains the capacity drop under

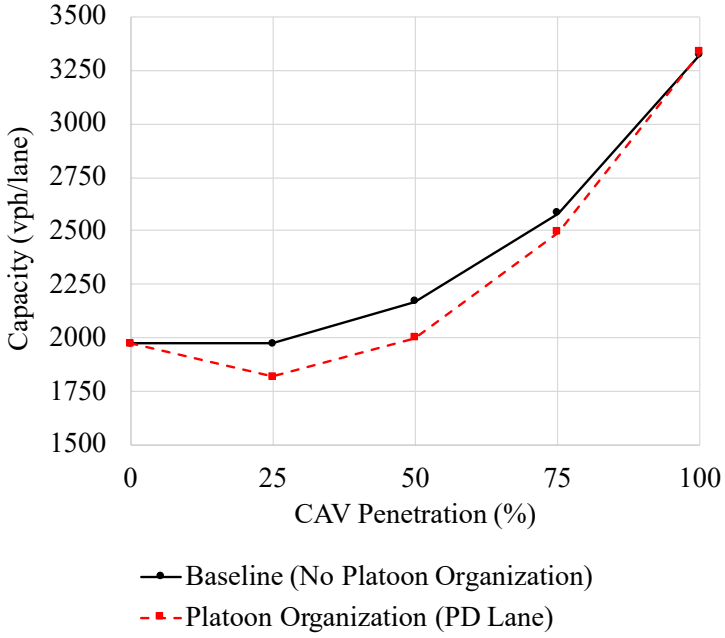

Figure 4.4: Capacity for Varying Market Penetrations of CAVs

platoon organization. When a system is at capacity, the output rate is bounded by the service rate. If the service rate decreases, the output rate decreases. Applying to our experiment, the platoon organization reduces the service rate by inducing more lane changes and inefficiently using the road. Therefore, the discharge flow (i.e., output rate) decreases. There is a need to prevent capacity drop under a naive implementation of platoon organization but still provide platooning benefits to the CAVs.

4.4 Methodology

In this section, we describe the methodology of the two following experiments. We first conduct a sensitivity analysis on platoon organization with various levels of traffic demand, which provides the evidence for proposing the Flow-Aware strategy of platoon organization. The Flow-Aware strategy of platoon organization ensures a maximal traffic flow and forms longer CAV platoons. Next, we validate the performance of the Flow-Aware strategy on a simulated freeway network.

Sensitivity Analysis on Traffic Demand

The sensitivity analysis explores how platoon organization impacts the traffic performance under various levels of traffic demands. We use the homogeneous road segment in Fig. 4.3,

where the CAV penetration is fixed at 50% and input demands are tested at 1000, 1500, 2000, and 2500 vph/lane. The traffic is simulated for an hour. For the first 20 minutes, no platoon organization is implemented as a warm-up period. For the next 40 minutes, the PD lane strategy is be implemented in the control section. The simulation results are compared in terms of the average number of lane changes, the average platoon length, the platooning probability, and the discharge flow, which are all measured after the first 20 minutes.

We define the *platoon length*, $L_i(\tau)$, as the number of CAVs in a platoon that the i-th CAV is a member of at time τ. The *average platoon length*, $\bar{L}$, is defined as the following:

$$\bar{L} = \frac{\sum_{i=1}^{N_{\text{CAV}}} \max_{\tau}\{L_i(\tau)\}}{N_{\text{CAV}}}, \tag{4.1}$$

where N_{CAV} is the total number of CAVs that travel the network. The average platoon length computes the average of the maximum platoon lengths experienced by individual CAVs. Note that a CAV has $L_i(\tau) = 1$ if it is not connected to any other CAVs at time τ.

We also define the *platooning probability*, P_{P}, as the probability that a CAV is ever in a platoon with other CAVs as the following:

$$\mathsf{P}_{\text{P}} = \mathsf{P}(\max_{\tau}\{L_i(\tau)\} > 1), \quad \forall i \in [1, N_{\text{CAV}}]. \tag{4.2}$$

We calculate the average number of lane changes as the total number of lane changes that occur in the network, divided by the total count of vehicles including CAVs and non-CAVs. The discharge flow is measured at the flow detector.

Flow-Aware Platoon Organization

We propose the *Flow-Aware strategy of platoon organization* that forms longer platoons of CAVs but ensures maximal traffic flow. The main idea is for the CAVs to execute platoon organization conditionally on the traffic state. Since the traffic demand may be difficult to monitor in practice, we use speed and count to estimate the traffic condition and determine whether platoon organization is allowed. We do not enforce a specific location or time for the CAVs to change lanes for platoon organization, which is often how the ingress and egress points of special purpose lanes are operated. Instead, we determine if the traffic can absorb the disturbance from lane changes, based on the constant thresholds of flow and speed as ρ_q (vph/lane) and ρ_v (km/hr), respectively.

Under the Flow-Aware strategy, a CAV gathers the average flow and speed measurements from the detectors nearby, as $\bar{q}$ and $\bar{v}$, respectively. The CAV evaluates the condition in Equation (4.3) to check if the flow measure is lower than the threshold and the speed measure is higher than the threshold.

$$\{\bar{q} < \rho_q\} \wedge \{\bar{v} > \rho_v\}. \tag{4.3}$$

If the condition is satisfied, we assume that the traffic can 'handle' disturbances like lane changes and the CAV performs platoon organization, such as the PD lane strategy.

Note that when the threshold values, ρ_q and ρ_v, are poorly calibrated, the Flow-Aware strategy may induce lane changes in traffic with high demand and create unnecessary congestion. As the CAV penetration increases, the flow threshold, ρ_q, can be increased because the capacity improves with more CAVs and traffic can absorb more shock at a given demand level. Also the threshold values must be calibrated for different road networks as their geometries and capacities vary. For the freeway network studied in this chapter, we calibrated the values of ρ_q and ρ_v for each CAV penetration rate by trial and error. We have reduced ρ_q and increased ρ_v so that an increase of lane changes does not decrease the network discharge flow significantly.

Validation of Flow-Aware Platoon Organization on Freeway

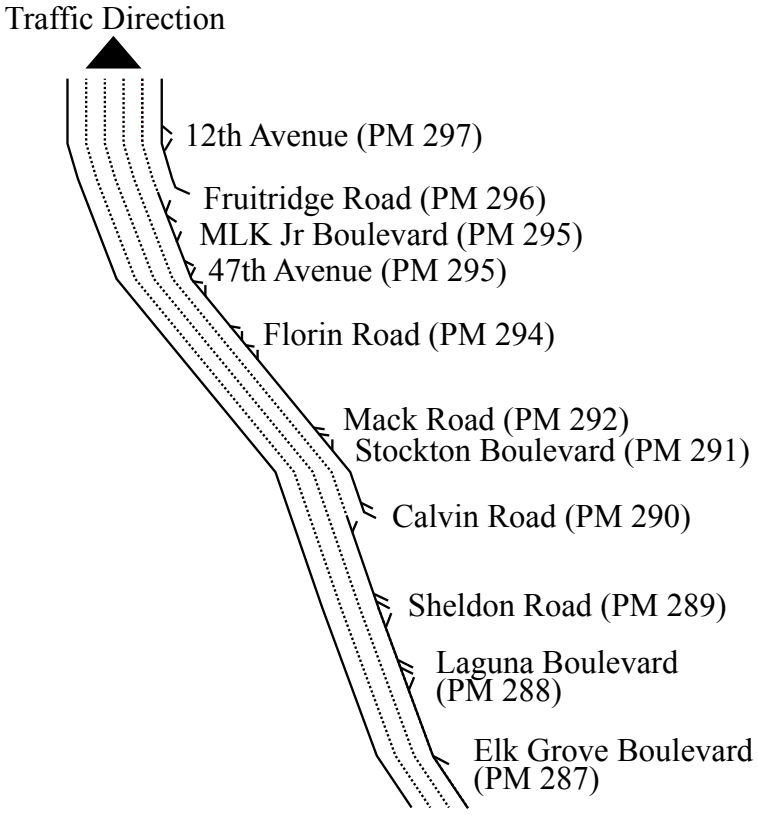

Figure 4.5: Simulated State Route 99 in Sacramento, California (PM: Post-mile)

We test the Flow-Aware platoon organization strategy proposed in Section 4.4 by simulating it on a realistic freeway network and evaluating if the strategy ensures a maximal

traffic flow and forms longer CAV platoons. We use the freeway network shown in Fig. 4.5. This freeway network is the State Route 99 in Sacramento, California, covering the Northbound 10-mile (approximately 16-km) corridor. It starts at Elk Grove Boulevard and ends at 12th Avenue, including 16 on-ramps and 11 off-ramps. The network originally includes High-Occupancy Vehicle lanes, however we exclude them in this chapter to isolate their effect on the capacity analysis. The traffic is simulated from 5AM to 9AM as the morning peak typically lasts from 6:30AM to 9AM. Bottlenecks recurrently form in the network, including one downstream of Elk Grove Boulevard due to high traffic demand. The free flow speed is around 105km/h for the freeway.

We assume that on the freeway network, detectors are installed around 50 meters upstream of all on-ramps and off-ramps, as well as around 50 meters downstream of all on-ramps. The detectors aggregate data in 5-minute intervals and broadcast the latest information on the vehicle count and speed. The CAVs can gather information from detectors located within 1 to 2km range. This allows the CAVs under the Flow-Aware strategy to evaluate the local traffic condition with Equation (4.3) and perform platoon organization accordingly. We also assume detectors to be installed at the end of each exit of the freeway, including the off-ramps and the main lanes after 12th Avenue, to collect the total discharge flow of the freeway network.

We test the CAV penetration from 0 to 100% at increments of 20%. At each entrance to the freeway, vehicles are generated according to a Poisson process. At each exit of the freeway, vehicles depart the freeway as Bernoulli trials with a departure rate depending on the exit. We simulate three cases - the traffic without platoon organization as a baseline, the traffic with the PD lane strategy from Section 4.2 with no consideration to the traffic condition, and the traffic with the Flow-Aware strategy from Section 4.5 with PD lane.

There is no rigidly defined sections of ingress and egress to the PD lane because the PD lane allows both CAVs and non-CAVs. In the original PD lane strategy, the CAVs consider the leftmost lane of entire freeway as the PD lane. This strategy is an example of a naive platooning operation of the CAVs. In the Flow-Aware PD lane strategy, the traffic condition in Equation (4.3) flexibly limits the execution of platooning maneuvers of CAVs. This strategy is an example of a platooning operation that controls the CAVs with awareness to the traffic flow.

The simulation procedure is as follows. First, we find the baseline demand for each CAV penetration level without platoon organization. We increase the network demand by scaling it with a constant factor, which we call *demand scale*, until the speed contour shows the recurrent bottlenecks of the freeway network. Second, we use the baseline demand to simulate the network traffic under the PD lane strategy and the Flow-Aware PD lane strategy, at each CAV penetration rate. The results are compared in terms of the network discharge flow, average number of lane changes, and average platoon length. The network discharge flow is measured as the sum of discharge flows measured at the detectors on the end of each freeway exit. Note that we analyze the results for each CAV penetration rate (not between different penetration rates), because the baseline traffic is simulated at different demand scale for each penetration rate.

4.5 Results

In this section, we find that at a low demand the CAVs can form longer platoons without reducing the discharge flow under platoon organization. Therefore, the Flow-Aware strategy conditions the CAVs to perform platoon organization only under a low demand condition so that the output flow does not drop with the induced lane changes. We confirm the performance of the Flow-Aware strategy of platoon organization by simulating the traffic on a realistic freeway network. We show that the Flow-Aware strategy ensures a maximal traffic flow and enhance CAV platooning performance.

Sensitivity Analysis on Traffic Demand

Table 4.3: Platoon Organization at Various Traffic Demands (Homogeneous Road in Fig. 4.3, CAV Penetration of 50%)

Traffic Demand (vph/lane)	Average Number of Lane Changes (count/veh) [2]		Average Platoon Length, $\bar{L}$, (CAV count)		Platooning Probability, P_P [3]		Discharge Flow (vph/lane)		
	B	PO	B	PO	B	PO	Q_B	Q_{PO}	Δ [4]
1000	0.05	0.49	2.6	5.0	0.73	0.89	1006.3	1006.7	0.04%
1500	0.07	0.51	3.0	5.1	0.74	0.89	1483.4	1478.3	-0.34%
2000	0.05	0.53	2.8	5.1	0.74	0.89	1961.7	1924.6	-1.89%
2500	0.04	0.56	3.3	5.4	0.78	0.91	2260.6	2045.0	-9.54%

B: Baseline, PO: Platoon Organization, Q_B: Baseline discharge flow, Q_{PO}: Discharge flow under PO

We analyze the traffic performance at various traffic demands under the PD lane strategy on a homogeneous road segment at CAV penetration of 50%. Table 4.3 presents the average numbers of lane changes, average platoon lengths, platooning probability, and the discharge flows at various traffic demands. Note that without platoon organization, a demand of 2,000 vph/lane results in a high but free flow. Without platoon organization, a demand

[2] Note that the number of lane changes increase both for CAVs and non-CAVs.

[3] Note that the platooning probability P_P around 0.75 in the baseline makes sense for the baseline traffic of 50% CAV penetration. Here is a simple explanation. Denote the CAV penetration rate as P_{CAV}. Then the platooning probability, P_p can be expressed as the probability that given the subject vehicle is a CAV, its leader and/or follower vehicle is a CAV, i.e., $P_p = 1 - (1 - P_{\mathrm{CAV}})^2$. For $P_{\mathrm{CAV}} = 0.5$, $P_p = 0.75$. The simulation well approximates this probability.

[4] Note that $\Delta = \dfrac{Q_{QO} - Q_B}{Q_B}$

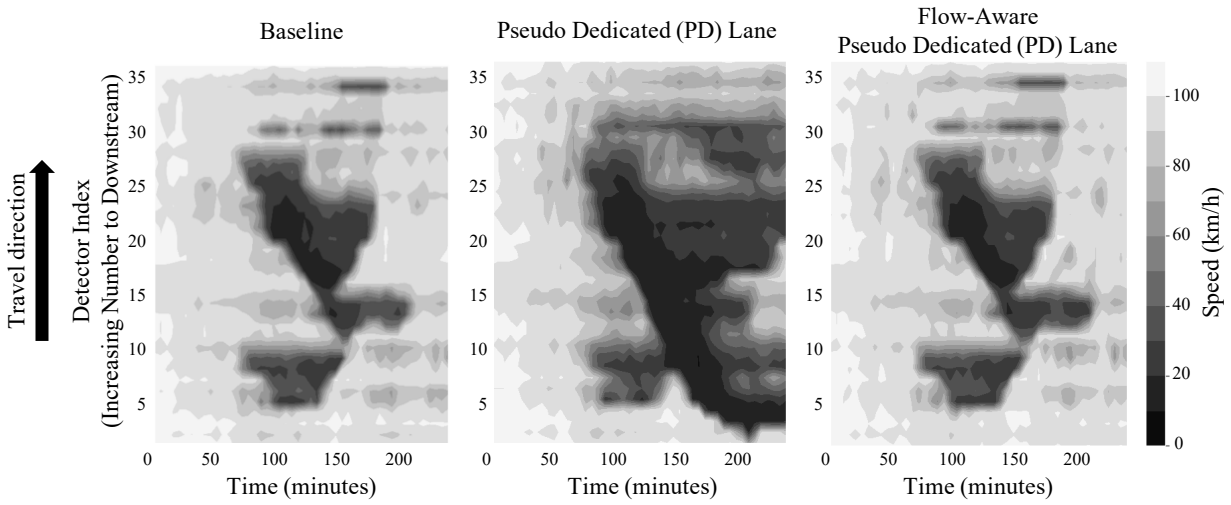

Figure 4.6: Speed Contours (Freeway Network in Fig. 4.5, CAV Penetration of 40%): the PD lane strategy reduces the speed significantly from the baseline, whereas the Flow-Aware strategy with PD lane does not.

at 2,500 vph/lane results in the capacity flow. We see that at all demand levels, platoon organization induces more lane changes (with higher average numbers of lane changes in the third column) and enhances platooning performance (with higher average platoon lengths in the fifth column and higher platooning probability in the seventh column). However, platoon organization affects the discharge flow very differently depending on the traffic demand; refer to the last column of Table 4.3.

At low demands (1,000 to 1,500 vph/lane), more lane changes under platoon organization do not change the discharge flow significantly. At moderately high demand (2,000 vph/lane), the lane changes under platoon organization breaks down the traffic and reduces the discharge flow by 1.89%. At a high demand (2,5000 vph/lane), the discharge flow reduces significantly by 9.5%. Therefore, platoon organization can be used when there is low demand, where the disturbance from lane changes can be absorbed easily. At a moderately high demand (2,000 vph/lane), platoon organization can also break down the traffic and cause a bottleneck. At a high demand, platoon organization is ill-advised. The Flow-Aware platoon organization is designed with this mechanism by estimating the traffic demand based on speed and count measurements and elongating the platoon lengths without flow disruption.

Flow-Aware Platoon Organization on a Freeway Network

We emulate the traffic on a freeway network to validate the strategy of Flow-Aware platoon organization. We assume that the CAVs perform PD lane strategy when the condition in Equation (4.3) is met at any post-mile of the freeway. We first validate the traffic simulation

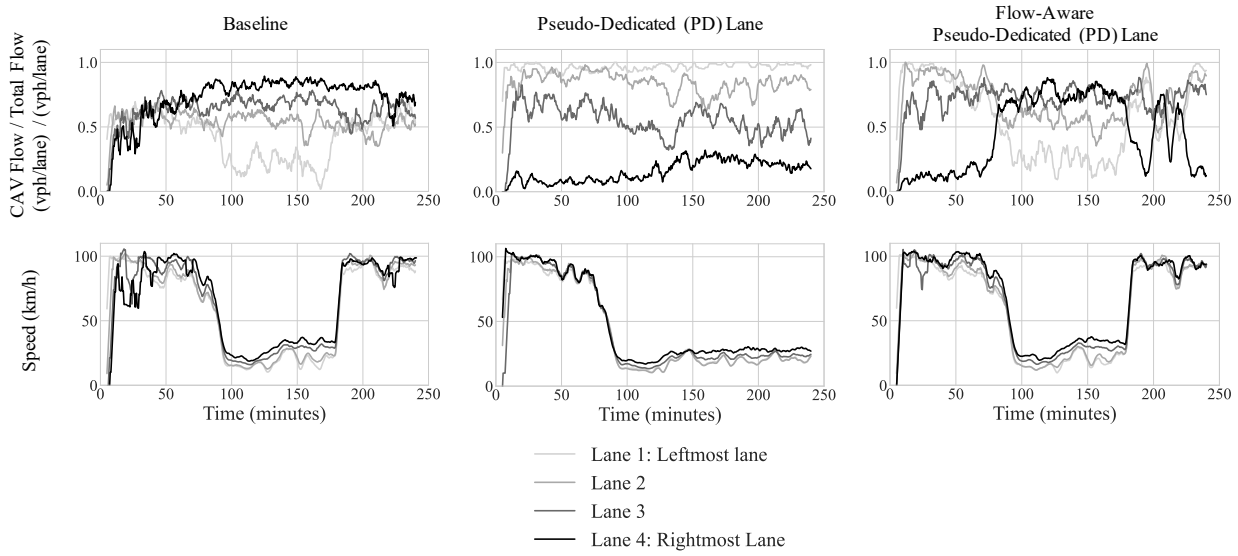

Figure 4.7: Ratio of CAV Flow to Total Flow (Freeway Network in Fig. 4.5, CAV Penetration of 40%): the PD lane strategy distributes the CAVs to the leftmost PD lane regardless of the traffic condition, whereas the Flow-Aware strategy with PD lane only does so in a free flow.

with Fig. 4.6, which shows three speed contours for the baseline, the PD lane strategy, and the Flow-Aware PD lane strategy at 40% CAV penetration. The simulation time is on the x-axis and space on the y-axis with detector index of an increasing number downstream. We observe that bottlenecks form in the baseline due to traffic demand larger than the network capacity. The PD lane strategy induces lane changes of CAVs regardless of the traffic condition and reduces speed significantly compared to the baseline. However, the Flow-Aware PD lane strategy results in a speed contour very similar to the baseline, indicating that the speed is not reduced significantly due to the platoon organization.

We also observe the distribution of CAVs across the lanes under platoon organization with Fig. 4.7 to validate the simulation further. The figure describes the traffic with 40% CAVs in the section immediately upstream of the second on-ramp at Florin Road (shown in Fig. 4.5) or around the detector index 22 (shown in Fig. 4.6), where a bottleneck queue reduces the speed significantly. In Fig. 4.7, the x-axis is the simulation time, the y-axes for the top figures show the CAV flow ratio, i.e., the ratio of the flow of CAVs to the flow of all vehicle types, and the y-axes for the bottom figures show the speed per lane. The lanes are differentiated by the shade, where the lightest line corresponds to the leftmost (or PD) lane. The baseline, the PD lane strategy, and the Flow-Aware PD lane strategy are shown on the left, the center, and the right, respectively.

The baseline results on the left column show that when this section is in a bottleneck queue from around 80 minutes to 170 minutes, the CAVs are more concentrated on the right

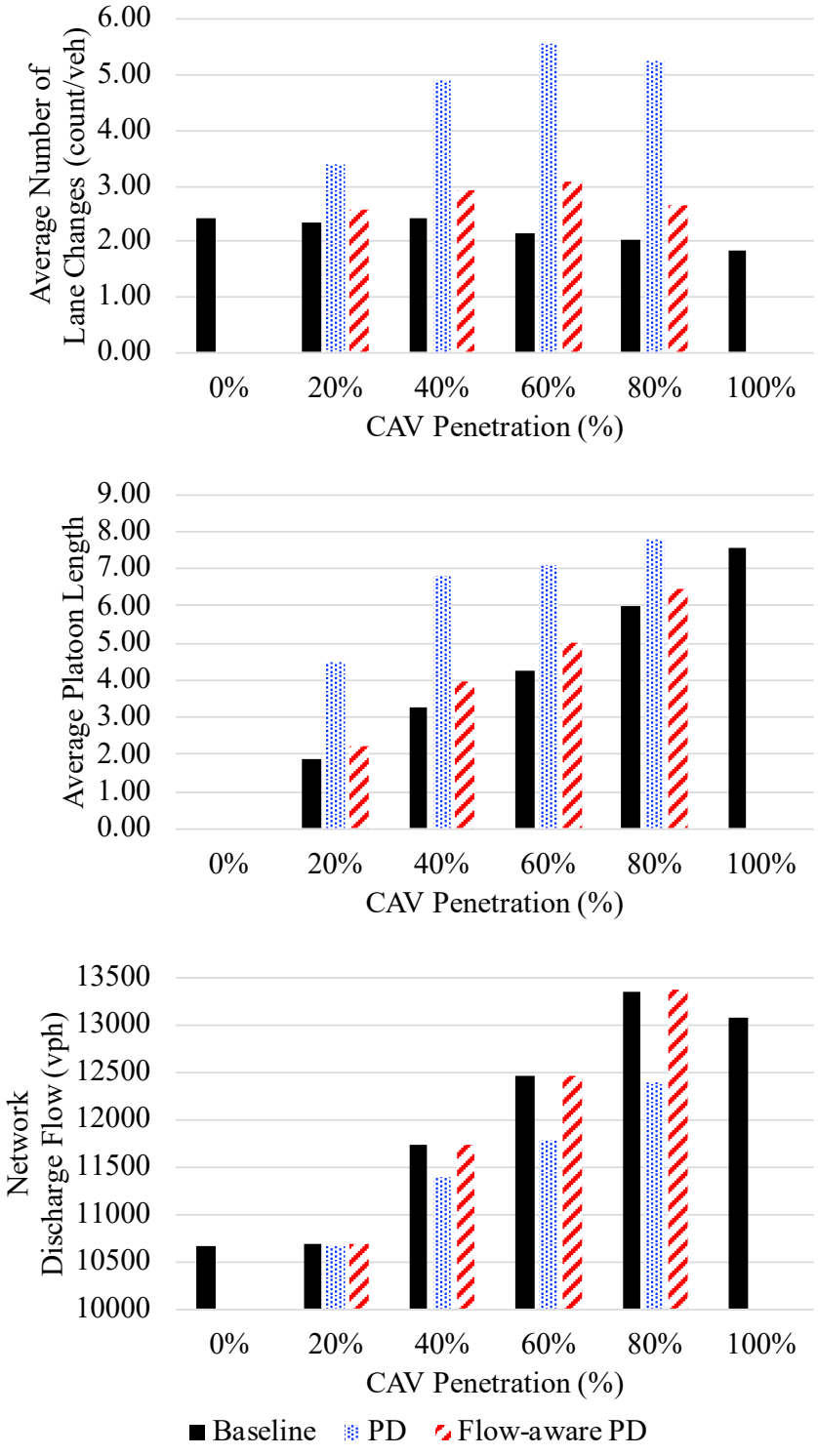

Figure 4.8: Increase of Lane Changes and Platoon Lengths without Flow Disruption under Flow-Aware Platoon Organization

lanes than the left lanes. The CAVs make up about 80% in the rightmost lane, whereas they make up about 20% in the leftmost lane. This is possibly because the human driven vehicles have moved toward the leftmost lanes to avoid the conflict with the on-ramp merging flow.

The results under PD lane strategy on the center column show an opposite distribution of CAVs across lanes to the baseline results. The CAVs are highly concentrated in the leftmost PD lane all throughout the simulation. With the naive implementation of the PD lane strategy, the CAVs join the PD lane regardless of the traffic condition. This cause a longer duration of congestion.

The results under the flow-aware PD on the right column are interesting, as the distribution of CAVs are similar to the PD lane during free flow, but similar to the baseline during congestion. During free flow (when speed is around 100km/h), the CAVs concentrate on the leftmost PD lane as the traffic condition in Equation (4.3) is met and their maneuvers do not disrupt the flow. During congestion (from around 80 minutes to 170 minutes), the CAVs refrain from platoon organization because the condition in Equation (4.3) is not satisfied. The CAVs concentrate higher in the right lanes like in the baseline case. Because of the restricted lane changes to the PD lane under congestion, the queue is dissipated at a similar time to the baseline.

We evaluate the traffic performance under the Flow-Aware platoon organization in comparison to the baseline and the PD lane strategy with Fig. 4.8. The detailed values for the figure are found in Table. 4.4 in the Appendix Section 4.6. Three figures present the average number of lane changes, average platoon length, and the network discharge flow, as functions of CAV penetration rates. At each penetration rate, the solid black bar shows the baseline result, the blue dotted bar shows the PD lane result with no condition on traffic, and the red dashed bar shows the result of Flow-Aware strategy with PD lane. Note that there is no result for the PD lane strategy and the Flow-Aware PD lane strategy for 0% and 100% CAV penetration rates because no CAV needs to be organized for longer platoons. The average platoon length is not applicable at 0% CAV penetration. The demand scales are 100%, 100%, 110%, 117%, 125%, and 127% for CAV penetration rates of 0%, 20%, 40%, 60%, 80%, and 100%, respectively.

The top figure in Fig. 4.8 shows that more lane changes are induced under both PD lane strategy and the Flow-Aware PD lane strategy, compared to the baseline. The PD lane strategy naively induces more lane changes than the Flow-Aware strategy, without checking on the flow conditions. The middle figure in Fig. 4.8 shows the PD lane strategy increases the platoon length the most, but the Flow-Aware PD lane strategy also significantly increases the average platoon length (by 8 to 20% as shown in Table. 4.4).

The bottom figure in Fig. 4.8 shows the network discharge flow. Compared to the baseline, the PD lane strategy significantly reduces the network flow (up to 7% at 80% as shown in Table. 4.4). However, the Flow-Aware PD lane strategy does not decrease the network flow significantly (only up to 0.1% as shown in Table. 4.4). The Flow-Aware PD lane strategy successfully forms longer platoons while ensuring the maximum level of traffic flow. In other words, the CAVs can form longer platoons without trading off the level of traffic flow. Agreeing with the preliminary analysis in Section 4.3, platoon organization does increase the

network flow further than the baseline.

Note that the network discharge flow in the baseline is lower at 100% than at 80%. Under the current simulation settings, the CAVs form and remain in a platoon if possible. The preference of CAV drivers to choose between forming a platoon and traveling in a faster lane is not well modeled or calibrated in this study; please refer to future work in Section 4.6) Discussion. At full CAV penetration, the CAVs form platoons soon after entering from the on-ramps because they find other CAVs immediately and stay in platoon on the right main lanes. So the highly dense traffic on the right lanes create conflicts with other merging flows downstream, resulting in a lower discharge flow than 80% CAV penetration. This issue is out of scope for the current study, as we compare the baseline at each CAV penetration rate, not across different penetration rates. However, please refer to [91] for further investigation on the need for a merging assistance system for a mixed traffic with CAVs and non-CAVs.

4.6 Discussion

In this chapter, we examine the potential problem of disrupting the traffic flow and causing unnecessary congestion with a naive platooning operation of CAVs. At low penetration, the CAVs will not deliver a large gain in the traffic capacity and the fuel economy because they are likely to form only few, short platoons. The CAVs can operate under a *platoon organization* strategy, where they can maneuver to follow other CAVs on the road by changing lanes and form longer platoons. However, a poorly designed strategy of platoon organization can deteriorate the traffic capacity by inducing lane changes that disrupt the flow. We explore this issue by implementing the realistic driving models of CACC and human-driven vehicles, which are validated by field experiments and model the disruptive effects of lane changes. The key findings from this research are as below.

- CAVs can form longer platoons by platoon organization, but may induce more lane changes on the road. At low traffic demand, the induced lane changes do not affect the traffic performance significantly as the traffic flows below capacity. However at high traffic demand, the induced lane changes can drop the capacity and create unnecessary traffic congestion.

- We propose the *Flow-Aware strategy of platoon organization* as a solution to enhance CAV platooning without degrading the traffic performance. Under the strategy, we estimate if the traffic can absorb the disturbances from additional lane changes by measuring the local flow and speed. If flow is below and speed is above the given thresholds, the CAVs execute platoon organization. If not, the CAVs refrain from platoon organization and avoid traffic disruption. We simulate the Flow-Aware strategy of platoon organization on a realistic freeway network (State Route 99 in California) and show that CAVs under this strategy indeed form longer platoons with no disruption to the traffic flow.

- The traffic capacity cannot increase further by forming longer CAV platoons on the road and reducing the headways within the platoons. Based on the queuing theory, an output flow is bounded by the input flow in a closed system. However, the input flow is composed of CAV platoons that are not longer, as platoon organization is yet to be performed. Therefore, the output flow is bounded by the input flow, i.e., the capacity cannot increase further by the maneuvers of CAVs on the road.

The CAVs may be motivated to form longer CAV platoons regardless of the capacity increase, due to the energy efficiency improvement [92]. There is an ongoing research to validate the improvement of energy efficiency in passenger vehicles by driving in platoons. For instance, Altinisik et al experimented with a platoon of two passenger cars and found a significant reduction in air drag in the leading vehicle [15]. Kaluva et al computed that a longer platoon reduced the average air drag coefficient of the platoon, saving energy [16]. Also, Liu et al show that vehicles driving in connectivity can improve traffic stability and fuel efficiency [31]. To facilitate the formation of long CAV platoons in a mixed traffic, we advocate for the Flow-Aware strategy of platoon organization to be implemented.

We believe our work can improve. In this study, we assume that lane changes are executed manually by human drivers in CAVs. It may be difficult for human drivers to implement the Flow-Aware strategy of platoon organization, which is based on the measurement of the local traffic condition. Because we do not know how well the human drivers will execute the platoon organization strategy, the estimated traffic performance may be biased. This bias can be overcome by assuming that the lane changes will be automated in the future and applying a model for the automated lane changing to execute the platoon organizations strategy. There is an on-going research on the lateral controller for automated vehicles. Although most works focus on safety and efficiency [93], some develop automated lane change controllers that consider the traffic flow. For instance, Wang et al [94] propose a centralized controller for cooperative lane changes that explicitly models the movement of vehicle upstream in the target lane. Their controller reduces the braking and waiting times of upstream vehicles following the lane-changing vehicle. The model for automated lane changing can replace the human-driving model for lane changing and better estimate the traffic impact of platoon organization.

Also, we lack the model to capture the preference of CAV drivers in choosing between traveling in a long CAV platoon or traveling in a faster lane without a platoon. It is possible that the adjacent lane of a CAV presents a higher probability of forming longer platoons, but flows at a lower speed than the current lane. It is also possible that the adjacent lane of a CAV flows faster than the current lane, but the CAV is travelling in a platoon already. In this chapter, we assume that under the PD lane strategy, the CAVs change lanes to reach the PD lane regardless of the speed difference between the current lane and the target lanes (although if the target lane is very crowded, the CAV is less likely to succeed in joining the target lane). A proper model of the CAV behavior in choosing between driving in a platoon and driving faster will better estimate the induction of lane changes under platoon organization. However, we would like to note that the Flow-Aware PD lane strategy is

designed with a condition of the local speed in Equation (4.3). A CAV performs platoon organization only when all lanes have a very high speed (above 90km/hr in this chapter). Therefore, the lack of a preference model between a longer platoon and a faster speed plays an insignificant role in the validation results of the Flow-Aware strategy.

There are many ways to improve the Flow-Aware strategy of platoon organization. First, we calibrated the threshold values, ρ_q and ρ_v, in Equation (4.3) by trial and error. We used only one value of flow threshold (vph/lane) for the entire network at a given CAV penetration, though the shock of lane changes may be absorbed differently at locations with various road geometries. Future research can design methods to calibrate the thresholds in a systematic manner that can be applied to various roads geometries.

Second, we assumed the availability of local measurements on vehicle count and speed and used these data to evaluate the condition in Equation (4.3). In practice, such data may not be available so that the CAVs need to use other sources of data to find if local traffic can absorb the shock of more lane changes. It's also possible that more sophisticated data will be available, such as individual vehicle data like gap, acceleration, and desired lane to travel. Different sources of data can be used to represent the traffic state for the Flow-Aware strategy of platoon organization with improved formulation of the condition in Equation (4.3).

Third, we can add sophistication to the Flow-Aware strategy, for instance by developing a learning controller that better models the complex dynamics of how a lane change can impact the traffic flow. The algorithm can model the traffic flow outcome of a lane change given various states measured by the sensors in CAVs, such as current gap, speed, acceleration, lane, and platoon length. This controller can replace the heuristic condition developed in the Equation (4.3) and perhaps allow a longer platoon length than the Flow-Aware PD lane strategy. A useful resource is 'Flow', an open-source deep learning platform developed in University of California, Berkeley, which supports microscopic traffic simulation as an environment [95].

In addition, the evaluation of the energy efficiency with platoon organization is missing in this chapter. It is possible that platoon organization will improve the energy efficiency of individual CAVs, while they systematically deteriorate the energy efficiency by creating congestion. If so, the Flow-Aware strategy must be implemented not only to ensure maximal traffic flow but also to avoid energy inefficiency as a whole. Future research must investigate the energy efficiency trade-off between individual vehicles and the traffic system under various operation scenarios of CAVs.

Appendix

The Microscopic Traffic Model

This section briefly describes the microscopic traffic model from [13] used in this study. The model has car-following algorithms and the lane-change algorithms. The car-following

algorithms are defined separately for human driving and automated driving with CACC. The algorithm for human drivers calculates the desired acceleration as the minimum of three values – acceleration from Newell's simplified car following model [96], Intelligent Driver Model's free flow acceleration [97], and Gipps acceleration with safe distance [98]. The algorithm for automated vehicles calculates the acceleration from a model calibrated with experimental data of production vehicles instrumented with CACC [84].

The lane-change algorithms in this model are similar for human driving and automated driving with CACC because the CACC does not provide automation for lane-changing task. In other words, human drivers in both CACC and non-CACC vehicles perform lane-change movements manually. However, the motivation for discretionary lane changes are different between the human driver and the CACC vehicles. The CACC vehicles is assumed to have a stronger motivation to stay in a platoon than to seek for higher speeds. In addition, the algorithms can emulate the complex lane-change behaviors, such as anticipatory lane changes in response to a slow speed downstream, cooperative behaviors to slow down to increase a gap for the lane-changers, and recovery responses after letting in a lane-changer with smaller reaction times and headway.

Supplementary Results on Flow-Aware Platoon Organization

Table. 4.4 presents the detailed results visualized in Fig. 4.8. PD indicates the PD lane strategy without considering the traffic state. Flow-Aware PD indicates the Flow-Aware strategy of PD lane that considers the traffic state by condition in Equation (4.3).

[5]In parenthesis is the percentage difference to the baseline result, i.e., (Current result - Baseline) / Baseline · 100%.

Table 4.4: Increase of Lane Changes and Platoon Lengths without Flow Disruption under Flow-Aware Platoon Organization (Supplementary Result to Fig. 4.8)

CAV (%)	Network Demand Scale Factor	Test Case	Network DischargeFlow (vph) [5]	Average Number of Lane Changes (count/veh)[5]	Average Platoon Length, $\bar{L}$, (CAV count)[5]
0	100%	B	10,675.8	2.40	NA
20	100%	B	10,687.3	2.35	1.87
		PD	10,675.8 (-0.1%)	3.40 (+45.0%)	4.47 (+138.9%)
		FPD	10,687.8 (+0.0%)	2.58 (+9.7%)	2.25 (+20.0%)
40	110%	B	11,739.8	2.40	3.28
		PD	11,402.0 (-2.9%)	4.90 (+103.9%)	6.81 (+107.2%)
		FPD	11,733.8 (-0.1%)	2.93 (+22.0%)	3.94 (+20.0%)
60	117%	B	12,449.3	2.15	4.27
		PD	11,780.3 (-5.4%)	5.55 (+157.6%)	7.12 (+66.6%)
		FPD	12,446.8 (-0.0%)	3.06 (+42.2%)	4.98 (+16.6%)
80	125%	B	13,347.0	2.03	5.97
		PD	12,378.8 (-7.3%)	5.24 (+157.9%)	7.78 (+30.4%)
		FPD	13,356.8 (+0.1%)	2.66 (+30.9%)	6.47 (+8.5%)
100	127%	B	13,069.0	1.82	7.55

B: Baseline, PD: Pseudo dedicated lane strategy, FPD: Flow-Aware pseudo dedicated lane strategy

Chapter 5

Conclusions

This dissertation explores critical problems from developing technologies without considering their impact on other related systems. Specifically, we identify the potential problems from vehicle electrification and automation in the energy grid, the charging infrastructure, and the traffic network. We propose the solutions by analyzing the real-world data, developing optimization models, and simulating the operation of mobility infrastructure. We show that our solutions help the infrastructure perform better with advanced vehicle technologies. We summarize the contributions of this dissertation as the following.

5.1 Research Contributions

This dissertation addresses three unintended problems from vehicle electrification and automation on the mobility infrastructure and proposes solutions via connectivity, modeling, and control.

Pareto optimal planning of an EV charging facility

In Chapter 2, we solve a challenging problem of planning an electric vehicle (EV) charging facility to simultaneously enhance the quality of service in charging and reduce the capital and operation costs. We develop a robust optimization model to find the sizing of a charging facility that can reliably satisfy the random charging demand. We study the impact of two demand management strategies, a local energy storage system and a rescheduling method of the EV charging sessions, to reduce the time-varying cost of the electrical grid consumption that penalizes a high demand peak. We analyze the complex relationships among the EV charging schedule, the capital and operation costs of the facility, and the electrical grid pricing and explain how to achieve the Pareto optimality in the service quality and the cost in planning an EV charging facility.

Optimal EV charging for electric grid benefits on a regional scale

In Chapter 3, we estimate the maximum potential gains to the electrical grid operation from managing the charging schedule of an EV fleet on a large regional scale. Our approach is novel in that we shift the charging sessions not only in time but also in the location. We propose the optimization models to reschedule various performance metrics of the grid operation, such as the cost, the renewable energy mix, and the greenhouse gas emissions. We estimate the gains to the electrical grid using the real driving and charging data of individual vehicles and the real grid operation data in the San Francisco bay area, California. We recommend an optimal rescheduling solution for the grid operators.

Platooning operation of CAVs for traffic flow performance

In Chapter 4, we identify a potential problem of disrupting the traffic flow by naively operating the Connected Automated Vehicle (CAV) platoons in mixed traffic with human-driven vehicles. This problem is critical as most literature recommends a CAV operation strategy without investigating its impact on the traffic flow. We study various strategies to form CAV platoons and simulate their impact on the traffic flow using a microscopic driving model and realistic parameters. We validate that the CAVs can severely disrupt the traffic flow and cause unnecessary congestion by changing lanes to form long platoons. We propose an effective strategy for CAVs to be 'aware' of their current traffic conditions regarding flow and speed measurements and form long platoons accordingly. We conclude that this flow-aware operation strategy forms longer CAV platoons while ensuring a maximal traffic flow.

5.2 Future Research

We believe that the research in this dissertation can be extended. In the following, we explain the possible next steps in detail.

Incorporation of human behavior

It is important to understand human behavior and its uncertainty for successfully implementing the proposed algorithms.

- In Chapters 2 and 3, we assume the perfect compliance of drivers to rescheduling the EV charging sessions in time and the location. Due to this unrealistic assumption, we may be overestimating the benefits of rescheduling to the charging infrastructure and the energy grid. There is an ongoing study on modeling and inducing a desirable behavior, such as [69]. Modeling the human behavior will help parametrize the success in rescheduling the EV charging sessions and estimate the impact of rescheduling more accurately.

- Human behavior is also critical when modeling the CAVs and their impact on the traffic. Although the CAVs can automate driving maneuvers, such as car-following and lane changes, it is uncertain how the humans in the CAVs and the human drivers around CAVs will respond to such maneuvers. The humans in the CAVs may override the automated controls due to personal preference or unexpected risk. Human drivers may also exhibit different behavior around CAVs than around other human drivers. In Chapter 4, we use the most realistic models of CAVs and human drivers from the literature. However, we assume that people will prefer to travel in a long CAV platoon to enhance fuel efficiency and driving comfort. People may prefer specific lanes and behave differently in real life. We must improve the modeling of human behavior as CAVs grow in the market.

Modeling of the future infrastructure

This dissertation evaluates the impact of vehicle electrification and automation on the mobility infrastructure, which is assumed to remain the same. However, the infrastructure may evolve as the mobility paradigm shifts.

- In Chapters 2 and 3, we assumed the operating conditions of the energy grid, such as the electricity pricing, renewable energy mix, and greenhouse gas emission rates, to remain constant. If the EVs become more widely adopted with an energy load that can significantly change the shape of the current demand, the energy grid may react to such change. The grid operator may impose a different business model or a pricing scheme specifically for the EVs or even upgrade the infrastructure. We must explore how the energy grid operators plan to adjust to the load to depict the interaction between the grid and the EV population on a mass scale and accurately estimate the impact of vehicle electrification on the energy grid.

- In Chapter 4, we assume that the transportation infrastructure and driving policies remain unchanged regardless of the increase in Autonomous Vehicle (AV) population on the road. However, there is an extensive discussion on building the infrastructure and policies that can facilitate the safe and efficient implementation of AVs [99], [100]. We do not know how the future traffic network will look like, especially as we already see some differences in the planning and expectations across cities on how the AVs will shape our future [101]. For instance, most cities (64%) in the US did not have any transportation plans related to AVs by January 2019, whereas San Francisco had a transportation plan in 2017 that incorporates AVs to achieve various goals, such as increase of street safety and mitigate traffic congestion [101]. Therefore, we must pay close attention to how the AVs are implemented and strategically plan the operation strategies of AVs accordingly to achieve safety and efficiency.

Assessment of practical challenges

It is critical to assess the practical challenges of implementing the proposed algorithms in this dissertation.

- In Chapter 2, we omit the discussion on the difficulty of installing local energy storage in an EV charging facility, though certain physical limitations on the electrical setup must exist on site.
- In Chapters 2 and 3 we do not explore the practical tasks in rescheduling of EV charging sessions. There are many issues to discuss, such as designing the driver's interface for informed decisions and choosing the type of device to use for active engagement with the drivers. The legal agreements are also critical to consider, for instance, to compensate for a failure to meet a charging demand and protect drivers' privacy with shared information.
- In Chapter 4, we do not explain how the drivers in CAVs will perceive or accept the lane change controls on a freeway. To implement a CAV operation strategy, one must decide whether to display the information on a vehicle console, use an audio message, or share the CAV control information with other vehicles.

Bibliography

[1] *World Vehicle Population Rose 4.6% in 2016*. https://wardsintelligence.informa.com/WI058630/World-Vehicle-Population-Rose-46-in-2016. Accessed: October 14th, 2021.

[2] *Inventory of U.S. Greenhouse Gas Emissions and Sinks: 1990–2019*. Tech. rep. Apr. 2021. URL: https://www.epa.gov/ghgemissions/inventory-us-greenhouse-gas-emissions-and-sinks.

[3] *Traffic Safety Facts: Overview of Motor Vehicle Crashes in 2019*. Tech. rep. Dec. 2020. URL: https://crashstats.nhtsa.dot.gov/Api/Public/Publication/813060.

[4] *Global EV Outlook 2020*. Tech. rep. June 2020. URL: https://www.iea.org/reports/global-ev-outlook-2020.

[5] *Fast Facts U.S.Transportation Sector Greenhouse Gas Emissions 1990-2017*. Tech. rep. United States Environmental Protection Agency, June 2019. URL: https://nepis.epa.gov/Exe/ZyPDF.cgi?Dockey=P100WUHR.pdf.

[6] Nadine Rauh, Thomas Franke, and Josef F. Krems. "Understanding the Impact of Electric Vehicle Driving Experience on Range Anxiety". In: *Human Factors: The Journal of the Human Factors and Ergonomics Society* 57.1 (Aug. 2014), pp. 177–187. DOI: 10.1177/0018720814546372. URL: https://doi.org/10.1177/0018720814546372.

[7] Quan Yuan, Wei Hao, Haotian Su, Guanwen Bing, Xinyuan Gui, and Abolfazl Safikhani. "Investigation on Range Anxiety and Safety Buffer of Battery Electric Vehicle Drivers". In: *Journal of Advanced Transportation* 2018 (June 2018), pp. 1–11. DOI: 10.1155/2018/8301209. URL: https://doi.org/10.1155/2018/8301209.

[8] Theo Lieven. "Policy measures to promote electric mobility – A global perspective". In: *Transportation Research Part A: Policy and Practice* 82 (Dec. 2015), pp. 78–93. DOI: 10.1016/j.tra.2015.09.008. URL: https://doi.org/10.1016/j.tra.2015.09.008.

[9] Dale Hall and Nic Lutsey. *Emerging Best Practices for Electric Vehicle Charging Infrastructure*. Oct. 2017. URL: https://theicct.org/sites/default/files/publications/EV-charging-best-practices_ICCT-white-paper_04102017_vF.pdf.

[10] Eric W. Wood, Clement L. Rames, Abdulkadir Bedir, Noel Crisostomo, and Jennifer Allen. *California Plug-In Electric Vehicle Infrastructure Projections: 2017-2025 - Future Infrastructure Needs for Reaching the State's Zero Emission-Vehicle Deployment Goals*. Tech. rep. Mar. 2018. DOI: 10.2172/1430826. URL: https://doi.org/10.2172/1430826.

[11] Till Gnann, Simon Funke, Niklas Jakobsson, Patrick Plötz, Frances Sprei, and Anders Bennehag. "Fast charging infrastructure for electric vehicles: Today's situation and future needs". In: *Transportation Research Part D: Transport and Environment* 62 (July 2018), pp. 314–329. DOI: 10.1016/j.trd.2018.03.004. URL: https://doi.org/10.1016/j.trd.2018.03.004.

[12] Nele Rietmann, Beatrice Hügler, and Theo Lieven. "Forecasting the trajectory of electric vehicle sales and the consequences for worldwide CO2 emissions". In: *Journal of Cleaner Production* 261 (July 2020), p. 121038. DOI: 10.1016/j.jclepro.2020.121038. URL: https://doi.org/10.1016/j.jclepro.2020.121038.

[13] Hao Liu, Xingan (David) Kan, Steven E. Shladover, Xiao-Yun Lu, and Robert E. Ferlis. "Modeling impacts of Cooperative Adaptive Cruise Control on mixed traffic flow in multi-lane freeway facilities". In: *Transportation Research Part C: Emerging Technologies* 95 (Oct. 2018), pp. 261–279. DOI: 10.1016/j.trc.2018.07.027. URL: https://doi.org/10.1016/j.trc.2018.07.027.

[14] Steven E. Shladover, Dongyan Su, and Xiao-Yun Lu. "Impacts of Cooperative Adaptive Cruise Control on Freeway Traffic Flow". In: *Transportation Research Record: Journal of the Transportation Research Board* 2324.1 (Jan. 2012), pp. 63–70. DOI: 10.3141/2324-08. URL: https://doi.org/10.3141/2324-08.

[15] Armagan Altinisik, Onur Yemenici, and Habib Umur. "Aerodynamic Analysis of a Passenger Car at Yaw Angle and Two-Vehicle Platoon". In: *Journal of Fluids Engineering* 137.12 (Aug. 2015), p. 121107. DOI: 10.1115/1.4030869. URL: https://doi.org/10.1115/1.4030869.

[16] Sai Teja Kaluva, Aditya Pathak, and Aybike Ongel. "Aerodynamic Drag Analysis of Autonomous Electric Vehicle Platoons". In: *Energies* 13.15 (Aug. 2020), p. 4028. DOI: 10.3390/en13154028. URL: https://doi.org/10.3390/en13154028.

[17] Jin I. Ge, Sergei S. Avedisov, Chaozhe R. He, Wubing B. Qin, Mehdi Sadeghpour, and Gábor Orosz. "Experimental validation of connected automated vehicle design among human-driven vehicles". In: *Transportation Research Part C: Emerging Technologies* 91 (June 2018), pp. 335–352. DOI: 10.1016/j.trc.2018.04.005. URL: https://doi.org/10.1016/j.trc.2018.04.005.

[18] Steven E. Shladover, Christopher Nowakowski, Xiao-Yun Lu, and Robert Ferlis. "Cooperative Adaptive Cruise Control". In: *Transportation Research Record: Journal of the Transportation Research Board* 2489.1 (Jan. 2015), pp. 145–152. DOI: 10.3141/2489-17. URL: https://doi.org/10.3141/2489-17.

[19] *California ISO: Today's Outlook*. http://www.caiso.com/todaysoutlook/pages/index.html. Accessed: September 30th, 2021.

[20] Matteo Muratori. "Impact of uncoordinated plug-in electric vehicle charging on residential power demand". In: *Nature Energy* 3.3 (Jan. 2018), pp. 193–201. DOI: 10.1038/s41560-017-0074-z. URL: https://doi.org/10.1038/s41560-017-0074-z.

[21] Martin Spitzer, Jonas Schlund, Elpiniki Apostolaki-Iosifidou, and Marco Pruckner. "Optimized Integration of Electric Vehicles in Low Voltage Distribution Grids". In: *Energies* 12.21 (Oct. 2019), p. 4059. DOI: 10.3390/en12214059. URL: https://doi.org/10.3390/en12214059.

[22] Syed Asad Abbas Rizvi, Ai Xin, Arsalan Masood, Sheeraz Iqbal, Mishkat Ullah Jan, and Haseebur Rehman. "Electric Vehicles and their Impacts on Integration into Power Grid: A Review". In: *2018 2nd IEEE Conference on Energy Internet and Energy System Integration (EI2)*. IEEE, Oct. 2018. DOI: 10.1109/ei2.2018.8582069. URL: https://doi.org/10.1109/ei2.2018.8582069.

[23] Julia K. Szinai, Colin J.R. Sheppard, Nikit Abhyankar, and Anand R. Gopal. "Reduced grid operating costs and renewable energy curtailment with electric vehicle charge management". In: *Energy Policy* 136 (Jan. 2020), p. 111051. DOI: 10.1016/j.enpol.2019.111051. URL: https://doi.org/10.1016/j.enpol.2019.111051.

[24] Bo Zhou, Guo Chen, Qiankun Song, and Zhao Yang Dong. "Robust chance-constrained programming approach for the planning of fast-charging stations in electrified transportation networks". In: *Applied Energy* 262 (Mar. 2020), p. 114480. DOI: 10.1016/j.apenergy.2019.114480. URL: https://doi.org/10.1016/j.apenergy.2019.114480.

[25] Sreten Davidov and Miloš Pantoš. "Planning of electric vehicle infrastructure based on charging reliability and quality of service". In: *Energy* 118 (Jan. 2017), pp. 1156–1167. DOI: 10.1016/j.energy.2016.10.142. URL: https://doi.org/10.1016/j.energy.2016.10.142.

[26] Amir Ghiasi, Omar Hussain, Zhen (Sean) Qian, and Xiaopeng Li. "A mixed traffic capacity analysis and lane management model for connected automated vehicles: A Markov chain method". In: *Transportation Research Part B: Methodological* 106 (Dec. 2017), pp. 266–292. DOI: 10.1016/j.trb.2017.09.022. URL: https://doi.org/10.1016/j.trb.2017.09.022.

[27] Xuedong Hua, Weijie Yu, Wei Wang, and Wenjie Xie. "Influence of Lane Policies on Freeway Traffic Mixed with Manual and Connected and Autonomous Vehicles". In: *Journal of Advanced Transportation* 2020 (Feb. 2020), pp. 1–20. DOI: 10.1155/2020/3968625. URL: https://doi.org/10.1155/2020/3968625.

[28] Jorge A. Laval and Carlos F. Daganzo. "Lane-changing in traffic streams". In: *Transportation Research Part B: Methodological* 40.3 (Mar. 2006), pp. 251–264. DOI: 10.1016/j.trb.2005.04.003. URL: https://doi.org/10.1016/j.trb.2005.04.003.

[29] Danjue Chen and Soyoung Ahn. "Capacity-drop at extended bottlenecks: Merge, diverge, and weave". In: *Transportation Research Part B: Methodological* 108 (Feb. 2018), pp. 1–20. DOI: 10.1016/j.trb.2017.12.006. URL: https://doi.org/10.1016/j.trb.2017.12.006.

[30] Jorge Laval, Michael Cassidy, and Carlos Daganzo. "Impacts of Lane Changes at Merge Bottlenecks: A Theory and Strategies to Maximize Capacity". In: *Traffic and Granular Flow'05*. Springer Berlin Heidelberg, pp. 577–586. DOI: 10.1007/978-3-540-47641-2_56. URL: https://doi.org/10.1007/978-3-540-47641-2_56.

[31] Hao Liu, Steven E. Shladover, Xiao-Yun Lu, and Xingan (David) Kan. "Freeway vehicle fuel efficiency improvement via cooperative adaptive cruise control". In: *Journal of Intelligent Transportation Systems* (Feb. 2020), pp. 1–13. DOI: 10.1080/15472450.2020.1720673. URL: https://doi.org/10.1080/15472450.2020.1720673.

[32] James Dixon, Peter Bach Andersen, Keith Bell, and Chresten Træholt. "On the ease of being green: An investigation of the inconvenience of electric vehicle charging". In: *Applied Energy* 258 (Jan. 2020), p. 114090. DOI: 10.1016/j.apenergy.2019.114090. URL: https://doi.org/10.1016/j.apenergy.2019.114090.

[33] Giuseppe Graber, Vito Calderaro, Pierluigi Mancarella, and Vincenzo Galdi. "Two-stage stochastic sizing and packetized energy scheduling of BEV charging stations with quality of service constraints". In: *Applied Energy* 260 (Feb. 2020), p. 114262. DOI: 10.1016/j.apenergy.2019.114262. URL: https://doi.org/10.1016/j.apenergy.2019.114262.

[34] Teng Zeng, Hongcai Zhang, and Scott Moura. "Solving Overstay and Stochasticity in PEV Charging Station Planning With Real Data". In: *IEEE Transactions on Industrial Informatics* 16.5 (May 2020), pp. 3504–3514. DOI: 10.1109/tii.2019.2955997. URL: https://doi.org/10.1109/tii.2019.2955997.

[35] Hongcai Zhang, Zechun Hu, Zhiwei Xu, and Yonghua Song. "An Integrated Planning Framework for Different Types of PEV Charging Facilities in Urban Area". In: *IEEE Transactions on Smart Grid* 7.5 (Sept. 2016), pp. 2273–2284. DOI: 10.1109/tsg.2015.2436069. URL: https://doi.org/10.1109/tsg.2015.2436069.

[36] Huimiao Chen, Zechun Hu, Haocheng Luo, Junjie Qin, Ram Rajagopal, and Hongcai Zhang. "Design and Planning of a Multiple-Charger Multiple-Port Charging System for PEV Charging Station". In: *IEEE Transactions on Smart Grid* 10.1 (Jan. 2019), pp. 173–183. DOI: 10.1109/tsg.2017.2735636. URL: https://doi.org/10.1109/tsg.2017.2735636.

[37] Leon Haupt, Michael Schöpf, Lars Wederhake, and Martin Weibelzahl. "The influence of electric vehicle charging strategies on the sizing of electrical energy storage systems in charging hub microgrids". In: *Applied Energy* 273 (Sept. 2020), p. 115231. DOI: 10.1016/j.apenergy.2020.115231. URL: https://doi.org/10.1016/j.apenergy.2020.115231.

[38] Huajie Ding, Zechun Hu, and Yonghua Song. "Value of the energy storage system in an electric bus fast charging station". In: *Applied Energy* 157 (Nov. 2015), pp. 630–639. DOI: 10.1016/j.apenergy.2015.01.058. URL: https://doi.org/10.1016/j.apenergy.2015.01.058.

[39] Hongcai Zhang, Zechun Hu, Zhiwei Xu, and Yonghua Song. "Optimal Planning of PEV Charging Station With Single Output Multiple Cables Charging Spots". In: *IEEE Transactions on Smart Grid* 8.5 (Sept. 2017), pp. 2119–2128. DOI: 10.1109/tsg.2016.2517026. URL: https://doi.org/10.1109/tsg.2016.2517026.

[40] Zachary J. Lee, George Lee, Ted Lee, Cheng Jin, Rand Lee, Zhi Low, Daniel Chang, Christine Ortega, and Steven H. Low. *Adaptive Charging Networks: A Framework for Smart Electric Vehicle Charging*. 2020. arXiv: 2012.02636 [eess.SY]. URL: https://arxiv.org/pdf/2012.02636.pdf.

[41] Mohammadreza Daneshvar, Behnam Mohammadi-ivatloo, Somayeh Asadi, Kazem Zare, and Amjad Anvari-Moghaddam. "Optimal Day-Ahead Scheduling of the Renewable Based Energy Hubs Considering Demand Side Energy Management". In: *2019 International Conference on Smart Energy Systems and Technologies (SEST)*. IEEE, Sept. 2019. DOI: 10.1109/sest.2019.8849131. URL: https://doi.org/10.1109/sest.2019.8849131.

[42] Wim Van Ackooij, Riadh Zorgati, René Henrion, and Andris Möller. "Chance constrained programming and its applications to energy management". In: *Stochastic Optimization—Seeing the Optimal for the Uncertain* (2011), pp. 291–320.

[43] Christian Milan, Michael Stadler, Gonçalo Cardoso, and Salman Mashayekh. "Modeling of non-linear CHP efficiency curves in distributed energy systems". In: *Applied Energy* 148 (June 2015), pp. 334–347. DOI: 10.1016/j.apenergy.2015.03.053. URL: https://doi.org/10.1016/j.apenergy.2015.03.053.

[44] Elpiniki Apostolaki-Iosifidou, Soomin Woo, Marco Pruckner, and Timothy Lipman. "Electric Vehicle Charge Management for Lowering Costs and Environmental Impact". In: *7th IEEE Conference on Technologies for Sustainability (SusTech2020)*. Apr. 2020.

[45] Thomas N. Taylor and Peter M. Schwarz. "The Long-Run Effects of a Time-of-Use Demand Charge". In: *The RAND Journal of Economics* 21.3 (1990), p. 431. DOI: 10.2307/2555618. URL: https://doi.org/10.2307/2555618.

[46] Zachary J. Lee, Tongxin Li, and Steven H. Low. "ACN-Data: Analysis and Applications of an Open EV Charging Dataset". In: *Proceedings of the Tenth International Conference on Future Energy Systems*. e-Energy '19. Phoenix, Arizona, June 2019.

[47] OpenEI. *Long-term electricity and gas consumption for LBNL Building 74*. URL: https://openei.org/datasets/dataset/lbnl-building-74.

[48] PG&E. *Time-of-Use Rates Charts*. URL: https://www.pge.com/en_US/business/rate-plans/rate-plans/time-of-use/time-of-use.page.

[49] Nicolò Daina, Aruna Sivakumar, and John W. Polak. "Electric vehicle charging choices: Modelling and implications for smart charging services". In: *Transportation Research Part C: Emerging Technologies* 81 (Aug. 2017), pp. 36–56. DOI: 10.1016/j.trc.2017.05.006. URL: https://doi.org/10.1016/j.trc.2017.05.006.

[50] Weeberb J. Requia, Moataz Mohamed, Christopher D. Higgins, Altaf Arain, and Mark Ferguson. "How clean are electric vehicles? Evidence-based review of the effects of electric mobility on air pollutants, greenhouse gas emissions and human health". In: *Atmospheric Environment* 185 (July 2018), pp. 64–77. DOI: 10.1016/j.atmosenv.2018.04.040. URL: https://doi.org/10.1016/j.atmosenv.2018.04.040.

[51] Yanchong Zheng, Songyan Niu, Yitong Shang, Ziyun Shao, and Linni Jian. "Integrating plug-in electric vehicles into power grids: A comprehensive review on power interaction mode, scheduling methodology and mathematical foundation". In: *Renewable and Sustainable Energy Reviews* 112 (Sept. 2019), pp. 424–439. DOI: 10.1016/j.rser.2019.05.059. URL: https://doi.org/10.1016/j.rser.2019.05.059.

[52] Florian van Triel and Timothy E. Lipman. "Modeling the Future California Electricity Grid and Renewable Energy Integration with Electric Vehicles". In: *Energies* 13.20 (Oct. 2020), p. 5277. DOI: 10.3390/en13205277. URL: https://doi.org/10.3390/en13205277.

[53] Joshua S. Graff Zivin, Matthew J. Kotchen, and Erin T. Mansur. "Spatial and temporal heterogeneity of marginal emissions: Implications for electric cars and other electricity-shifting policies". In: *Journal of Economic Behavior & Organization* 107 (Nov. 2014), pp. 248–268. DOI: 10.1016/j.jebo.2014.03.010. URL: https://doi.org/10.1016/j.jebo.2014.03.010.

[54] Emre C. Kara, Jason S. Macdonald, Douglas Black, Mario Bérges, Gabriela Hug, and Sila Kiliccote. "Estimating the benefits of electric vehicle smart charging at non-residential locations: A data-driven approach". In: *Applied Energy* 155 (Oct. 2015), pp. 515–525. DOI: 10.1016/j.apenergy.2015.05.072. URL: https://doi.org/10.1016/j.apenergy.2015.05.072.

[55] Brian Tarroja, Joshua D. Eichman, Li Zhang, Tim M. Brown, and Scott Samuelsen. "The effectiveness of plug-in hybrid electric vehicles and renewable power in support of holistic environmental goals: Part 1 – Evaluation of aggregate energy and greenhouse gas performance". In: *Journal of Power Sources* 257 (July 2014), pp. 461–470. DOI: 10.1016/j.jpowsour.2013.09.147. URL: https://doi.org/10.1016/j.jpowsour.2013.09.147.

[56] Linni Jian, Yanchong Zheng, and Ziyun Shao. "High efficient valley-filling strategy for centralized coordinated charging of large-scale electric vehicles". In: *Applied Energy* 186 (Jan. 2017), pp. 46–55. DOI: 10.1016/j.apenergy.2016.10.117. URL: https://doi.org/10.1016/j.apenergy.2016.10.117.

[57] Fei Teng, Marko Aunedi, and Goran Strbac. "Benefits of flexibility from smart electrified transportation and heating in the future UK electricity system". In: *Applied Energy* 167 (Apr. 2016), pp. 420–431. DOI: 10.1016/j.apenergy.2015.10.028. URL: https://doi.org/10.1016/j.apenergy.2015.10.028.

[58] Kate E. Forrest, Brian Tarroja, Li Zhang, Brendan Shaffer, and Scott Samuelsen. "Charging a renewable future: The impact of electric vehicle charging intelligence on energy storage requirements to meet renewable portfolio standards". In: *Journal of Power Sources* 336 (Dec. 2016), pp. 63–74. DOI: 10.1016/j.jpowsour.2016.10.048. URL: https://doi.org/10.1016/j.jpowsour.2016.10.048.

[59] Christopher G. Hoehne and Mikhail V. Chester. "Optimizing plug-in electric vehicle and vehicle-to-grid charge scheduling to minimize carbon emissions". In: *Energy* 115 (Nov. 2016), pp. 646–657. DOI: 10.1016/j.energy.2016.09.057. URL: https://doi.org/10.1016/j.energy.2016.09.057.

[60] Kanwardeep Singh, Narayana Prasad Padhy, and Jaydev Sharma. "Influence of Price Responsive Demand Shifting Bidding on Congestion and LMP in Pool-Based Day-Ahead Electricity Markets". In: *IEEE Transactions on Power Systems* 26.2 (May 2011), pp. 886–896. DOI: 10.1109/tpwrs.2010.2070813. URL: https://doi.org/10.1109/tpwrs.2010.2070813.

[61] Peter Alstone, Jennifer Potter, Mary Ann Piette, Peter Schwartz, Michael A. Berger, Laurel N. Dunn, Sarah Josephine Smith, Michael D. Sohn, Arian Aghajanzadeh, Sofia Stensson, and Julia Szinai. *Demand Response Potential for California SubLAPs and Local Capacity Planning Areas: An Addendum to the 2025 California Demand Response Potential Study - Phase 2*. Tech. rep. Apr. 2017.

[62] California ISO. *CAISO SubLAPs*. URL: https://www.pge.com/pge_global/common/pdfs/save-energy-money/energy-management-programs/demand-response-programs/2018-demand-response/2018-demand-response-auction-mechanism/PGE-Sub-Lap-Map-201703.pdf.

[63] Steven Diamond and Stephen Boyd. "CVXPY: A Python-embedded modeling language for convex optimization". In: *Journal of Machine Learning Research* 17.83 (2016), pp. 1–5.

[64] Department of Energy. *Alternative Fuels Data Center. Maps and Data - Electric Vehicle Registrations by State*. URL: https://afdc.energy.gov/data/10962.

[65] California Public Utilities Commission. *RPS Program Overview*. URL: https://www.cpuc.ca.gov/rps_overview/ (visited on 04/13/2021).

[66] California Public Utilities Commission. *Greenhouse Gas Cap-and-Trade Program*. URL: https://www.cpuc.ca.gov/general.aspx?id=5932 (visited on 04/13/2021).

[67] California Public Utilities Commission. *Zero-Emission Vehicles*. URL: https://www.cpuc.ca.gov/zev/ (visited on 04/13/2021).

[68] Pacific Gas and Electric Company. *Electric Schedule EV Residential Time-of-Use Service for Plug-in Electric Vehicle Customers*. URL: https://www.pge.com/tariffs/assets/pdf/tariffbook/ELEC_SCHEDS_EV%20(Sch).pdf.

[69] Teng Zeng, Sangjae Bae, Bertrand Travacca, and Scott Moura. "Inducing Human Behavior to Maximize Operation Performance at PEV Charging Station". In: *IEEE Transactions on Smart Grid* 12.4 (July 2021), pp. 3353–3363. DOI: 10.1109/tsg.2021.3066998. URL: https://doi.org/10.1109/tsg.2021.3066998.

[70] Bart van Arem, Cornelie J. G. van Driel, and Ruben Visser. "The Impact of Cooperative Adaptive Cruise Control on Traffic-Flow Characteristics". In: *IEEE Transactions on Intelligent Transportation Systems* 7.4 (Dec. 2006), pp. 429–436. DOI: 10.1109/tits.2006.884615. URL: https://doi.org/10.1109/tits.2006.884615.

[71] Alireza Talebpour, Hani S. Mahmassani, and Amr Elfar. "Investigating the Effects of Reserved Lanes for Autonomous Vehicles on Congestion and Travel Time Reliability". In: *Transportation Research Record: Journal of the Transportation Research Board* 2622.1 (Jan. 2017), pp. 1–12. DOI: 10.3141/2622-01. URL: https://doi.org/10.3141/2622-01.

[72] Danjue Chen, Soyoung Ahn, Madhav Chitturi, and David A. Noyce. "Towards vehicle automation: Roadway capacity formulation for traffic mixed with regular and automated vehicles". In: *Transportation Research Part B: Methodological* 100 (June 2017), pp. 196–221. DOI: 10.1016/j.trb.2017.01.017. URL: https://doi.org/10.1016/j.trb.2017.01.017.

[73] Lanhang Ye and Toshiyuki Yamamoto. "Impact of dedicated lanes for connected and autonomous vehicle on traffic flow throughput". In: *Physica A: Statistical Mechanics and its Applications* 512 (Dec. 2018), pp. 588–597. DOI: 10.1016/j.physa.2018.08.083. URL: https://doi.org/10.1016/j.physa.2018.08.083.

[74] Chao-Tsung Ma. "System Planning of Grid-Connected Electric Vehicle Charging Stations and Key Technologies: A Review". In: *Energies* 12.21 (Nov. 2019), p. 4201. DOI: 10.3390/en12214201. URL: https://doi.org/10.3390/en12214201.

[75] Alireza Talebpour, Hani S. Mahmassani, and Samer H. Hamdar. "Modeling lane-changing behavior in a connected environment: A game theory approach". In: *Transportation Research Part C: Emerging Technologies* 59 (Oct. 2015), pp. 216–232. DOI: 10.1016/j.trc.2015.07.007. URL: https://doi.org/10.1016/j.trc.2015.07.007.

[76] Zijia Zhong and Joyoung Lee. "The effectiveness of managed lane strategies for the near-term deployment of cooperative adaptive cruise control". In: *Transportation Research Part A: Policy and Practice* 129 (Nov. 2019), pp. 257–270. DOI: 10.1016/j.tra.2019.08.015. URL: https://doi.org/10.1016/j.tra.2019.08.015.

[77] Lin Xiao, Meng Wang, and Bart van Arem. "Traffic Flow Impacts of Converting an HOV Lane Into a Dedicated CACC Lane on a Freeway Corridor". In: *IEEE Intelligent Transportation Systems Magazine* 12.1 (2020), pp. 60–73. DOI: 10.1109/mits.2019.2953477. URL: https://doi.org/10.1109/mits.2019.2953477.

[78] Lin Xiao, Meng Wang, Wouter Schakel, Steven Shladover, and Bart van Arem. "Modeling lane change behavior on a highway with a high occupancy vehicle lane with continuous access and egress". In: *TRB 96th Annual Meeting Compendium of Papers*. 2017.

[79] Lin Xiao, Meng Wang, and Bart van Arem. "Realistic Car-Following Models for Microscopic Simulation of Adaptive and Cooperative Adaptive Cruise Control Vehicles". In: *Transportation Research Record: Journal of the Transportation Research Board* 2623.1 (Jan. 2017), pp. 1–9. DOI: 10.3141/2623-01. URL: https://doi.org/10.3141/2623-01.

[80] Christopher Nowakowski, Jessica O'Connell, Steven E. Shladover, and Delphine Cody. "Cooperative Adaptive Cruise Control: Driver Acceptance of Following Gap Settings Less than One Second". In: *Proceedings of the Human Factors and Ergonomics Society Annual Meeting* 54.24 (Sept. 2010), pp. 2033–2037. DOI: 10.1177/154193121005402403. URL: https://doi.org/10.1177/154193121005402403.

[81] Vicente Milanes, Steven E. Shladover, John Spring, Christopher Nowakowski, Hiroshi Kawazoe, and Masahide Nakamura. "Cooperative Adaptive Cruise Control in Real Traffic Situations". In: *IEEE Transactions on Intelligent Transportation Systems* 15.1 (Feb. 2014), pp. 296–305. DOI: 10.1109/tits.2013.2278494. URL: https://doi.org/10.1109/tits.2013.2278494.

[82] Vicente Milanés and Steven E. Shladover. "Handling Cut-In Vehicles in Strings of Cooperative Adaptive Cruise Control Vehicles". In: *Journal of Intelligent Transportation Systems* 20.2 (Apr. 2015), pp. 178–191. DOI: 10.1080/15472450.2015.1016023. URL: https://doi.org/10.1080/15472450.2015.1016023.

[83] Xiao-Yun Lu, Xingan (David) Kan Steven Shladover, Dali Wei, and Robert Ferlis. "An Enhanced Microscopic Traffic Simulation Model for Application to Connected Automated Vehicles". In: *TRB 96th Annual Meeting Compendium of Papers*. 2017.

[84] Vicente Milanés and Steven E. Shladover. "Modeling cooperative and autonomous adaptive cruise control dynamic responses using experimental data". In: *Transportation Research Part C: Emerging Technologies* 48 (Nov. 2014), pp. 285–300. DOI: 10.1016/j.trc.2014.09.001. URL: https://doi.org/10.1016/j.trc.2014.09.001.

[85] Xingan (David) Kan, Lin Xiao, Hao Liu, Meng Wang, Wouter J. Schakel, Xiao-Yun Lu, Bart van Arem, Steven E. Shladover, and Robert A. Ferlis. "Cross-Comparison and Calibration of Two Microscopic Traffic Simulation Models for Complex Freeway Corridors with Dedicated Lanes". In: *Journal of Advanced Transportation* 2019 (Mar.

2019), pp. 1–14. DOI: 10.1155/2019/8618476. URL: https://doi.org/10.1155/2019/8618476.

[86] Lanhang Ye and Toshiyuki Yamamoto. "Modeling connected and autonomous vehicles in heterogeneous traffic flow". In: *Physica A: Statistical Mechanics and its Applications* 490 (Jan. 2018), pp. 269–277. DOI: 10.1016/j.physa.2017.08.015. URL: https://doi.org/10.1016/j.physa.2017.08.015.

[87] Li Jin, Mladen Čičić, Saurabh Amin, and Karl H. Johansson. "Modeling the Impact of Vehicle Platooning on Highway Congestion". In: *Proceedings of the 21st International Conference on Hybrid Systems: Computation and Control (part of CPS Week)*. ACM, Apr. 2018. DOI: 10.1145/3178126.3178146. URL: https://doi.org/10.1145/3178126.3178146.

[88] Alireza Talebpour and Hani S. Mahmassani. "Influence of connected and autonomous vehicles on traffic flow stability and throughput". In: *Transportation Research Part C: Emerging Technologies* 71 (Oct. 2016), pp. 143–163. DOI: 10.1016/j.trc.2016.07.007. URL: https://doi.org/10.1016/j.trc.2016.07.007.

[89] Ye Li, Hao Wang, Wei Wang, Lu Xing, Shanwen Liu, and Xueyan Wei. "Evaluation of the impacts of cooperative adaptive cruise control on reducing rear-end collision risks on freeways". In: *Accident Analysis & Prevention* 98 (Jan. 2017), pp. 87–95. DOI: 10.1016/j.aap.2016.09.015. URL: https://doi.org/10.1016/j.aap.2016.09.015.

[90] Lin Xiao, Meng Wang, Wouter Schakel, and Bart van Arem. "Unravelling effects of cooperative adaptive cruise control deactivation on traffic flow characteristics at merging bottlenecks". In: *Transportation Research Part C: Emerging Technologies* 96 (Nov. 2018), pp. 380–397. DOI: 10.1016/j.trc.2018.10.008. URL: https://doi.org/10.1016/j.trc.2018.10.008.

[91] Hao Liu, Xingan (David) Kan, Steven E. Shladover, Xiao-Yun Lu, and Robert E. Ferlis. "Impact of cooperative adaptive cruise control on multilane freeway merge capacity". In: *Journal of Intelligent Transportation Systems* 22.3 (Apr. 2018), pp. 263–275. DOI: 10.1080/15472450.2018.1438275. URL: https://doi.org/10.1080/15472450.2018.1438275.

[92] Matteo Muratori, Jacob Holden, Michael Lammert, Adam Duran, Stanley Young, and Jeffrey Gonder. "Potentials for Platooning in U.S. Highway Freight Transport". In: *SAE International Journal of Commercial Vehicles* 10.1 (Mar. 2017), pp. 45–49. DOI: 10.4271/2017-01-0086. URL: https://doi.org/10.4271/2017-01-0086.

[93] Zhen Wang, Xiaowei Shi, and Xiaopeng Li. "Review of Lane-Changing Maneuvers of Connected and Automated Vehicles: Models, Algorithms and Traffic Impact Analyses". In: *Journal of the Indian Institute of Science* 99.4 (Oct. 2019), pp. 589–599. DOI: 10.1007/s41745-019-00127-7. URL: https://doi.org/10.1007/s41745-019-00127-7.

[94] Di Wang, Manjiang Hu, Yunpeng Wang, Jianqiang Wang, Hongmao Qin, and Yougang Bian. "Model predictive control–based cooperative lane change strategy for improving traffic flow". In: *Advances in Mechanical Engineering* 8.2 (Feb. 2016), p. 168781401663299. DOI: 10.1177/1687814016632992. URL: https://doi.org/10.1177/1687814016632992.

[95] Cathy Wu, Aboudy Kreidieh, Kanaad Parvate, Eugene Vinitsky, and Alexandre M Bayen. *Flow: A Modular Learning Framework for Autonomy in Traffic*. 2017. eprint: arXiv:1710.05465.

[96] G.F. Newell. "A simplified car-following theory: a lower order model". In: *Transportation Research Part B: Methodological* 36.3 (Mar. 2002), pp. 195–205. DOI: 10.1016/s0191-2615(00)00044-8. URL: https://doi.org/10.1016/s0191-2615(00)00044-8.

[97] Martin Treiber, Ansgar Hennecke, and Dirk Helbing. "Congested traffic states in empirical observations and microscopic simulations". In: *Physical Review E* 62.2 (Aug. 2000), pp. 1805–1824. DOI: 10.1103/physreve.62.1805. URL: https://doi.org/10.1103/physreve.62.1805.

[98] Biagio Ciuffo, Vincenzo Punzo, and Marcello Montanino. "Thirty Years of Gipps' Car-Following Model". In: *Transportation Research Record: Journal of the Transportation Research Board* 2315.1 (Jan. 2012), pp. 89–99. DOI: 10.3141/2315-10. URL: https://doi.org/10.3141/2315-10.

[99] Fábio Duarte and Carlo Ratti. "The Impact of Autonomous Vehicles on Cities: A Review". In: *Journal of Urban Technology* 25.4 (July 2018), pp. 3–18. DOI: 10.1080/10630732.2018.1493883. URL: https://doi.org/10.1080/10630732.2018.1493883.

[100] Dimitris Milakis, Nikolas Thomopoulos, and Bert Van Wee. *Policy Implications of Autonomous Vehicles*. Academic Press, 2020.

[101] Yonah Freemark, Anne Hudson, and Jinhua Zhao. "Are Cities Prepared for Autonomous Vehicles?" In: *Journal of the American Planning Association* 85.2 (Apr. 2019), pp. 133–151. DOI: 10.1080/01944363.2019.1603760. URL: https://doi.org/10.1080/01944363.2019.1603760.